The stochastic movements of individual streambed grains

by

J. Kevin Pierce

B.S., West Virginia University, 2013

M.Sc., University of British Columbia, 2016

A THESIS SUBMITTED IN PARTIAL FULFILLMENT
OF THE REQUIREMENTS FOR THE DEGREE OF

Doctor of Philosophy

in

THE FACULTY OF GRADUATE AND POSTDOCTORAL STUDIES
(Geography)

The University of British Columbia
(Vancouver)

September 2021

The following individuals certify that they have read, and recommend to the Faculty of Graduate and Postdoctoral Studies for acceptance, the thesis entitled:

The stochastic movements of individual streambed grains

submitted by **J. Kevin Pierce** in partial fulfillment of the requirements for the degree of **Doctor of Philosophy** in **Geography**.

Examining Committee:

Marwan Hassan, Professor, Geography, University of British Columbia
Supervisor

Brett Eaton, Professor, Geography, University of British Columbia
Supervisory Committee Member

Rui Ferreira, Associate Professor, Civil Engineering, Instituto Superior Técnico
Supervisory Committee Member

Michael Church, Professor Emeritus, Geography, University of British Columbia
University Examiner

Roger Beckie, Professor, Civil Engineering, University of British Columbia
University Examiner

Peter Ashmore, Professor, Geography and Environment, Western University
External Examiner

Abstract

Bedload transport is the movement of coarse grains through river channels by bouncing, rolling, and sliding. Because coarse grains control river stability, predicting the rate of bedload transport is a fundamental problem in river science. This problem is usually approached with continuum mechanics, but this approach is questionable considering that coarse sediment grains rarely move in densities approximating a continuum.

An alternative approach describes bedload transport from the trajectories of individual grains using statistical physics. This approach has become increasingly popular in recent decades, but many fundamental issues prevent this approach from being widely adopted. In particular, the connection between individual particle trajectories and transport rates remains unclear, and particle trajectory models remain highly simplified. Feedbacks between topography and sediment transport remain challenging to analyze, and basic properties of bedload motions like downstream travel velocities remain incompletely understood. Buried particles cannot appreciably move downstream, but even this simple observation has not been comprehensively described in the statistical physics approach.

This thesis presents four projects completed in my PhD which overcome these issues to provide new understanding of bedload transport from a statistical point of view. First, I demonstrate how to calculate the sediment flux from the dynamics of individual grains, and I model the trajectories of grains alternating through motion and rest having fluctuating velocities in the motion state. This links the sediment flux to the grain-scale dynamics and describes particle trajectories with additional detail compared

to earlier descriptions. Second, I include feedbacks between local bed elevations and sediment transport, quantifying the interplay of bed elevation changes and sediment transport rates and predicting how long particles can stay buried in the river bed. Third, I incorporate the sediment burial process into a model of downstream sediment transport, predicting how grains move downstream when they can become buried. Finally, I describe bedload dynamics on short timescales, predicting the movement velocities of bedload particles using methods adopted from granular physics. I conclude by summarizing these developments, discussing their implications for the statistical description of bedload transport, and suggesting how we can use this modeling progress to better understand landscapes.

Lay Summary

Predicting the flow rates of gravel through river channels is important to manage environmental issues involving rivers. Most approaches to predict gravel flow consider gravel as if it were a heavy fluid. These descriptions oversimplify the problem, since gravel flow is actually composed of individual grains bouncing and rolling downstream, which is hardly like a fluid.

In this thesis, I consider gravel flow as the result of individual grains. Using physics and probability, I calculate how fast individual grains move downstream, then I demonstrate how to use their downstream movement paths to predict overall gravel flow rates. This research produces a more realistic description of gravel movement in rivers which helps us understand how rivers change through time.

Preface

This thesis is entirely the original research of Kevin Pierce, including all figures, writing, and calculations. The supervisory committee and especially the research supervisor Marwan Hassan provided guidance in the research. Suggestions from Michael Church, Rui Ferreira, Roger Beckie, Peter Ashmore, Bernard Laval, and Brett Eaton improved the clarity of the writing.

The thesis includes two published works, Chapters 3 and 4, available in *Journal of Geophysical Research: Earth Surface* and *Geophysical Research Letters* respectively, with Marwan Hassan as coauthor (*Pierce and Hassan*, 2020a,b). Chapters 2 and 5 will be submitted for publication following acceptance of the thesis.

Contents

List of Tables

List of Figures

Acknowledgments

Attending university long enough to earn a PhD is an unbelievable privilege, and I only had access to it thanks to an incredible amount of guidance and support.

Most of all, to my mom Calisa Pierce, dad Jim Pierce, sisters Kelsey and Kim, and grandmother Wilma Avis, it's impossible to explain how thankful I am for your guidance. Thanks also to my great aunt Alice who graciously paid for my undergraduate education.

Thanks to my early teachers who put in the extra care to keep me on track, Jonathan Ramey, Linda Ball, Damon Spurlock, Linda Mendez, Linda Afzalirad, Phyllis Adkins, Brandon Willard, Marty Ojeda, and Red Hamlin among many others.

Thanks also to my professors at Southern WV Community College who fostered my way of thinking and provided many of the tools I used for the research in this thesis. At SWVCC, I'd like to thank especially Mindy Saunders, Tex Wood, Anne Klein, Charles Wood, Don Saunders, and George Trimble. SWVCC was a personal transformation and a great privilege.

At WVU, I'd like to thank Alan Bristow, Tudor Stanescu, and Leo Golubovic in particular. Alan and Tudor, thank you for providing my first opportunities in research. Leo, you are the key person in my development as a researcher.

To my extended cohort at WVU physics, Payne, Megat, Collins, Scott, Dustin, Rice, Wolfe, Samet, Craig, April, Evan, Larry, Robert, Stephen, Rick, Matt, Caleb, John, and all of you others, thanks for the collaboration and the hilarious times. May the lounge live on forever!

To Marwan Hassan, some time ago now I wandered into your office saying I liked rivers and wanted to describe sediment transport with statistical physics. I realize now when I said "statistical physics" your eyes lit up with visions of Einstein, Nakagawa, Yano, and so many other names I now know well. I was lucky to use the right trigger words. Marwan, thanks for all of the guidance, for lending me many dozens of books and papers, for the freedom to explore ideas, and most of all for showing me that it's ok (and implicitly expected) to be human in science.

My friends in geography have also been great. Thanks to the whole extended research family: Shawn, Matteo, Conor, Nisreen, Yinlue, Alex, Kyle, Leo, Dave, Tobias, Katie, Maria, Elli, Jiamei, Xingyu, Niannian, and Emma, plus the outsider Eaton-ites, Will, Dave, Rose, and Anya. In particular thanks to Shawn for all of the shared speculations.

Thank you Rui Ferreira and Brett Eaton! Rui, you welcomed me to Portugal, offered me guidance in the laboratory, and educated me on turbulence and hydraulics. Thanks especially for the thoughtful comments on my thesis. Brett, you were the first person to welcome me to UBC, and I'll always appreciate your effort to teach me how to write, interpret flume experiments, and understand simplified modeling in light of real world complexity.

To David Furbish, before I started my PhD when I was still a physics kid exclusively, I recall attending your colloquium at UBC with Marwan's invitation. At the end I asked a vague question about whether Langevin equations might be useful for describing sediment transport, and the answer was "absolutely yes". Now I have a thesis on it. Thanks for the confirmation! And to the Furbish people – Rachel, Sarah W, Sarah Z, Nakul, Tyler, Erika, and Shawn, thanks sincerely for letting me board the spaceship.

Among UBC Geographers I'd like to thank Nina Hewitt in particular. It was always a pleasure to work for you on your courses, which are so uniquely organized and student-focused. UBC Geography is a much greater department with you in it.

Finally, Mary! My PhD has not been great in terms of work-life balance. Thanks for putting up with my late bedtimes, early wake-ups, rambling science jargon, and skipped social events. It's done!

Completing a PhD looks like a personal achievement, but it's really not. It's an expression of 30 years of influence and guidance from other people at every stage, my parents, my sisters, my grandmother, and a huge network of teachers and mentors. Thank you all!

Chapter 1

Sediment transport and channel evolution

Landscapes evolve when water, wind, and ice erode along the gradients produced by tectonics. Channels initiate along faults and depressions wherever climatic conditions are suitable, incising networks in the landscape and transferring sediments from uplands to lowlands. Earth's biota colonize these networks which form conduits for migration, transmitting water, genetic information, and organic material alike, while biota and chemical decomposition convert sediments to soils, staging the joint evolution of life and landscapes which has occurred across geological time.

Human impacts on these old patterns have become severe, in what has been characterized as an environmental and social crisis (*Slaymaker et al.*, 2021). Research demonstrates unprecedented recent shifts in ancient climatic (*Sivan et al.*, 2004; *Slater et al.*, 2021), denundational (*Hooke*, 2000; *Szabo et al.*, 2010), and biotic patterns (*Walther et al.*, 2002; *Willis and Bhagwat*, 2009), requiring effective aquatic habitat restoration, contaminant management, and engineering strategies more than ever before.

In this context river geomorphology as a scientific discipline has shifted toward more quantitative methods that enable concrete predictions about the natural world (*Church*, 2005, 2010). Sediment transport in river channels is especially amenable to this quantitative approach since it is mechanisti-

cally the result of fluid and granular physics. Sediment moves in different modes depending on the relative importance of the fluid forces against the weight of sediment grains (*Bagnold*, 1956). When particles are coarse, as in gravel-bed rivers, fluid forces are relatively weak and particles move as "bedload", by bouncing, rolling, and sliding along the bed surface (*Kalinske*, 1947). In bedload transport conditions, fluid turbulence and the irregular bed surface adopt particular control over the sediment dynamics (*Ferreira et al.*, 2015).

Bedload transport exerts unique influence over channel morphology and stability (*Church*, 2006; *Recking et al.*, 2016), in part because the coarsest grains in a river provide a partially-immobile skeleton upon which sedimentary deposits can develop (*Eaton et al.*, 2020; *Hassan et al.*, 2008). A longstanding problem in river science is therefore to determine the bedload flux, or the rate of coarse sediment movement. Unfortunately, existing approaches to compute the bedload flux are inadequate, and predictions often deviate from measured values by orders of magnitude (*Barry et al.*, 2004; *Bathurst*, 2007; *Gomez and Church*, 1989; *Recking et al.*, 2012). Given that the problem has been researched intensively for over a century now (*Gilbert*, 1914), it is clear that new research strategies are needed (*Ancey*, 2020a).

Predicting bedload fluxes is challenging because transport is not always well correlated to average characteristics of the flow and bed material. Local fluxes can range through orders of magnitude as details of turbulent fluctuations and bed organization vary, while average characterizations of flow and sediment remain constant (*Charru et al.*, 2004; *Hassan et al.*, 2008; *Sumer et al.*, 2003; *Venditti et al.*, 2017). The same turbulence and sediment organization details which correlate with the bedload flux are also modified by it. Turbulent impulses drive sediment motion (*Amir et al.*, 2014; *Celik et al.*, 2014; *Shih et al.*, 2017; *Valyrakis et al.*, 2010), but moving sediment affects turbulence characteristics (*Liu et al.*, 2016; *Santos et al.*, 2014; *Singh et al.*, 2010). The surface arrangement and consolidation of grains affects sediment mobility (*Dwivedi et al.*, 2012; *Miller and Byrne*, 1966; *Paintal*, 1971), but transport rearranges grains and consolidates the bed (*Allen and Kudrolli*, 2018; *Charru et al.*, 2004; *Kirchner et al.*, 1990; *Masteller et al.*,

2019; *Pretzlav et al.*, 2020). Bedload fluxes are in cyclical feedback with their controls (*Jerolmack and Mohrig*, 2005), and this challenges us to step beyond descriptions based on averaged values (*Ancey*, 2020b).

The approach taken in this thesis is to consider bedload transport as an aggregate result of many individual transported grains whose movements have probabilistic characteristics. This departs from the traditional strategy of correlating transport rates to the average flow and sedimentary characteristics (*Meyer-Peter and Müller*, 1948; *Parker*, 1990; *Wilcock*, 2001). Because the trajectories of individual grains are governed by Newtonian mechanics, this approach brings powerful tools to the problem, but it is nonetheless complicated because the forces driving and resisting sediment motion vary through space and time due to fluid turbulence and the erratic interactions of moving particles with the bed.

To address these complications, I develop in this thesis a handful of new bedload transport models using methods adopted from statistical physics. To provide context and motivation, the thesis begins by reviewing earlier approaches to bedload transport which my work is most related to, rephrasing works as necessary to indicate common themes, highlight the shortcomings to be addressed, and show continuity with my own developments which follow in subsequent chapters.

1.1 Theories of individual particle movement

A basic problem in sediment transport modeling is to predict the downstream movements of individual particles. At first glance, this seems an elementary problem in general physics, but numerous challenges appear. Particles moving as bedload are driven downstream by a turbulent fluid flow, but relationships between the fluid flow and the applied forces are known only approximately (*Michaelides*, 1997; *Schmeeckle et al.*, 2007). Downstream movement is resisted by frictional encounters between moving particles and the bed (skidding, pivoting, colliding), but since the bed is a granular surface, its geometry is difficult to characterize (*Gordon et al.*, 1972), and the role of bed interactions is challenging to describe (*Niño and García*, 1998;

Sekine and Kikkawa, 1992).

Entrainment and deposition provide an additional layer of complexity. Moving particles that encounter the bed with sufficiently low velocities can settle into pockets which protect them from the flow (*Miller and Byrne*, 1966) and cause deposition (*Charru et al.*, 2004). These pockets are not permanent shelter because rearrangement of the surrounding bed by entrainment of neighboring particles or subsurface creep (*Frey*, 2014; *Houssais et al.*, 2016) can re-expose particles to the flow, and sufficiently strong turbulent fluctuations (e.g. *Cameron et al.*, 2020) can overcome shelter even if its geometry is not disturbed (*Celik et al.*, 2014; *Valyrakis et al.*, 2010). As a result, particles generally alternate through sequences of entrainment and deposition, but the exact times at which these alternations occur are difficult to characterize (*Einstein*, 1937).

Particles at rest on the bed surface can also become covered by other transported particles (*Yang and Sayre*, 1971). These buried particles cannot move appreciably until those burying them have been transported away (*Nakagawa and Tsujimoto*, 1981), generating long periods of relative immobility (*Ferguson and Hoey*, 2002; *Hassan and Church*, 1994).

Individual trajectories of particles therefore involve a number of contributing processes which occur over different characteristic timescales, from seconds to years (*Pretzlav et al.*, 2021), and each of these processes has so far evaded any exact description.

Nikora et al. (2001a, 2002) provided a conceptual framework which helps to organize this complexity. Nikora et al. divided the downstream trajectories of individual particles into three timescales, or "ranges", termed local, intermediate, and global. The local range refers to the period of motion between subsequent interactions with the bed, when the particles accelerate downstream within the turbulent flow. The intermediate range reflects particle motions through sequences of bed encounters, when particles alternately accelerate and decelerate. The global range refers to particle trajectories through sequential entrainment and deposition events as they cycle between motion and rest. *Hassan and Bradley* (2017) added an additional range, referred to as "geomorphic", to reflect the even longer period over

which particles become buried within the subsurface or embedded among sedimentary deposits (*Bradley*, 2017). This set of timescales – local, intermediate, global, and geomorphic – are used below to organize the literature describing trajectories of individual grains.

1.1.1 Motivation: Tracers and basic understanding

An early motivation to understand individual particle motions was to predict the efficiency of sediment transport measurements (*Ettema and Mutel*, 2004), and this motivation still drives a great deal of research into individual particle motions today (*Hassan and Bradley*, 2017; *Pretzlav et al.*, 2021). A common technique to estimate sediment transport is to seed a stream with tracer stones and track their progress downstream (*Einstein*, 1937; *Pretzlav et al.*, 2021; *Takayama*, 1965). In principle, tracers provide a proxy for the population of grains in a stream, so one can estimate virtual velocities of tracers, then multiply by an estimate of the number of grains available for motion to calculate the overall sediment flux (*Ferguson and Hoey*, 2002; *Wilcock and McArdell*, 1997). In practice, challenges arise due to the distinct behavior of tracers over the local, intermediate, global, and geomorphic timescales. Apparently, tracer virtual velocities depend on the observation time, in a phenomenon which has been called "advective slowdown" (*Ferguson and Hoey*, 2002; *Haschenburger*, 2011, 2013; *Pelosi et al.*, 2016). This observation-time dependence obscures the relationship between measured tracer virtual velocities and actual sediment fluxes, exposing a need for further research into how exactly individual particle motions depend on observation scale and what processes generate advective slowdown.

1.1.2 Einstein's random walk model

Einstein was probably the first to model the movements of individual particles through streams (*Einstein*, 1937). Watching painted tracers move through a flume, Einstein came to the conclusion that the movement characteristics of any one particle could not be predicted, so he turned to probabilistic methods to characterize their transport.

Einstein's key insight was to represent particle motions as an alternating sequence of movements and rests having random characteristics. As his interest was on the global range of particle motion when many motion-rest alternations have occurred, and because the duration of particle motions is usually short compared to rests, Einstein made the approximation that individual motions (between entrainment and deposition) are mathematically instantaneous. With this approximation, the downstream movement of sediment becomes an alternate cycle of instantaneous steps of random length and rests of random duration. Implicitly, this concept of sediment trajectories assumes that movement velocities are infinite.

Einstein's experiments indicated that both step lengths and resting times were well-described by exponential distributions, and the focus of his Ph.D. was to find the probability density $P(x,t)$ that a particle had traveled a net distance x after a time t has elapsed. In the course of this research, Einstein formulated an example of what is now called the continuous time random walk, but this approach not formalized until much later (*Montroll*, 1964). In Earth science, random walks have been widely applied to hydrologic problems (*Berkowitz et al.*, 2006), but their application to Earth surface processes remains relatively uncommon (e.g. *Schumer et al.*, 2009).

Einstein's assumptions of infinite movement velocity, random resting duration, and random movement distance imply that the particle position $x(t)$ can be expressed by the dynamical equation

$$\dot{x}(t) = \mu(t), \tag{1.1}$$

where $\dot{x} = dx/dt$, and $\mu(t)$ is a Poisson pulse noise (*Van Den Broeck*, 1983), which is essentially a sequence of pulses having random heights with mean height ℓ (the mean step length), and random locations in time with mean separation $1/k_E$ (the mean resting time, interpreted as the reciprocal of the entrainment rate k_E). A particular realization of this pulsed noise can be written

$$\mu(t) = \sum_{i=1}^{N(t)} s_i \delta(t - t_i). \tag{1.2}$$

Here $N(t)$ is the number of particle entrainments in time t which is a Poisson random variable, distributed as $P(N) = e^{-k_E t}(k_E t)^N/N!$. The t_i are the times at which particle entrainment events occur. These are separated by resting times $\tau = t_{i+1} - t_i$ distributed as $P(\tau) = k_E \exp(-k_E \tau)$. The s_i are step lengths distributed according to $P(s) = \ell^{-1} \exp(-s\ell^{-1})$. Fig. 1.1 panel (a) sketches the pulsed noise $\mu(t)$, and panel (b) sketches the resulting global range bedload sediment trajectories as an alternating sequence of steps and rests.

Eq. 1.1 is a phenomenological equation representing how the position of a sediment grain evolves through time (*Kubo et al.*, 1978), similar to Newtonian mechanics (*Goldstein*, 1997) but with random driving term 1.2 and involving the sediment velocity, not acceleration.

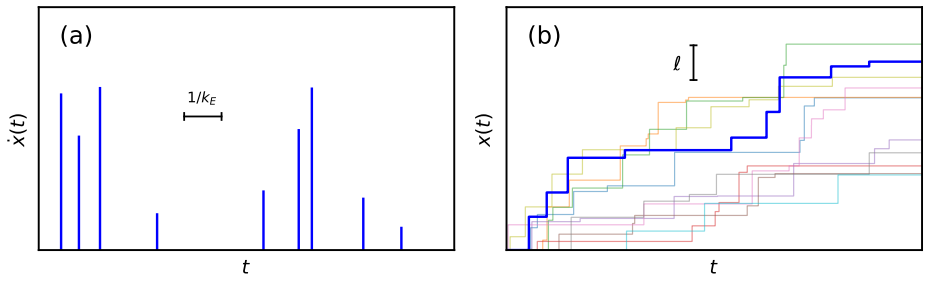

Figure 1.1: Panel (a) indicates the representation of Einstein's model as an idealized Poisson pulse noise, as indicated in Eq. 1.2, while panel (b) shows the "stair-step" trajectories of sediment particles moving downstream through cycles of steps (which are instantaneous) and rests (which have mean duration $1/k_E$).

The governing equation of the distribution $P(x,t)$ to find the particle at x can be calculated as an ensemble average of $\delta(x - x(t))$ over all possible realizations of the noise (*Moss and McClintock*, 1989; *Risken*, 1984). Different methods exist to compute such averages (*Balakrishnan*, 1993; *Hänggi*, 1978, 1984; *Van Den Broeck*, 1983), but whatever the approach, the governing equation for the distribution comes out as

$$\big(\ell\partial_x\partial_t + k_E\ell\partial_x + \partial_t\big)P(x,t) = 0. \tag{1.3}$$

This equation can be solved by standard methods (series solutions or transform calculus) (*Arfken*, 1985; *Prudnikov et al.*, 1992) to reproduce the original result of *Einstein* (1937) for the probability distribution of position of a sediment particle:

$$P(x,t) = \left[\delta(x)e^{-k_E t} + e^{-k_E t - x/\ell}\sqrt{\frac{k_E t}{\ell x}}\mathcal{I}_1\left(2\sqrt{\frac{k_E x t}{\ell}}\right)\right]\theta(x)\theta(t). \qquad (1.4)$$

Here, $\mathcal{I}_\nu$ is a modified Bessel function of order ν. The probability distribution Eq. 1.4 fully characterizes the downstream movement of an individual particle alternating randomly through steps and rests.

This distribution displays both advection and diffusion. Advection occurs because particles move downstream. Diffusion occurs because step lengths and entrainment times vary from one particle to the next.

One can calculate all moments of the position by multiplying Eq. 1.3 by x^n and integrating over space. This gives the mean position of the particle

$$\langle x(t)\rangle = k_E \ell t. \qquad (1.5)$$

This equation indicates that in Einstein's model, sediment grains move with virtual velocity $V_{\text{virt}} = k_E\ell$ given by the product of the single-particle entrainment rate k_E and mean step length ℓ.

The rate at which particles spread apart due to differences in their trajectories can be represented by the variance of position, $\sigma_x^2 = \langle x^2\rangle - \langle x\rangle^2$. This gives

$$\sigma_x^2(t) = 2k_E\ell^2 t, \qquad (1.6)$$

so particles in Einstein's model spread apart as a normal diffusion process $\sigma_x^2 = 2D_{\text{eff}}t$ (*Sokolov*, 2012), with an effective diffusivity $D_{\text{eff}} = k_E\ell^2$.

1.1.3 Inclusion of the movement duration

Einstein's model provides an adequate description of global range particle transport when the period of interest is much larger than the timescales of individual particle movements (local and intermediate ranges) and much

smaller than the timescales over which particles become embedded in sedimentary deposits (geomorphic range).

The advent of high speed camera experiments produced new insight into the local and intermediate ranges of bedload motion (*Abbott and Francis*, 1977; *Drake et al.*, 1988; *Francis*, 1973) which *Einstein* (1937) probably did not intend for his model to describe. In the local range, particles move with a fluctuating velocity due to the variable drag of the turbulent flow (*Fathel et al.*, 2015; *Lajeunesse et al.*, 2010) and changes in the particle height within the flow profile (*van Rijn*, 1984; *Wiberg and Smith*, 1985). In the intermediate range, particle-bed collisions impart additional variability to sediment velocities (*Gordon et al.*, 1972; *Martin*, 2013). Einstein's instantaneous movement assumption obscures the timescales over which these processes occur.

Studies by *Lisle et al.* (1998), and *Lajeunesse et al.* (2017) generalized the Einstein theory to include intermediate timescales. They approximated particle velocities as constant (neglecting fluctuations), and they assumed that the movement times are exponentially-distributed random variables just like resting times, but this time characterized by a deposition rate k_D, whose reciprocal is the average period of time a particle spends in motion between entrainment and deposition. The analogue of Einstein's model Eq. 1.1 with a finite movement velocity V can be written

$$\dot{x} = V\eta(t), \tag{1.7}$$

where the noise is now a "dichotomous Markov noise" (*Bena*, 2006; *Van den Broeck*, 1990), which is essentially a random switch or telegraph signal that alternates between "on" ($\eta(t) = 1$, meaning the particle is moving) and "off" ($\eta(t) = 0$, meaning the particle is resting) (*Cox and Miller*, 1965; *Horsthemke and Lefever*, 1984; *Masoliver and Weiss*, 1991; *Masoliver et al.*, 1996). This noise is displayed in Fig. 1.2 panel (a). Some particle trajectories produced by Eq. 1.7 are displayed in Fig. 1.2 panel (b).

The governing equation of the position probability distribution $P(x, t) =$

$\langle \delta(x - \int_0^t V\eta(t')dt') \rangle$ becomes (cf. *Balakrishnan*, 1993)

$$\big(\partial_t^2 + V\partial_x\partial_t + k_E V\partial_x + k\partial_t\big)P(x,t) = 0, \tag{1.8}$$

where k_E and k_D are the entrainment and deposition rates, V is the particle velocity during the motion state, and $k = k_E + k_D$. This partial differential equation is called an asymmetric telegrapher's equation (*Rossetto*, 2018), and although the symmetric analogue of this equation is well-studied (*Masoliver and Lindenberg*, 2017; *Weiss*, 2002), the asymmetric problem is not often encountered.

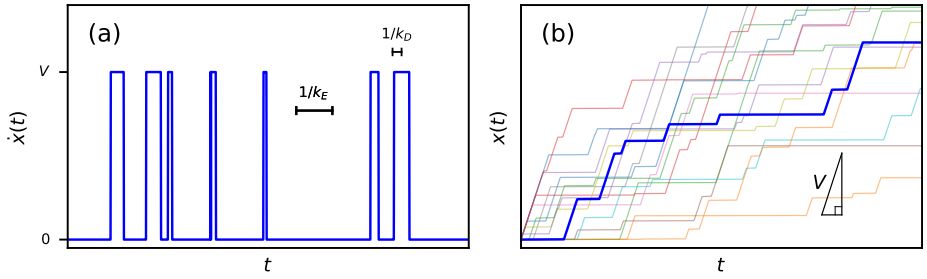

Figure 1.2: Panel (a) indicates the generalization of Einstein's model to include the interval of sediment motion between entrainment and deposition, now represented with dichotomous noise Eq. 1.7, while panel (b) shows the tilted stair-step trajectories of sediment particles moving downstream in cycles of motion at velocity V (with mean duration $1/k_D$) and rest (with mean duration $1/k_E$).

For the initial condition that particles have a probability k_E/k to start in motion, reflecting steady-state conditions as far as alternation between motion and rest are concerned (e.g. *Ancey et al.*, 2006), the solution of Eq. 1.8 is (*Lisle et al.*, 1998)

$$P(x,t) = e^{-\chi-\tau}\Big[\frac{k_E}{V}\delta(\tau) + \frac{k_E}{V}\sqrt{\frac{\chi}{\tau}}\mathcal{I}_1(2\sqrt{\chi\tau}) + \frac{k_D}{V}\mathcal{I}_0(2\sqrt{\chi\tau}) + \frac{k_E k_D}{kV}\sqrt{\frac{\tau}{\chi}}\mathcal{I}_1(2\sqrt{\chi\tau}) + \frac{k_E k_D}{kV}\delta(\chi)\Big]\theta(\chi)\theta(\tau), \tag{1.9}$$

where $\chi = k_D x/V$ and $\tau = k_E(t - x/V)$ are shorthand notations. Incorporating the duration of sediment motion, the mean position of the sediment grain remains linear in time: $\langle x(t) \rangle = k_E V t/k$, representing movement with a virtual velocity $V_{\text{virt}} = k_E V/k$, which is the fraction of time spent in motion (k_E/k) (*Ancey et al.*, 2006) multiplied by the velocity during the motion state. In contrast to the instantaneous step model, the variance now develops a two range scaling. Computing σ_x^2 provides

$$\sigma_x(t)^2 = \frac{2k_E k_D V^2}{k^3}\Big(t + \frac{1}{k}e^{-kt} - \frac{1}{k}\Big), \tag{1.10}$$

which is a non-trivial result. At short times, for $t \ll 1/k$, Eq. 1.10 shows diffusion $\sigma_x^2 \sim t^2$, which is a faster "ballistic" rate of spreading than the Einstein model predicts (*Sokolov*, 2012). At long times ($t \gg 1/k$), the diffusion becomes normal again ($\sigma_x^2 = 2D_{\text{eff}}t$), with an effective diffusion constant $D_{\text{eff}} = k_E k_D V^2/k^3$. The rapid spreading of particles at short timescales occurs because some are completely stationary while others move with velocity V.

The eventual transition to normal diffusion occurs because particles eventually become well-mixed among motion and rest states. An analogous diffusion phenomenon is described in *Taylor* (1920).

In this trajectory model, both intermediate and global ranges are adequately represented, but local and geomorphic are not, the former since fluctuations of the velocity between entrainment and deposition have been neglected, and the latter since particle burial was not incorporated.

1.1.4 The Newtonian approach

Some authors have modeled local and intermediate ranges of individual particle trajectories by writing approximate Newtonian equations for the dynamics of individual particles and integrating them numerically. Early efforts applied time-averaged fluid forces linked to a logarithmic mean flow velocity profile (*van Rijn*, 1984; *Yalin*, 1963), and later efforts included collision models to modify particle velocities upon bed contact (*Niño and García*, 1998; *Sekine and Kikkawa*, 1992; *Wiberg and Smith*, 1985).

Researchers eventually included realistic granular interactions in many-particle simulations of bedload transport using the discrete element method (e.g. *Cundall and Strack*, 1979; *Wachs*, 2019). The early works utilizing this approach used a two-dimensional domain with a simplified "slab" flow geometry (*Gotoh and Sakai*, 1997; *Jiang and Haff*, 1993), while later works included synthetic turbulence to drive particles (*Maurin et al.*, 2015; *Schmeeckle and Nelson*, 2003) or clever reduced-complexity representations of the flow (*Clark et al.*, 2015, 2017).

The state of the art within this category of sediment transport models is to simulate both fluid and particle phases simultaneously. Particle-particle interactions are represented with the discrete element method, while the fluid flow is modeled either by large eddy simulation or direct numerical simulation of the Navier-Stokes equations. A majority of these approaches simulate the fluid without including the no-slip boundary conditions on individual particles (e.g. *González et al.*, 2017; *Schmeeckle*, 2014; *Vowinckel et al.*, 2014), although some works have resolved these particle-scale fluid boundary conditions with the immersed boundary method (e.g. *Elghannay and Tafti*, 2018; *Ji et al.*, 2013, 2014; *Youse et al.*, 2020). These computational physics models produce impressive insight into the underlying granular and fluid mechanics producing bedload transport (*Frey and Church*, 2011), but analytical models are nevertheless desired for further insight into the problem.

1.1.5 Mechanistic-stochastic models for the sediment velocity distribution

One category of analytical models describes bedload particle velocities during the motion state using Langevin equations (*Ancey and Heyman*, 2014; *Fan et al.*, 2014), whereby the particle dynamics are driven by Gaussian white noise (*Kubo et al.*, 1978).

Experimental studies on bedload velocities have provided two major conclusions for the shape of the particle velocity distribution. One subset of observations shows that bedload velocities follow exponential distributions (*Fathel et al.*, 2015; *Furbish et al.*, 2012a; *Lajeunesse et al.*, 2010), and an-

other subset shows Gaussian distributions (*Ancey and Heyman*, 2014; *Heyman et al.*, 2016; *Martin et al.*, 2012).

Fan et al. (2014) set out to describe exponentially-distributed bedload particle velocities with the Langevin equation

$$\dot{u}(t) = -\Delta \mathrm{sgn}(u) + F + \sqrt{2D}\xi(t). \tag{1.11}$$

This equation drives the particle velocity u by a fluid drag $F + \sqrt{2D}\xi(t)$, where F is a constant, D is a diffusivity that characterizes the magnitude of drag fluctuations, and $\xi(t)$ is a Gaussian white noise with unit variance and vanishing mean (*Gardiner*, 1983). This drag is resisted by a heuristic Coulomb friction term $-\Delta \mathrm{sgn}(u)$, introduced as a proxy for particle-bed collisions. This model is reminiscent of Brownian motion models with Coulomb friction from the physics literature (e.g. *De Gennes*, 2005; *Menzel and Goldenfeld*, 2011; *Touchette et al.*, 2010). The equation governing the probability distribution $P(u,t)$ of the particle velocity is called a Fokker-Planck equation, and this can be derived from Eq. 1.11 as (*Risken*, 1984; *Van Kampen*, 2007)

$$\frac{\partial}{\partial t}P(u,t) = -\Delta \frac{\partial}{\partial u}\Big[\mathrm{sgn}(u)P\Big] + D\frac{\partial^2 P}{\partial u^2}, \tag{1.12}$$

implying that the steady-state velocity distribution ($\partial_t P(x,t) = 0$) provided by Eq. 1.11 is

$$P(u) = \frac{\Delta^2 - F^2}{2\Delta D} \exp\Big(-\frac{-\Delta|u| + Fu}{D}\Big). \tag{1.13}$$

This is the (two-sided) exponential distribution observed in one subset of experiments.

Ancey and Heyman (2014) formulated a different Langevin model to describe the Gaussian velocity distributions observed in the other subset of experiments. They wrote for the streamwise velocity

$$t_r \dot{u}(t) = -(U - u) + \sqrt{2D}\xi(t), \tag{1.14}$$

where U represents the mean velocity of particles, D characterizes the mag-

nitude of velocity fluctuations, and $\xi(t)$ is again a Gaussian white noise with vanishing mean and unit variance. The timescale t_r is a relaxation time over which velocity fluctuations decay. This time, the Fokker-Planck equation is

$$\frac{\partial}{\partial t}P(u,t) = -\frac{\partial}{\partial u}\Big[\frac{U-u}{t_r}P\Big] + \frac{D}{t_r^2}\frac{\partial^2 P}{\partial u^2}, \tag{1.15}$$

and the steady-state solution becomes

$$P(u) = \sqrt{\frac{t_r}{2\pi D}}\exp\Big(-\frac{t_r(u-U)^2}{2D}\Big), \tag{1.16}$$

which is the Gaussian velocity distribution from the other subset of the experiments. These two models of bedload velocity distributions are summarized in Fig. 1.3. Although these descriptions describe two end-member sediment velocity distributions, Gaussian and exponential, the underlying mechanical reason why bedload transport has shown multiple velocity distributions remains an open question, and several experiments have revealed other distributions besides exponential and Gaussian which still lack any physical description (e.g. *Houssais and Lajeunesse*, 2012; *Liu et al.*, 2019). A comprehensive model of the full range of bedload transport observations remains a desirable target.

1.1.6 The definition of the flux

Perhaps a surprising summary of bedload transport research is that no one definition of the sediment flux has been agreed upon despite over a century of research (*Ballio et al.*, 2018). Today, there are two main complementary definitions of the bedload flux being applied in stochastic modeling (but see *Ballio et al.* (2014, 2018) for other definitions).

The first definition is reminiscent of continuum mechanics and formulates the flux as a current of sediment across a control surface S (*Ballio et al.*, 2014; *Furbish et al.*, 2012a; *Heyman et al.*, 2016):

$$q = \int_S c(\mathbf{x},t)\mathbf{u}\cdot d\mathbf{S}. \tag{1.17}$$

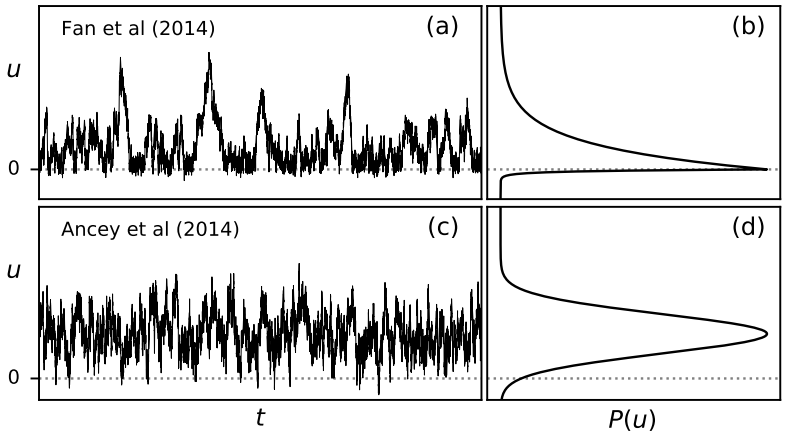

Figure 1.3: Panel (a) demonstrates the trajectory of a particle within the Fan et al. model, where Coulomb friction impedes turbulent drag. Panel (b) shows the resulting exponential particle velocity distribution, having relatively large fluctuations with mode at $u = 0$. Panel (c) shows the analogous trajectory from the Ancey et al. model, where fluctuating Stokes drag generates the Gaussian velocity distribution seen in panel (d). The latter has relatively narrow and symmetric fluctuations, with a positive mode well above $u = 0$.

This definition involves the volumetric concentration c of particles and their velocities at the instant they cross the control surface. These quantities require careful interpretation because bedload particles do not constitute a continuous field (*Furbish et al.*, 2012b). Typically one represents the concentration as a sum of indicator or Dirac delta functions (cf. *Gardiner*, 1983, Sec. 8.5.1).

The second definition formulates the downstream flux in terms of the number of particles moving within a control volume V:

$$\Phi = \frac{1}{L} \sum_{i \in V} u_i. \tag{1.18}$$

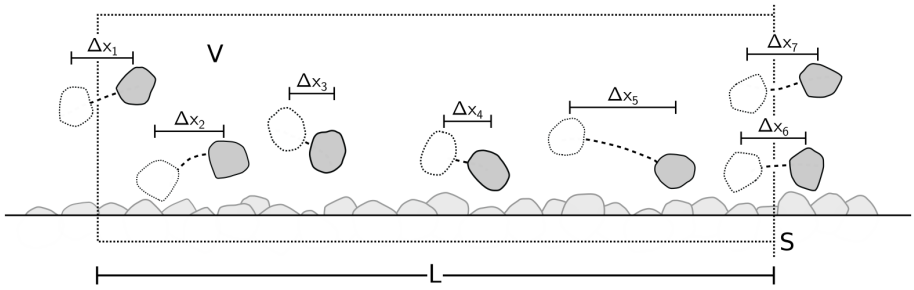

Figure 1.4: Particle fluxes can be defined with a control volume V or a control surface S. Here, particles are shown moving from time $t - \Delta t$ (faint white particles) to time t (grey particles). The downstream displacement Δx_i for each particle is indicated. These displacements define the downstream velocities $u_i \approx \Delta x_i / \Delta t$. At the instant t, the surface definition of the flux Eq. 1.17 gives $q = \frac{1}{L}(u_6 + u_7)$, while the volume definition Eq. 1.18 gives $\Phi = \frac{1}{L}(u_1 + \cdots + u_5)$, showing the non-equivalence of these two definitions.

Here, the flux is evaluated as a sum over all downstream velocities of particles within the volume (of which there are a fluctuating number), and the division by the downstream length of the control volume is incorporated to count only that proportion of particles near the downstream boundary of the volume. These two definitions, q defined with a surface and Φ defined with a volume, are generally not equivalent (*Ballio et al.*, 2014).

1.1.7 The scaling arguments of Bagnold

One of the most influential formulations of the bedload flux is due to *Bagnold* (1956, 1966), who derived a formula for the mean sediment flux using an energy balance approach. Bagnold understood sediment transport as a process which converts flow energy to heat via the effective friction (e.g. *Bagnold*, 1954) of grains against the bed as they move downstream through a succession of collisions (*Bagnold*, 1973). He assumed that the flow power P_f available to move sediment in a volume scales as $P_f \propto \tau - \tau_c$, where τ is the average bed shear stress and τ_c is the threshold shear stress at which

particles first begin to move. Considering that the average volumetric flux of particles is Φ, and particles move with mean velocity proportional to the fluid velocity near the bed, Bagnold hypothesized that the power P_g required to sustain particle motion in a volume scales as $P_g \propto \Phi/\tau^{1/2}$. Balancing flow energy against frictional dissipation ($P_f = P_g$) then provides Bagnold's sediment transport formula

$$\Phi = k(\tau - \tau_c)\tau^{1/2}, \tag{1.19}$$

which has shown good correspondence with laboratory data provided the constant factors k and τ_c are carefully calibrated.

The large shear stress limit $\Phi \sim \tau^{3/2}$ of Bagnold's formula is shared in common with many other empirical formulas describing the mean downstream flux of bedload (e.g. *Meyer-Peter and Müller*, 1948; *Parker*, 1990; *Wilcock and Crowe*, 2003; *Yalin*, 1972). A distinguishing feature of Bagnold's formula is its derivation from mechanistic reasoning, although many of Bagnold's assumptions have since turned out to be incorrect. Bagnold's assumption that the power available to move sediment scaled with the excess shear stress leads to unphysical results over arbitrarily sloping beds (*Seminara et al.*, 2002), and the flow power dissipated by sediment transport shows only a weak correlation with the sediment flux (*Ancey et al.*, 2008), while Bagnold assumed they were directly proportional. These issues are hinted at when calibrating Bagnold's formula to data, where the parameters k and τ_c take on unphysical values at low transport rates (*Niño and García*, 1996). Bagnold's formulation also faces the notorious challenge of defining the critical shear stress τ_c for the initiation of sediment transport (*Allen and Kudrolli*, 2018; *Clark et al.*, 2017; *Houssais et al.*, 2015; *Kirchner et al.*, 1990; *Pähtz et al.*, 2020; *Paintal*, 1971). The difficulties with Bagnold's approach have motivated many revisions of his theory. These are often based on more carefully incorporating the properties of individual particle motions into the sediment transport energy budget (*Engelund and Fredsoe*, 1976; *Luque and van Beek*, 1976; *Martin and Church*, 2000; *Niño and García*, 1998).

1.1.8 Einstein's probabilistic approach

Among revisions of Bagnold, one category shows a return to the probabilistic ideas of Einstein (*Ancey et al.*, 2006; *Parker et al.*, 2003). Einstein formulated his original model of individual particle trajectories in terms of entrainment and deposition rates using the idealization of grains moving downstream through a sequence of instantaneous steps (*Einstein*, 1937). Later, Einstein calculated the sediment flux with these same probabilistic ideas (*Einstein*, 1942, 1950). This formulation of the sediment flux now provides an alternative to Bagnold's scaling approach. The conceptual picture that Einstein considered is depicted in Fig. 1.5.

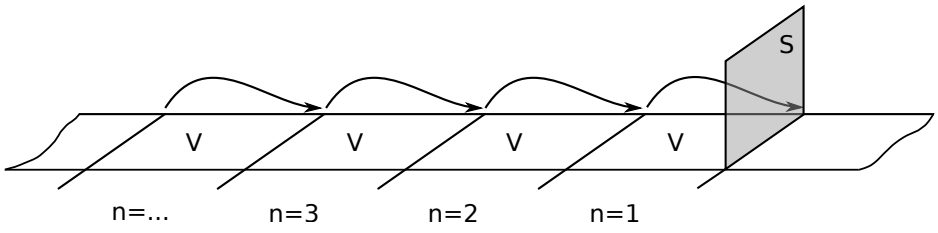

Figure 1.5: Einstein's conceptual picture, modified from *Yalin* (1972), involves an array of adjacent control volumes. Particles move in discrete jumps of length ℓ from left to right. The bedload flux is the rate of particles crossing the surface S per unit width and time, collected from all upstream control volumes.

Einstein partitioned the channel into a sequence of identical control volumes (V) and calculated the average rate at which particles cross a control surface (S) by aggregating the contributions from each upstream control volume. Each control volume has downstream length ℓ which is also the average particle step length. Denoting by P_n the probability that an individual grain undergoes at least n jumps of length ℓ in a time interval T, meaning it travels at least a distance $n\ell$, and considering that there is a density ρ of particles at rest on the bed, it follows that on average $\rho\ell P_n$ particles will displace a distance $n\ell$ or more from within each control volume during the

time interval T. As a result, since grains crossing S in a time T could have come from any upstream location, the number of grains crossing S in T is a sum over all control volumes: $\sum_{n=1}^{\infty} \rho \ell P_n$. Dividing by the time T to get the average rate of grains crossing S provides the mean flux:

$$q = \frac{\rho \ell}{T} \sum_{n=1}^{\infty} P_n. \tag{1.20}$$

The final quantity to evaluate is P_n, the probability a particle entrains *at least* n times in a time T.

Einstein originally constructed this probability by assuming that each particle had n independent entrainment opportunities in the period T, each with probability p, so that $P_n = p^n$, giving $q \propto p/(1-p)$ by a geometric series, but this approach has been criticized by *Yalin* (1972) and others (*Armanini*, 2017; *Armanini et al.*, 2015; *Cheng*, 2004; *Paintal*, 1971). Some authors have argued convincingly that instead, one should calculate P_n as an exceedance probability. The central critique is that there is a distinct difference between *exactly* and *at least* n entrainment events in T.

If the entrainment rate of an individual grain is k_E (probability per unit time), then the probability that it entrains *exactly* n times in time T, denoted by p_n (distinct from P_n) is a Poisson distribution (*Cox and Miller*, 1965):

$$p_n = \frac{(k_E T)^n}{n!} e^{-k_E T}. \tag{1.21}$$

This implies that the probability that it entrains *at least* n times is $P_n = \sum_{i=n}^{\infty} \frac{(k_E T)^i}{i!} e^{-k_E T}$, so Einstein's mean sediment flux across the control surface (Eq. 1.20) becomes

$$q = \frac{\rho \ell}{T} \sum_{n=1}^{\infty} \sum_{i=n}^{\infty} \frac{(k_E T)^i}{i!} e^{k_E T} = \frac{\rho \ell}{T} \sum_{n=1}^{\infty} n \frac{(k_E T)^n}{n!} e^{-k_E T} = \rho k_E \ell. \tag{1.22}$$

Noticing that ρk_E is the entrainment rate of a single grain multiplied by the density of grains available for entrainment on the bed, we can summarize

the Einstein theory as

$$q = E\ell, \tag{1.23}$$

where the quantity $E = \rho k_E$ is the "areal entrainment rate", representing the number of grains entrained per unit streambed area (*Furbish et al.*, 2012a; *Wilcock and McArdell*, 1997).

Einstein's formulation requires expressions of the single particle entrainment rate k_E and step length ℓ in terms of the flow and sediment characteristics. Although Einstein and many followers have attempted to formulate these connections (e.g. *Einstein*, 1950; *Grass*, 1970; *Paintal*, 1971), there are still no comprehensive solutions. Linking Einstein's entrainment and deposition rates to the grain scale mechanics remains an active area of research with many open problems (e.g. *Dey and Ali*, 2018; *Tregnaghi et al.*, 2012).

1.1.9 Fusing Einstein and Bagnold: The erosion-deposition model

One uniquely successful strategy to relate Einstein's model to flow and sediment characteristics was developed by Charru et al. (*Charru*, 2006; *Charru et al.*, 2004). This "erosion-deposition model" phrases sediment transport as a mass balance within a control volume using Einstein's entrainment rate E and the complementary deposition rate D. These rates are related to flow and sediment properties using scaling relations obtained from experiments (*Charru*, 2006; *Charru et al.*, 2004; *Lajeunesse et al.*, 2010, 2015; *Seizilles et al.*, 2014). The Charru et al. approach can be characterized as a mixture of the Einstein and Bagnold strategies for its incorporate of both probabilistic rates and scaling relations.

The erosion-deposition model is

$$\partial_t \gamma + \partial_x V\gamma = E - D. \tag{1.24}$$

In this equation, γ is the "particle activity", which is the number of moving particles per unit area (*Furbish et al.*, 2012a), V is the ensemble averaged movement velocity of sediment grains (which in unsteady conditions may

depend on space and time), E is the areal entrainment rate (the number of particles transitioning into motion per unit area and time), and D is the areal deposition rate (the number of particles coming to rest on the bed per unit area and time).

Scaling arguments provide relations for E, D, and V in terms of the fluid shear stress τ, particle size d, particle settling velocity V_s, and critical shear stress τ_c:

$$E = \alpha_1 \frac{\tau - \tau_c}{d^3 V_s}, \tag{1.25}$$

$$D = \alpha_2 \frac{\gamma V_s}{d}, \tag{1.26}$$

$$V = \alpha_3 + \alpha_4(\sqrt{\tau} - \sqrt{\tau_c}). \tag{1.27}$$

The constant coefficients α_i are calibrated in experiments.

Eq. 1.24 indicates that the mean flux in steady transport and flow conditions is the implicit solution to the equation $E = D$. Using the scaling Eqs. 1.25 and 1.27 produces the mean particle activity

$$\gamma = \frac{\alpha_1}{\alpha_2} \frac{\tau - \tau_c}{d^2 V_s^2}. \tag{1.28}$$

Expressing the mean flux as $\Phi = \gamma V$, the relationship between flux and bed shear stress becomes

$$\Phi = \frac{\alpha_1}{\alpha_2 d^2 V_s^2} \big(\tau - \tau_c\big) \big[\alpha_3 + \alpha_4(\sqrt{\tau} - \sqrt{\tau_c})\big]. \tag{1.29}$$

This recovers the Bagnold scaling $\Phi \propto \tau^{3/2}$ at large bed shear stresses.

1.1.10 The nonlocal formulation

Einstein's model of the bedload flux is inherently nonlocal in that it aggregates particle motions from all upstream locations (*Martin et al.*, 2012; *Schumer et al.*, 2009; *Tucker and Bradley*, 2010). Originally *Nakagawa and Tsujimoto* (1976) and later *Parker et al.* (2000) formalized this by writing

the sediment flux in an explicitly nonlocal form:

$$q(x,t) = \int_0^\infty dx' F(x',t) E(x-x',t). \tag{1.30}$$

In this equation, motions are considered instantaneous, and $F(x,t)$ is the probability that a particle entrained at $t = 0$ steps at least a distance x before deposition at time t.

Furbish et al. (2012a, 2017) generalized the Parker model to include a finite duration of motion. They wrote

$$q(x,t) = \int_0^\infty dx' \int_0^\infty dt' F(x',t') E(x-x',t-t'), \tag{1.31}$$

where $F(x,t)$ now represents the probability density that just-entrained particles move at least a distance x in time t before deposition. In general, this approach can handle non-uniform conditions by including space and time dependence in E and F.

For a simple example of the Furbish et al. formalism, consider that particles move with a constant velocity V and have a deposition rate k_D. Then the probability density that a particle moves *exactly* a distance x in time t is $\delta(x-Vt)k_D \exp(-k_D t)$, so the probability that it moves *at least* a distance x in t is

$$F(x,t) = \int_x^\infty \delta(x-Vt)k_D \exp(-k_D t) dx = \theta(Vt-x)k_D \exp(-k_D t). \tag{1.32}$$

Considering uniform conditions with a density ρ_s of particles available for motion on the bed surface, each having entrainment rate k_E, the areal entrainment rate can be expressed as $E = \rho_s k_E$, and Eq. 1.31 provides a mean flux

$$q = \rho_s k_E \int_0^\infty dx' \int_0^\infty dt \theta(Vt-x) k_D \exp(-k_D t) = \rho_s k_E V/k_D. \tag{1.33}$$

Since $1/k_D$ is the average time spent in motion, V/k_D is the average step length ℓ, and Eq. 1.33 provides another perspective on Einstein's central

result $q = E\ell$, but with the added ability to describe unsteady conditions (*Furbish et al.*, 2012a).

1.1.11 Channel evolution

Exner (1925) was probably the first to write a mathematical formula linking sediment transport to topographic change in a river channel. He wrote

$$(1-\phi)\frac{\partial z}{\partial t}(\mathbf{x},t) = -\nabla q(\mathbf{x},t). \tag{1.34}$$

This equation links the temporal evolution of the bed elevation z at a location $\mathbf{x} = (x, y)$ to spatial gradients in the sediment flux q. The parameter ϕ is the bed porosity.

Nakagawa and Tsujimoto (1976) and *Tsujimoto* (1978) developed an alternative statement of the Exner equation using Einstein's entrainment and deposition rates. According to their formulation, spatial gradients in the sediment flux arise due to local discrepancies in entrainment and deposition:

$$\partial_x q(x,t) = E - D. \tag{1.35}$$

In combination with Eq. 1.34, this expression of the sediment flux gradient implies the relation

$$(1-\phi)\partial_x z(x,t) = D - E \tag{1.36}$$

by which bed evolution can be described in terms of Einstein's rates. In a nonlocal framework, as in Eq. 1.31, sediment deposition can be interpreted as the eventual result of entrainment from all upstream locations, giving

$$(1-\phi)\partial_x z(x,t) = \int_0^\infty dx' \int_0^\infty dt' E(x-x', t-t')F(x',t') - E(x,t). \tag{1.37}$$

This "entrainment form of the Exner equation" (*Furbish et al.*, 2017; *Nakagawa and Tsujimoto*, 1976; *Parker et al.*, 2000) relates channel morphodynamics to a probabilistic interpretation of sediment transport.

The major limitation of these approaches are that they assume river beds are continuous. This can be justified as an average over the detailed

spatial configurations of individual bed grains (*Coleman and Nikora*, 2009). This averaging process is expected to obscure the relevant morphological evolution processes whenever individual grains are large compared to the scales of interest (e.g. *Shobe et al.*, 2021).

1.1.12 Fluctuations and scale dependence

Sediment transport rates always fluctuate (*Hoey*, 1992; *Kuhnle and Southard*, 1988; *Recking et al.*, 2012), even under the most controlled laboratory conditions available (*Ancey et al.*, 2006; *Roseberry et al.*, 2012). At short timescales, fluctuations arise from the intermittent arrivals of individual grains (*Ballio et al.*, 2018; *Böhm et al.*, 2004). At moderate timescales they emerge from waves of moving grains (*Heyman et al.*, 2014) or the episodic entrainment of clusters of grains (*Papanicolaou et al.*, 2018; *Strom et al.*, 2004). At the longest timescales, they originate from migrating bedforms (*Guala et al.*, 2014), cycles of aggradation and degradation in pools (*Dhont and Ancey*, 2018). These mechanisms generally occur in conjunction with other sources of bedload transport fluctuations like grain size sorting (*Cudden and Hoey*, 2003; *Iseya and Ikeda*, 1987), flow discharge variations (*Mao*, 2012; *Redolfi et al.*, 2018; *Wong and Parker*, 2006), and sediment supply perturbations (*Elgueta-Astaburuaga and Hassan*, 2019; *Lisle et al.*, 1993; *Madej et al.*, 2009).

Despite widespread acceptance that sediment transport rates always fluctuate, we still have relatively little understanding of how to describe these fluctuations. *Hamamori* (1962) was probably the first to calculate a probability distribution for the sediment flux, but this subject fell into relative obscurity for a long period, until it was revisited by *Nikora et al.* (1997), *Sun and Donahue* (2000), *Ancey et al.* (2006), and others.

Recognition that sediment transport rates fluctuate requires careful interpretation of sediment transport measurements. In practice, sediment transport measurements always involve time or space averaging, whether measurements are obtained by light tables (*Chartrand et al.*, 2018; *Zimmermann et al.*, 2008), impact sensors (*Mendes et al.*, 2016; *Rickenmann*

and McArdell, 2007), computer vision (*Ancey and Heyman*, 2014; *Roseberry et al.*, 2012), or sediment traps (*Bunte et al.*, 2004; *Papangelakis and Hassan*, 2016).

The averaging process in conjunction with transport fluctuations introduces scale-dependence to sediment transport measurements, whereby mean sediment transport rates (and other statistical moments) depend on the averaging timescale (*Ancey and Pascal*, 2020; *Campagnol et al.*, 2012; *Turowski*, 2010). A fundamental question raised by scale-dependence is how large averaging windows must be for sediment flux measurements to converge. To date, very few mathematical models have addressed this issue (e.g. *Ancey and Pascal*, 2020).

1.1.13 Birth-death models for bedload fluctuations

The prevalence of large bedload fluctuations motivated *Ancey et al.* (2006, 2008) to revisit Einstein's assumptions to develop a model of the bedload flux as a random process. They derived the probability distribution of the flux by counting the number of moving particles in a control volume, considering that this number changes through time as a result of particles migrating into the volume from upstream, entraining, depositing, and migrating out of the volume to downstream.

To obtain realistically-wide fluctuations in particle activity, Ancey et al. introduced a positive feedback they called "collective entrainment", whereby the entrainment rate of grains increases in proportion to the number of moving grains in the control volume (*Ancey et al.*, 2008; *Heyman et al.*, 2013).

Their governing equations are completely analogous to a stochastic population model (*Cox and Miller*, 1965; *Pielou*, 1977) where arrivals of moving particles to the volume are "births" and departures are "deaths". Ancey et al. formulated the probability distribution $P(n,t)$ of the number of moving

grains in the control volume at time t as

$$\partial_t P(n,t) = \big[\lambda + (n-1)\mu\big]P(n-1,t) \\ - [n+1]\alpha P(n+1,t) - \big[\lambda + n(\alpha+\mu)\big]P(n,t). \quad (1.38)$$

The terms on the right hand side of this equation describe respectively particle entrainment and migration in with rate λ, collective entrainment with rate μ, and deposition and migration out with rate α. The final term encodes the possibility that n stays constant for a period of time. These coupled equations (one for each $n = 0, 1, \dots$) can be solved by generating functions (*Cox and Miller*, 1965), providing the steady-state distribution

$$P(n) = \frac{\Gamma(r+n)}{\Gamma(r)n!}p^r(1-p)^n, \quad (1.39)$$

where $r = \lambda/\mu$ and $p = 1 - \mu/\alpha$. This is a negative binomial distribution, which is a wide-tailed generalization of the Poisson distribution.

From Eq. 1.39, the mean number of moving particles is

$$\langle n \rangle = \frac{\lambda}{\alpha - \mu}, \quad (1.40)$$

and the variance is

$$\sigma_n^2 = \frac{\lambda\alpha}{(\alpha-\mu)^2}. \quad (1.41)$$

Owing to the collective entrainment process, particle activity fluctuations can be arbitrarily wide: $\sigma_n^2/\langle n \rangle = \alpha/(\alpha - \mu)$, whereas in the absence of collective entrainment ($\mu = 0$), the strength of fluctuations is always pinned to a fixed value, $\sigma_n^2/\langle n \rangle = 1$, as the distribution Eq. 1.39 limits to a Poisson distribution where the mean and variance are equal (e.g. *Ancey et al.*, 2006).

Using the probability distribution of the number of moving particles Eq. 1.18, the probability distribution of the bedload flux can be computed with the control volume definition assuming that the particle velocities and the number of moving particles are independent. Writing $P_k(u)$ as the probability distribution for the sum of k independent particle velocities

$(u = u_1 + \cdots + u_k)$, the sediment flux probability distribution $P(\Phi)$ becomes (*Ancey and Pascal*, 2020)

$$P(\Phi) = L \sum_{k=0}^{\infty} P_k(L\Phi) P(n = k). \tag{1.42}$$

A limitation of this approach is that in reality, entrainment and deposition modify the bed elevation, which in turn modifies the rates of entrainment and deposition (*Sawai*, 1987; *Wong et al.*, 2007). This highlights a need to incorporate bed elevation change in statistical sediment transport models.

1.1.14 Renewal models for scale dependence

The final bedload transport model to summarize calculates the sediment flux probability distribution from an "inter-arrival time distribution" representing the statistics of times between subsequent arrivals of particles to a control surface (*Ancey*, 2020a; *Heyman et al.*, 2013; *Turowski*, 2010).

The sediment flux distribution obtained from these approaches shifts depending on the observation time T over which particle arrivals are counted, so approaches based on inter-arrival times explicitly model scale dependence. In statistics, the problem of counting probabilistic arrival events is called renewal theory (*Cox*, 1962).

Earlier studies have considered different arrival time distributions to calculate the probability distribution of the time-averaged sediment flux, but only the simplest exponential case is reviewed here. The exponential inter-arrival time distribution is $P(t) = \Lambda \exp(-\Lambda t)$, so the rate of particle arrivals is Λ. In this case, the flux observed over a period T can be represented with a Poisson pulse noise, similar to the particle position in the Einstein model reviewed in Sec. 1.1.2:

$$q(T) = \frac{1}{T} \int_0^T dt' \mu(t'). \tag{1.43}$$

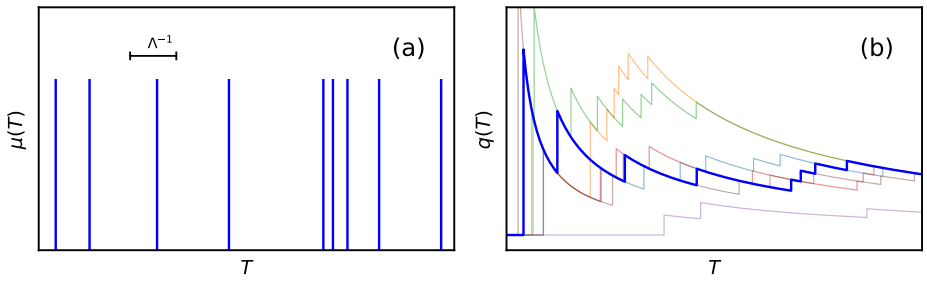

Figure 1.6: The scale-dependent sediment flux is described as a renewal process. Panel (a) indicates the arrivals of particles at rate Λ, while panel (b) shows an ensemble of realizations of the sediment flux versus the observation time T. Note that different realizations of the flux converge toward the same value at large observation times, whereas at small observation times, uncertainty in the flux is large. This is scale dependence. The properties of this convergence depend on the particle dynamics in a manner which has not yet been specified.

Here, the noise is

$$\mu(t) = \sum_{i=1}^{N(t)} \delta(t - t_i), \tag{1.44}$$

as indicated in Fig. 1.6 panel (a). In this equation, $N(t)$ is distributed as $P(N) = (\Lambda t)^N / N! \exp(-\Lambda t)$. The flux in Eq. 1.43 is a random variable as indicated in Fig. 1.6 panel (b). Its probability distribution $P(q|T)$, which is contingent on the observation time T, can be derived by evaluating $P(q|T) = \langle \delta(q - \int_0^T \mu(t')dt'/T) \rangle$. This equation entails an average over all possible realizations of the noise in Eq. 1.44, producing (*Van Kampen*, 2007)

$$P(q|T) = \sum_{l=0}^{\infty} \frac{(\Lambda T)^l}{l!} e^{-\Lambda T} \delta(q - \frac{l}{T}), \tag{1.45}$$

which is a scale-dependent Poisson distribution for the sediment flux across the control surface.

The mean flux $\langle q(T) \rangle = \int_0^\infty dq P(q|T)$ derived from this renewal scheme

becomes

$$\langle q(T) \rangle = \Lambda, \tag{1.46}$$

which is independent of the observation scale, while the magnitude of bedload transport fluctuations scales with $1/T$:

$$\sigma_q^2(T) = \frac{\Lambda^2}{T}. \tag{1.47}$$

Even this simple model gives a non-trivial conclusion that the relative uncertainty in a measurement of bedload transport depends on the observation time: $\sigma_q(T)/\langle q(T) \rangle \propto T^{-1/2}$. Our uncertainty in a sediment transport measurement diverges as the observation time becomes short.

A limitation of renewal approaches to calculate the flux is that they do not obviously relate to the dynamics of individual particles. In renewal models as they are phrased now, the inter-arrival time distribution not based on the underlying mechanics of particle transport.

1.2 Summary

This literature review has indicated that successful bedload transport descriptions have been developed to describe individual particles and bedload fluxes, although many limitations are left in need of further research attention.

All of the works reviewed so far are either mean field models that do not include fluctuations, or stochastic models that calculate probability distributions for the quantities of interest. The common thread of all of these models is that they take advantage of various devices to side step the complex interplay of turbulence and granular physics which ultimately controls bedload transport.

In the case of mean field models, the devices are heuristic scaling arguments and semi-empirical formulas, while in the case of stochastic models, they are phenomenological equations driven by idealized noises, like sequences of pulses, alternating switches, and erratic fluctuations. This thesis applies the latter methodology to many of the limitations highlighted in

the review. An outline of the problems to be addressed follows below.

1.3 Outline of the thesis

1.3.1 Problem 1: The scale-dependent flux from individual particle dynamics

The original model by *Einstein* (1937) described particle trajectories as a sequence of instantaneous steps. This model was subsequently improved to include a finite duration of motion at constant velocity (*Lajeunesse et al.*, 2017; *Lisle et al.*, 1998).

In reality, particle velocities fluctuate during movements due to turbulence and particle-bed collisions, so there is a need to go one step further and account also for the velocity fluctuations of moving particles in Einstein-type models.

In addition, although the scale-dependent sediment flux has been calculated from renewal models (*Ancey and Pascal*, 2020; *Turowski*, 2010), these approaches are not based on the dynamics of individual particles in transport, so it remains unclear how the sediment flux distribution and its scale dependence originate from the transport characteristics of individual grains.

Chapter 2 introduces a new model of individual bedload trajectories that includes velocity fluctuations in the motion state. The chapter demonstrates how these trajectories can be used to calculate the scale-dependent probability distribution of the bedload flux. This work joins together and extends studies from *Einstein* (1937) to *Ancey and Pascal* (2020) to develop new understanding of individual particle motions and the scale-dependent sediment flux.

1.3.2 Problem 2: Feedbacks between sediment transport fluctuations and bed elevation change

Birth-death models calculate the flux probability distribution assuming that entrainment and deposition do not change the local bed elevation (*Ancey and Heyman*, 2014; *Heyman et al.*, 2013), but this assumption violates con-

servation of mass.

Bed elevation changes imply sediment burial, and although sediment burial is known to affect tracer particle motions at geomorphic timescales (*Ferguson and Hoey*, 2002; *Hassan and Bradley*, 2017), our understanding of how long sediment can remain buried is limited.

Chapter 3 generalizes the model of *Ancey et al.* (2008) to include bed elevation changes in order to evaluate the effect of bed elevation change on bedload transport fluctuations and to study how the timescales of sediment burial relate to the movement characteristics of individual grains.

1.3.3 Problem 3: The effect of sediment burial on downstream transport of sediment tracers

Modeling sediment transport as an alternating sequence of motion and rest intervals implies particles are either moving or resting on the bed surface. Although this provides a useful description of bedload transport across local and intermediate timescales, it requires modification to describe longer global and geomorphic timescales. At longer timescales, particle burial moderates the downstream movements of grains (*Bradley*, 2017; *Hassan and Bradley*, 2017), yet the burial process has not been incorporated into Einstein-type models of particle trajectories.

Chapter 4 generalizes the model of *Lisle et al.* (1998) and *Lajeunesse et al.* (2017) to incorporate a new sediment burial state as suggested by the observations of *Bradley* (2017). The resulting model evaluates sediment trajectories including sediment motion, rest, and burial. This provides the first description of sediment trajectories over local, intermediate, global, and geomorphic timescales.

1.3.4 Problem 4: The control of particle-bed collisions over bedload particle velocity distributions

Finally, the Langevin models of *Fan et al.* (2014) and *Ancey and Heyman* (2014) describe the velocity distributions of sediment moving downstream in the local and intermediate ranges between entrainment and deposition.

These models produce two different end-member sediment velocity distributions, but no descriptions have yet been constructed which produce the full range of distributions observed in experiments.

Chapter 5 presents a stochastic Langevin model including episodic particle-bed collisions formulated by analogy with the theory of granular gases (*Brilliantov and Poschel*, 2004). The episodic representation improves on the static Coulomb-like friction representing collisions in earlier models. The improved model is demonstrated to describe all of the different bedload velocity distributions which have been reported in experiments.

Chapter 2

From particle dynamics to the scale-dependent flux

2.1 Introduction

A relativity weak flow shearing a bed of sediment entrains individual particles into a state of motion controlled by turbulent forcing and intermittent collisions with other grains at rest on the bed, generating wide fluctuations in the sediment velocity (*Fathel et al.*, 2015; *Heyman et al.*, 2016). Bedload particles move downstream until they are disentrained when they happen to encounter sufficiently sheltered pockets on the bed surface to interrupt their motions (*Charru et al.*, 2004; *Gordon et al.*, 1972). Eventually, the bed around them rearranges and destroys this shelter, or turbulent fluctuations overcome the shelter (*Celik et al.*, 2014; *Valyrakis et al.*, 2010), and resting particles are once again entrained. Bedload transport is thus a kind of intermittent motion, characterized by alternation between fluctuating movements and periods of rest.

To date, descriptions of bedload transport have simplified the problem in various ways to enable modeling progress. The foundational work is due to Einstein, who considered bedload motions as instantaneous so he could describe bedload transport as an alternating sequence of "steps" and rests having random length and duration (*Einstein*, 1937), in a pioneering ap-

plication of the continuous time random walk (*Montroll*, 1964). Einstein concluded that particles move downstream with a mean velocity $\langle u \rangle = k_E \ell$, where k_E is the rate at which the individual bed particle is entrained into motion, and ℓ is the mean length of each downstream step. Later, Einstein applied these ideas to calculate the mean downstream flux due to the movements of many such particles (*Einstein*, 1950). Einstein reasoned that if the density of resting particles on the bed is ρ_b, the overall areal entrainment rate of particles can be written $E = \rho_b k_E$, giving a mean sediment flux $\langle q \rangle = \rho_b \langle u \rangle = E\ell$.

Many researchers have since refined Einstein's approach to provide more realistic descriptions of individual particle motions than his instantaneous step model. One set of efforts has neglected the particle deposition process to calculate the downstream velocity distributions of moving particles using mechanistic equations with noise terms representing turbulent fluid forces and particle-bed collisions (*Ancey and Heyman*, 2014; *Fan et al.*, 2014). Another set of works have described particles alternating between motion and rest considering that motions occur with a constant velocity (*Lajeunesse et al.*, 2017; *Lisle et al.*, 1998). No models have yet been formulated which describes particles alternating between motion and rest while motions have realistic fluctuating velocities, even though this is how bedload particles actually move.

Parallel to these efforts to better describe individual particle trajectories, a complementary set of studies have roduced stochastic formulations of the sediment flux which improve on the mean field description provided by Einstein (*Ancey*, 2020a; *Furbish et al.*, 2012b; *Turowski*, 2010). Sediment fluxes generally exhibit wide fluctuations due to variations in the number of moving particles and their velocities (*Ancey et al.*, 2006; *Böhm et al.*, 2005; *Furbish et al.*, 2012b), the migration of bedforms and sediment waves (*Guala et al.*, 2014; *Recking et al.*, 2012), and a host of other processes (*Dhont and Ancey*, 2018). Because these fluctuations occur over disparate timescales, measurements of mean sediment fluxes depend on the timescale over which they are collected, a phenomenon called scale dependence (*Ancey*, 2020a; *Dhont and Ancey*, 2018; *Saletti et al.*, 2015; *Singh et al.*, 2009; *Turowski*,

2010). To date, very few models have calculated the probability distribution of the bedload sediment flux due to individual particle motions (*Ancey and Heyman*, 2014; *Ancey et al.*, 2008), and even fewer have described any observation-scale dependence of the flux (*Ancey and Pascal*, 2020; *Turowski*, 2010). Among those that do include scale dependence, none formulate the sediment flux in terms of the trajectories of individual grains.

This survey provides context for the two problems addressed in this chapter. First, we lack the capability to describe individual sediment trajectories through motion and rest including velocity fluctuations in the motion state; and second, we need more understanding of how to connect individual particle trajectories through motion and rest to the overall streamwise sediment flux, including its probability distribution and the dependence of its statistical moments on the observation time. These two problems limit our understanding of the sediment flux and undermine our ability to phrase fluvial processes like bedform initiation (e.g. *Ashley et al.*, 2021) and bedrock erosion (e.g. *Li et al.*, 2020) in terms of the dynamics of individual grains.

Here, I develop a new statistical physics-based formalism which addresses both of these problems by describing individual particle trajectories with a stochastic Langevin equation. This dynamical equation describes alternation between motion and rest at random intervals while particles in motion have velocities that fluctuate around a mean value. Using the probability distribution of particle position generated by this model, I construct a formalism to derive analytically the probability distribution of the sediment flux. This distribution exhibits observation-scale dependence as a result of velocity fluctuations among moving particles. Below, I develop the new formalism in Sec. 2.2, solve it in Sec. 2.4, and discuss the implications of these results and future research ideas in Secs. 2.5 and 2.6.

2.2 Description of motion-rest alternation with velocity fluctuations

The starting point for this analysis is an idealized one-dimensional domain, infinite in extent, populated with sediment particles on the surface of a

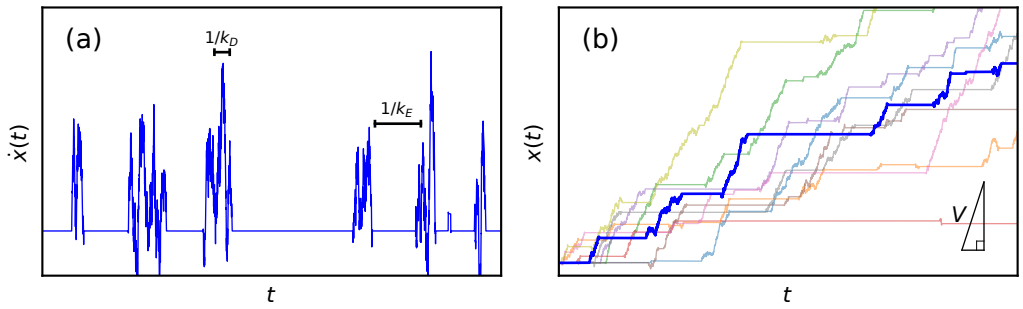

Figure 2.1: Panel (a) sketches a realization of the noise in Eq. 2.1, while panel (b) shows the trajectory derived from it (in blue) alongside other possible trajectories. Keys in panel (a) indicate the average movement time $1/k_D$ and rest time $1/k_E$, while the key in panel (b) shows the average movement velocity V. Velocity fluctuations produce tilted stair-step trajectories with unsteady slopes in the $x-t$ plane. This can be compared with Fig. 1.2 which does not include fluctuations.

sedimentary bed. Particles are set in motion by the turbulent flow and move downstream until they deposit, and the cycle repeats. The downstream coordinate is x, so that $\dot{x}$ describes a velocity in the downstream direction. The flow is considered weak enough that interactions among moving grains are very rare, although interactions between moving particles and the bed may be common, characteristic of rarefied transport conditions (e.g. *Furbish et al.*, 2017; *Kumaran*, 2006). Particles are considered to have similar enough shapes and sizes so as to have nearly identical mobility characteristics. These conditions allow for all particles to be described as independent from one another but governed by the same underlying dynamical equations.

2.2.1 Dynamical equation for grain-scale sediment transport

From these assumptions, the first target is to write an equation of motion for the individual sediment particle encompassing two features. First, particles should alternate between motion and rest. Entrainment occurs with

probability per unit time (or rate) k_E, while deposition occurs with rate k_D. Second, velocities of moving particles should jitter around a mean value V due to turbulent drag and particle-bed collisions.

The simplest equation of motion including these features is

$$\dot{x}(t) = [V + \sqrt{2D}\xi(t)]\eta(t). \tag{2.1}$$

Here, V is the mean particle velocity while D is a diffusivity [units L^2/T^3] representing the magnitude of velocity fluctuations. $\xi(t)$ is a Gaussian white noise having zero mean and unit variance which produces the velocity fluctuations. $\eta(t)$ is a dichotomous noise generating the motion-rest alternation. This noise takes on values $\eta = 1$, representing motion, and $\eta = 0$, representing rest. The transition rate from $\eta = 0$ to $\eta = 1$ is k_E, and the transition rate from $\eta = 1$ to $\eta = 0$ is k_D. Times spent in motion and rest are respectively distributed as $P(t) = k_D \exp(k_D t)$ and $P(t) = k_E \exp(k_E t)$. The notation $k = k_E + k_D$ is a shorthand used throughout this chapter.

Equation 2.1 describes the downstream movement of particles alternating through motion and rest with velocity fluctuations in the motion state. This model can be viewed as a generalization of the "flashing diffusion" models developed by Luczka and coworkers in physics (*Łuczka et al.*, 1992; *Luczka et al.*, 1993, 1995). Some trajectories produced by the Langevin equation 2.1 are sketched in Fig. 2.1. The driving term in panel (a) displays erratic fluctuations due to the assumption that velocities evolve as Gaussian white noise with no temporal correlations, but the particle trajectories in panel (b) which integrate these fluctuations are well-behaved and visually similar to those of earlier studies (cf. *Bialik et al.*, 2015; *Fan et al.*, 2016). Eq. 2.1 generalizes the constant velocity model of *Lisle et al.* (1998) and *Lajeunesse et al.* (2017) that was presented in Sec. 1.1.3, providing the first extension of these works aimed at a refined description of bedload particle trajectories through motion and rest.

2.2.2 Derivation of the master equation for the sediment position distribution

The solution of Eq. 2.1 for a given realization of the two noises $\eta(t)$ and $\xi(t)$ gives one possible trajectory of a particle. The probability distribution $P(x,t)$ that a particle which started at position $x = 0$ at time $t = 0$ has traveled to position x by time t can be formulated as an average over the ensemble of all possible trajectories.

This probability distribution of position is formed as $P(x',t) = \left\langle \delta(x' - x(t)) \right\rangle_{\eta,\xi}$, where $x(t)$ is the formal solution of Eq. 2.1 and the average is over both noises. This symbolic equation is not directly useful as taking averages over both noises is a challenging mathematical problem (e.g. *Hänggi*, 1978). This calculation is completed in the appendix Sec. A.1, providing the master equation

$$(\partial_t^2 + V\partial_x\partial_t + k_E V\partial_x + k\partial_t - D\partial_x^2\partial_t - k_E D\partial_x^2)P(x,t) = 0 \qquad (2.2)$$

for the position probability distribution. The master equation 2.2 is a diffusion-like equation governing the probability distribution of position for individual particles alternating between motion and rest, with the movement velocity considered as a fluctuating quantity.

One can see in particular that taking the entrainment rate k_E very large, meaning that particles are very often moving, implies a classical advection-diffusion equation $(\partial_t + V\partial_x - D\partial_x^2)P = 0$ for the position, characteristic of a particle moving downstream with Gaussian velocity fluctuations. Otherwise, there is a possibility that the particle comes to rest and the advection-diffusion process is interrupted, giving rise to the additional terms in Eq. 2.2 and providing an asymmetrical structure reminiscent of Eq. 1.8 from the earlier motion-rest model.

2.3 Formalism for the downstream sediment flux

The probability distribution of the sediment flux can be calculated using the probability distribution of particle position $P(x,t)$ derived as the solution of

Eq. 2.2. The method I present here is modified from the approach recently developed by Banerjee and coworkers in physics (*Banerjee et al.*, 2020). This approach generalizes the nonlocal formulation of Sec. 1.1.10 to provide the probability distribution of the flux, and it re-frames the renewal approach of Sec. 1.1.14 in terms of the mechanics of individual particles in transport.

The basic idea, as depicted in Fig. 2.2, is to initially distribute N particles in all states of motion along the domain $-L \leq x \leq 0$. Later, the number of particles N and the size L of the domain will be extended to infinity such that their ratio $\rho = N/L$ remains constant. This limit will provide a configuration similar to the one constructed in the nonlocal formation of Sec. 1.1.10.

From this initial configuration, particles move downstream through time according to Eq. 2.1. The flux is calculated as the average rate of particles crossing to the right of the control surface at $x = 0$ after the sampling time T. This time-averaged flux is

$$q(T) = \frac{1}{T} \sum_{i=1}^{N} I_i(T). \tag{2.3}$$

In this equation, the $I_i(T)$ are indicator functions which equal 1 if the ith particle has passed the control surface ($x = 0$) at the observation time T and 0 otherwise. All particles which have not crossed the control surface (or which have crossed and then crossed back) do not contribute to the flux.

The probability distribution of the flux is then the average of Eq. 2.3 across all possible initial configurations of particles and their trajectories

$$P(q|T) = \Big\langle \delta\Big(q - \frac{1}{T} \sum_{i=1}^{N} I_i(T)\Big) \Big\rangle. \tag{2.4}$$

These averages are again most easily conducted in Laplace space. Taking the Laplace transform over q (i.e. forming the characteristic function of

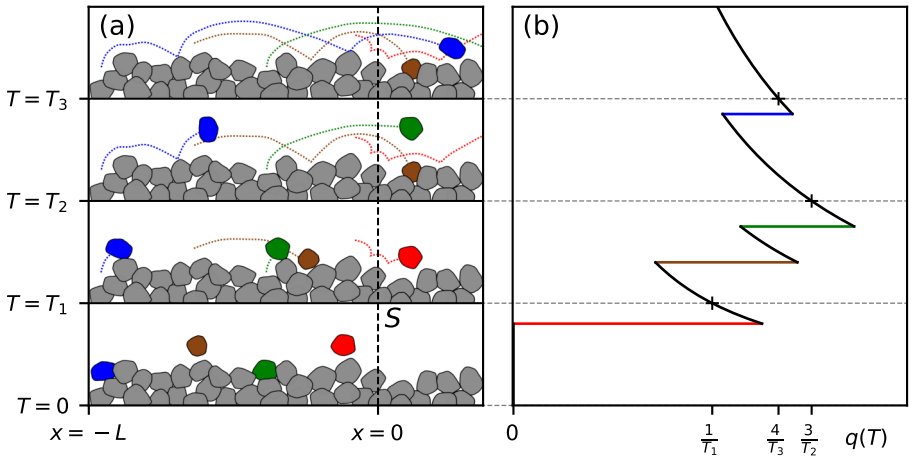

Figure 2.2: The left panel indicates the configuration for the flux. Here, the observation time increases from the bottom to the top. The particle trajectories within demonstrate alternation between rest and motion with fluctuating velocities. Particles begin their transport with positions $-L \leq x \leq 0$ at $T = 0$, and as depicted in the right panel, the flux is calculated with the number of particles $N_>(T)$ which lie to the right of $x = 0$ at the observation time T, divided by T: $q(T) = N_>(T)/T$. The probability distribution of $q(T)$ is determined from all possible realizations of the trajectories and initial positions as N and L tend to infinity while the density of particles $\rho = N/L$ to the left of the control surface is held constant.

$P(q|T)$) obtains

$$\begin{aligned}\tilde{P}(s|T) &= \Big\langle \exp\Big(\frac{s}{T}\sum_{i=1}^{N} I_i(T)\Big)\Big\rangle \\ &= \prod_{i=1}^{N}\Big\langle \exp\Big(-\frac{s}{T}I_i(T)\Big)\Big\rangle \\ &= \prod_{i=1}^{N}\Big[1-\big(1-e^{-s/T}\big)\big\langle I_i(T)\big\rangle\Big].\end{aligned} \tag{2.5}$$

This progression relies on the independence of averages for each particle (so that the average of a product is the product of averages) and the observation that $e^{aI} = 1 - (1 - e^a)I$ because I is either 0 or 1.

The average over initial conditions and possible trajectories for the ith particle involved in this characteristic function can be written

$$\langle I_i(t) \rangle = \frac{1}{L} \int_{-L}^{0} dx' \int_{0}^{\infty} dx P(x - x', t), \tag{2.6}$$

where $P(x, t)$ is the position probability distribution which solves Eq. 2.2. Eq. 2.6 describes the probability that the ith particle is found to the right of control surface by time T provided it started at a random location somewhere to the left. These $\langle I_i(t) \rangle$ are the components of the flux that depend on the particle dynamics.

Inserting Eq. 2.6 into Eq. 2.5 and taking the limits $L \to \infty$ and $N \to \infty$ as the density of particles $\rho = N/L$ remains constant, producing the configuration of the nonlocal formulation in Sec. 1.1.10, provides

$$\begin{aligned} \tilde{P}(s|T) &= \lim_{N \to \infty} \Big(1 - \frac{1}{N} \big(1 - e^{-s/T} \big) \Lambda(T) \Big)^N \\ &= \exp \Big[- \big(1 - e^{-s/T} \big) \Lambda(T) \Big]. \end{aligned} \tag{2.7}$$

where $\Lambda(T) = \rho \int_0^\infty dx \int_0^\infty dx' P(x + x', T)$ is a rate *function*, similar to the rate *constant* in the renewal process models of Sec. 1.1.14, except that it is now formulated in terms of individual particle trajectories via the probability distribution of particle position $P(x, t)$, which itself originates from the Langevin equation 2.1 governing the particle dynamics.

Eq. 2.7 is the characteristic function of a Poisson distribution (*Cox and Miller*, 1965). Expanding in $e^{-s/T}$ and inverting the Laplace transforms provides a key equation of this chapter, the probability distribution of the flux held contingent on the sampling time T:

$$P(q|T) = \sum_{l=0}^{\infty} \frac{\Lambda(T)^l}{l!} e^{-\Lambda(T)} \delta(q - \frac{l}{T}). \tag{2.8}$$

This equation implies that the mean flux is $\langle q(T) \rangle = \int_0^\infty qP(q|T)dq = \Lambda(T)/T$. Similarly the variance is $\sigma_q^2(T) = \Lambda(T)/T^2$. For the case when $\Lambda(T)$ is proportional to the observation time ($\Lambda \propto T$), these formulas become identical to the renewal theory approach reviewed in Sec. 1.1.14. This correspondence demonstrates that the renewal approach can be formulated equivalently by considering the dynamics of individual particles as a starting point.

2.4 Results

2.4.1 Position probability distribution of sediment particles

The master equation 2.2 describes the evolution of the probability distribution of position through time. The solution of this equation should be some combination of the *Einstein* (1937) model for particle transport (Sec. 1.1.2) with the Gaussian solution of the advection-diffusion equation (e.g. *Morse and Feshbach*, 1953a).

Because the master equation is second order in time, it requires initial conditions for both P and $\partial_t P$. Considering that particles start at rest in a mixture of motion and rest states, with a fraction k_E/k starting in motion and a fraction k_D/k starting in rest, these conditions derive from the initial state

$$P(x,0) = \lim_{t \to 0} \frac{k_E}{k} \sqrt{\frac{1}{4\pi D t}} \exp\Big[- \frac{(x - Vt)^2}{4Dt} \Big] + \frac{k_D}{k} \delta(x) \qquad (2.9)$$

which gives $P(x,0) = \delta(x)$ and $\partial_t P(x,0) = \frac{k_E}{k} \big[D\delta''(x) - V\delta'(x) \big]$ (cf. *Weiss*, 2002).

The master equation 2.2 is solved by transform calculus in Sec. A.2 of

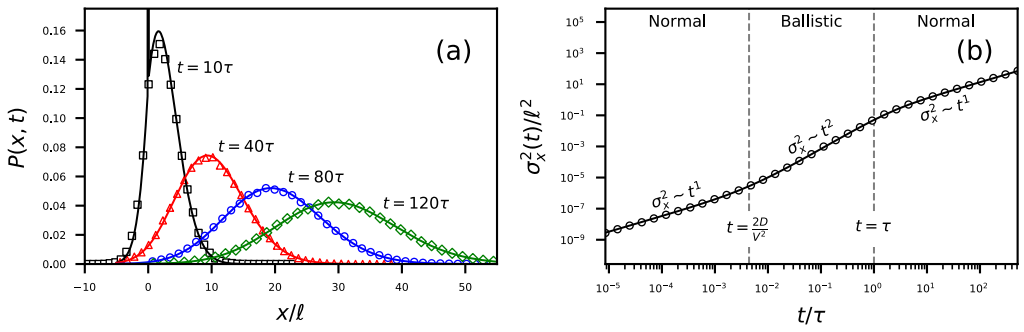

Figure 2.3: Panel (a) indicates the probability distribution of particle position 2.10 as it evolves through time. From the initial mixture of motion and rest states, particles advect downstream as they diffuse apart from one another due to differences in their velocities and transition times between motion and rest. In panel (a), the initial position persists as a delta function spike for the black $t = 10\tau$ curve. Panel (b) shows the resulting particle diffusion (Eq. 2.13). At timescales $t \ll 2D/V^2$, the diffusion is normal since the movement is approximately a standard Brownian diffusion process. For larger timescales, $2D/V^2 \ll t \ll \tau$, particles undergo ballistic diffusion similar to *Lisle et al.* (1998) as a result of some particles being stationary as others advect. Finally at times longer than the timescale $\tau = 1/k$ associated with entrainment and deposition, diffusion is again normal since particles are well-mixed among motion and rest states. All results are scaled by the mean hop length $\ell = V/k_D$ and the timescale $\tau = 1/k$ of the motion-rest alternation. In both plots, the lines are analytical results while the points are the results of Monte Carlo simulations based on evaluating cumulative transition probabilities on a small timestep (e.g. *Barik et al.*, 2006).

the appendix, providing

$$P(x,t) = \big[-\varphi D\partial_x^2 + V\varphi\partial_x + k + \delta(t) + \partial_t \big] \times \int_0^t \mathcal{I}_0\Big(2\sqrt{k_E k_D u(t-u)}\Big) e^{-k_E(t-u)-k_D u} \times \sqrt{\frac{1}{4\pi D u}} \exp\Big[-\frac{(x-Vu)^2}{4Du} \Big] du, \quad (2.10)$$

where $\varphi = k_D/k$ is the probability the particle starts at rest and $\mathcal{I}_0$ is a modified Bessel function. This equation generalizes the earlier result Eq. 1.9 for alternation between motions and rests to include velocity fluctuations within the motion state.

The distribution Eq. 2.10 is shown evolving through time in Fig. 2.3 panel (a), where the advection and diffusion characteristics of Eq. 2.2 are both evident. The integral in Eq. 2.10 encodes the earlier expectation of Einstein model-like behavior mixed with a Gaussian propagator, in that it convolves the Bessel function probability that the particle has been in motion for a period u out of a time t with the Gaussian probability that a particle has traveled a distance x in time u within the motion state. The prefactors of this integral term can be understood as adapting this distribution to the initial conditions.

2.4.2 The moments of particle position through motion-rest alternation

The moments of position produced by Eq. 2.10 could be derived by integrating it directly, but this is difficult. Instead, the moments can be calculated from the master equation 2.2 (e.g. *Cox and Miller*, 1965).

Multiplying Eq. 2.2 by x^l and integrating over all x provides

$$\partial_t^2\langle x^l\rangle - Vl\partial_t\langle x^{l-1}\rangle - k_E Vl\langle x^{l-1}\rangle + k\partial_t\langle x^l\rangle - Dl(l-1)\partial_t\langle x^{l-2}\rangle - k_E Dl(l-1)\langle x^{l-2}\rangle = 0. \quad (2.11)$$

For $l = 1$, this equation generates the mean position $\langle x\rangle(t) = k_E Vt/k$,

which is unaffected by diffusion (since Gaussian velocity fluctuations are symmetric). The case $l = 2$ provides the second moment, implying the variance of position is

$$\sigma_x(t)^2 = \frac{2k_E k_D V^2}{k^3}\Big(t + \frac{1}{k}e^{-kt} - \frac{1}{k}\Big) + 2\frac{k_E D}{k}t. \tag{2.12}$$

This equation describes a non-trivial multi-scale diffusion phenomenon, whereby the rate at which particles spread apart from one another depends on how long their dynamics have been ongoing.

Provided that $2D/V^2 \ll k_D/k^2$, series expansion of Eq. 2.12 in t and $1/t$ reveals three different scaling behaviors:

$$\sigma_x^2 \sim \begin{cases} t, & t \ll \frac{2Dk}{V^2 k_D}, \\ t^2, & \frac{2Dk}{V^2 k_D} \ll t \ll \frac{1}{k}. \\ t, & t \gg \frac{1}{k} \end{cases} \tag{2.13}$$

In the physical condition when $k \approx k_D$, which is generally satisfied for bedload transport since motions are typically short compared to rests (*Hassan et al.*, 1991; *Wu et al.*, 2019a), the above condition for existence of three ranges becomes $Pe \gg 1$, where $Pe = V^2/(2k_D D)$ is a Péclet number (e.g. *Heyman et al.*, 2014). This dimensionless number measures the relative importance of advection and diffusion to the downstream movements of particles.

The large Péclet limit ($Pe \gg 1$) is the physically-relevant condition for bedload transport, where velocity fluctuations are typically small compared to mean downstream movement velocities, so that particles rarely move upstream any appreciable distance (e.g. *Fathel et al.*, 2015). This limit also generates the three-range diffusion exemplified by Eq. 2.13, so we should expect bedload particles to spread apart with three different scaling ranges depending on how long they have been observed (cf. *Nikora et al.*, 2001a, 2002), at least within the assumptions of the model. Fig. 2.3 panel (b) sketches the predicted three-range diffusion, which is discussed further in Sec. 2.5.2.

Below, this anomalous diffusion behavior (cf. *Sokolov*, 2012) is shown to affect the rate constant $\Lambda(t)$ in the sediment flux. As a result of these multi-scale particle dynamics, the sediment flux becomes scale-dependent in a richer way than the renewal model of Sec. 1.1.14.

2.4.3 Calculation of the sediment flux

From the formalism in Sec. 2.3, the central parameter of the sediment flux distribution is the rate function

$$\Lambda(t) = \rho \int_0^\infty dx_i \int_0^\infty dx P(x + x_i, t). \tag{2.14}$$

This represents the number of particles crossing $x = 0$ at the observation time T given they started somewhere to left of $x = 0$ at $T = 0$.

Using the probability distribution of position Eq. 2.10, the integrals in Eq. 2.14 are performed in appendix Sec. A.3, providing the rate function

$$\begin{aligned}\Lambda(t) = \rho \int_0^t \mathcal{I}_0\Big(2\sqrt{k_E k_D u(t-u)}\Big) e^{-k_E(t-u)-k_D u} \\ \times \left[\sqrt{\frac{D}{\pi u}}\Big([\overleftarrow{\partial}_t + k]u - \frac{k_D}{2k}\Big)e^{-V^2 u/4D} \right. \\ \left. + \frac{V}{2}\Big([\overleftarrow{\partial}_t + k]u - \frac{k_D}{k}\Big)\,\mathrm{erfc}\left(-\sqrt{\frac{V^2 u}{4D}}\right)\right] du. \end{aligned} \tag{2.15}$$

In this equation, the notation $\overleftarrow{\partial}_t$ means that the partial time derivative acts from the left of all terms in which it is involved, as in $f(t)\overleftarrow{\partial}_t g(t) = \partial_t[f(t)g(t)]$.

This is an intricate result for the rate function in the sediment flux distribution Eq. 2.8. This mathematical complexity may not be surprising given that Eq. 2.1 involves two interacting diffusion processes. As displayed in Fig. 2.4, as a result of Eq. 2.15 the mean sediment flux takes on a non-trivial scale-dependence, characterized by a decay toward the Einstein prediction $q_0 = \rho k_E V/k \approx E\ell$ as the observation time becomes much larger than $1/(k_D Pe)$.

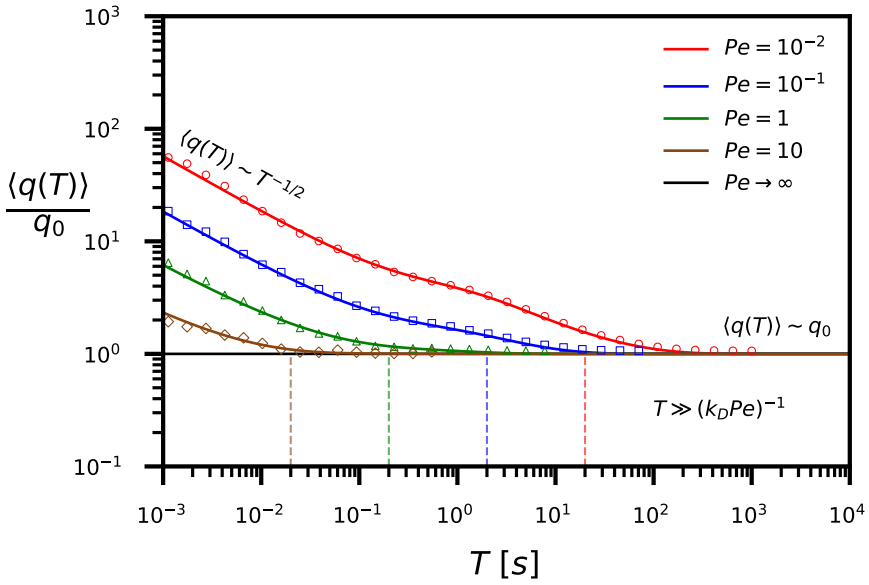

Figure 2.4: The mean sediment flux is plotted for different values of the Péclet number $Pe = V^2/(2k_D D)$, characterizing the relative significance of particle velocity fluctuations during motion. The flux is normalized by the prediction $q_0 = E\ell$ of the Einstein model (Sec. 1.1.8). For nonzero velocity fluctuations in the motion state (moderate Pe), the Einstein limit is approached as the observation time T grows. Stronger velocity fluctuations (smaller Pe) slow the convergence to this limit. In all cases, convergence of the mean flux is achieved when the observation time satisfies $T \gg 1/(k_D Pe)$, as expected by Eq. 2.16. Plotted lines are the analytical result Eq. 2.15, while the points are the results of Monte Carlo simulations. Vertical dotted lines indicate the convergence time $T = (k_D Pe)^{-1}$ for each simulation.

Further insight into the rate constant of the sediment flux distribution can be gained by investigating extreme cases of the observation time. As shown in appendix Sec. A.4, Eq. 2.15 takes on relatively simple forms at extreme values of T:

$$\Lambda(T) = \begin{cases} \frac{\rho k_E}{k}\sqrt{\frac{DT}{\pi}} & T \ll (k_D Pe)^{-1} \\ \frac{\rho k_E V T}{k} & T \gg (k_D Pe)^{-1}. \end{cases} \tag{2.16}$$

Since the mean flux is $\langle q(T)\rangle = \Lambda(T)/T$, the condition on the observation time so that the flux converges to the Einstein value $q_0 = \rho k_E V/k = E\ell$ can be expressed as $T \gg (k_D Pe)^{-1}$. It is related to the Péclet number and is proportional to the time particles spend in motion ($1/k_D$). As a result, when particle velocity fluctuations during motions become appreciable in comparision to the mean particle velocity, Eq. 2.16 indicates that the flux becomes slow to converge to the Einstein result.

2.5 Discussion

This chapter has generalized earlier descriptions of individual sediment trajectories (e.g. *Lajeunesse et al.*, 2017; *Lisle et al.*, 1998) to include velocity fluctuations in the motion state.

Using results from this generalized model as an example, I demonstrated how to calculate the sediment flux probability distribution, phrasing earlier renewal theory approaches (e.g. *Ancey*, 2020a; *Turowski*, 2010) more directly in terms of the underlying particle dynamics. This method can also be viewed as a generalization of the nonlocal formulation (Sec. 1.1.10) to describe sediment flux probability distributions, rather than just mean values.

2.5.1 Fluctuations and collective motions

The sediment flux probability distribution 2.8 represents a Poisson distribution with an observation scale-dependent rate. Poisson distributions have relatively narrow tails, meaning their fluctuations are typically small (*An-*

cey et al., 2006). In reality, sediment flux distributions are only Poissonian at high transport rates, whereas in other conditions they have wide tails representing the possibility of extremely large transport fluctuations (*Ancey et al.*, 2008; *Saletti et al.*, 2015; *Turowski*, 2010) which appear as bursts (e.g. *Goh and Barabási*, 2008) in the sediment flux timeseries (*Benavides et al.*, 2021; *Dhont and Ancey*, 2018; *Singh et al.*, 2009). This highlights a need to generalize the mechanistic description of the sediment flux I developed here to produce wider transport rate fluctuations.

Descriptions of sediment transport based on population dynamics in a control volume have produced realistically-wide fluctuations by incorporating a positive feedback between the number of moving particles and the particle entrainment rate called collective entrainment (*Ancey and Heyman*, 2014; *Ancey et al.*, 2008). This feedback generates waves of moving particles (*Ancey and Heyman*, 2014; *Heyman et al.*, 2014) and produces non-exponential inter-arrival time distributions (*Heyman et al.*, 2013) which imply wide-tailed flux distributions when incorporated in the renewal theory (e.g. *Ancey*, 2020a; *Turowski*, 2010).

Collective entrainment has been attributed to particle-particle interactions such as small granular avalanches and collision-induced entrainment (e.g. *Lee and Jerolmack*, 2018; *Pähtz et al.*, 2020), and to fluid-particle interactions, such as coherent structures entraining particles en masse as they sweep downstream (*Ancey and Heyman*, 2014; *Cameron et al.*, 2020). Given the prevalence of large coherent structures, gravel beds must often times be conditioned to them. Therefore particle-particle interactions seem more plausible as a mechanism for collective entrainment. In particular, contact forces within granular media are known to organize into "force chains", where a minority of contacts provide a majority of the strength (e.g. *Azéma and Radjaï*, 2012; *Radjai et al.*, 1996). Fluid entrainment of a key particle within a near-surface force chain could entail a collective release of the particles relying on it for stability. Likewise, collisions between moving particles and stationary particles might induce entrainment of otherwise stable surface particles.

Such particle-particle interactions would be challenging to include in a

mechanistic model for the sediment flux like I developed here, but the basic structure can be sketched. Eq. 2.1 would generalize to a stochastic Newtonian form $\ddot{x}_i(t) = F_i(x_i, \dot{x}_i, t) + \sum_{i \neq j} G_{ij}(\{x_j\}, t)$, where the F_i are the driving forces unique to each particle while the G_{ij} are some (generally stochastic) terms representing interactions between the ith and jth particles (*Goldstein*, 1997). As an approximation, this forcing structure might alternate between moving and resting modes as a dichotomous process (e.g. *Bena*, 2006).

The resulting joint distribution of particle positions and velocities – $P(x_1, v_1, \ldots, x_{N(t)}, v_{N(t)}, t)$ – might be formulated by analogy to the theory of reaction-diffusion systems (*Cardy*, 2008; *Pechenik and Levine*, 1999), granular gases (*Brilliantov and Poschel*, 2004), or other interacting particle systems available in physics literature (*Escaff et al.*, 2018; *Hernández-García and López*, 2004).

A suitable generalization of the model developed in this chapter to include particle-particle interactions should be capable of producing realistically-wide sediment transport fluctuations. Such a development will be a challenging next step for research. The present chapter only lays the groundwork.

2.5.2 Velocity correlations and bedload diffusion

Fig. 2.3 panel (b) indicates that bedload sediment particles described by the model spread apart with a rate which depends upon observation scale, transitioning through three different ranges consistent with the concept of *Nikora et al.* (2001b, 2002). Nikora et al. originally proposed that sediment diffusion would be super-diffusive at local timescales, normal at intermediate timescales, and sub-diffusive at global timescales. Here, the local range diffusion is normal, not super-diffusive, indicating a discrepancy between the Nikora et al. concept and the model of this chapter.

This discrepancy could originate from the representation of velocity fluctuations in Eq. 2.1 as Gaussian noise with a vanishing correlation time. In actuality, particle velocities are temporally correlated, and this will modify the diffusion characteristics on timescales comparable to the correlation

time. The simplest modification of Eq. 2.1 to include velocity correlations would be to replace the Gaussian white noise with an Ornstein-Uhlenbeck noise (e.g. *Hänggi and Jung*, 1995; *Łuczka*, 2005). A more challenging (but perhaps more realistic) modification would be to describe the evolution of position by a second-order equation, as in $\ddot{x} = F(x, \dot{x}, t)\eta(t)$, where F is an appropriate stochastic driving term switched on and off by the dichotomous noise $\eta(t)$ (e.g. *Masoliver*, 1993). Either of these alternatives would introduce correlations to particle velocities and modify the resulting short-range diffusion characteristics, unfortunately at the cost of mathematical difficult.

The short-timescale diffusion may also be affected by the assumption that entrainment and deposition processes are instantaneous within dichotomous noise models. *Campagnol et al.* (2015) showed from experimental data that particle "unsteadiness" during entrainment and deposition can give rise to diffusion exponents even larger than those for ballistic motion. Likely, the representation of entrainment and deposition with an instantaneous alternation obscures the local-timescale physics of these processes (e.g. *Celik et al.*, 2014; *Valyrakis et al.*, 2010). The simplest modification to include the timescales of entrainment and deposition would introduce a uniform acceleration during entrainment and deposition, in effect "tilting" the sharp motion-rest alternation of the dichotomous noise. The relatively lower velocities of particles during the acceleration phase should modify the predicted local-timescale particle diffusion characteristics, possibly producing a faster-than-ballistic spreading as proposed by *Campagnol et al.* (2015).

2.5.3 Scale-dependent fluxes and channel evolution

Fig. 2.4 indicates that the sediment flux described by Eq. 2.15 converges when $T \gg (k_D\ Pe)^{-1}$ to its eventual value $q_0 = E\ell$ predicted by the Einstein model. Because particles move for durations $1/k_D$ on average, the typical variance of velocity among moving particles can be estimated as $\sigma_V^2 = 2D/k_D$. In terms of this quantity, the convergence condition for the flux is $T \gg \sigma_V^2/(k_D V^2)$, now phrased in terms of easily measurable quantities – the velocity of particles, the average time spent in motion, and the

magnitude of velocity fluctuations.

The Exner equation of Sec. 1.1.11 used to describe channel evolution is derived by evaluating mass balance within a control volume (e.g. *Coleman and Nikora*, 2009). When the sediment flux changes values for observation scales $t < T$, as in this chapter, how the channel evolution predicted by the Exner equation is affected remains an open question. Future studies should include fluctuating and scale-dependent sediment transport rates into the Exner equation to evaluate their implications.

Presumably, the inclusion of a scale-dependent stochastic transport rate generates a stochastic bed elevation field $h(x)$, producing a probability distribution of field configurations $P(h(x), t)$ which depends on the observation scale. *Jerolmack and Mohrig* (2005) included a stochastic sediment transport rate within the Exner equation, although they only investigated particular realizations of $h(x)$, not the probability distribution of bed configurations or its scale dependence. Mathematical tools to formulate such a stochastic Exner equation might be adopted from works on surface growth and polymer physics, where the evolution of random fields is common topic of inquiry (e.g. *Barabasi and Stanley*, 1995; *Kardar*, 2007; *Kawakatsu*, 2001).

2.5.4 Collective motions

It has long been recognized that many processes lend variability to the sediment flux, including bedform migration (*Guala et al.*, 2014; *Hamamori*, 1962) and entrainment of clusters (*Papanicolaou et al.*, 2018; *Strom et al.*, 2004). Understanding these processes has been a challenging problem, in part because different sources of fluctuations mix within measured transport signals (e.g. *Dhont and Ancey*, 2018; *Hoey*, 1992; *Saletti et al.*, 2015; *Singh et al.*, 2009).

Although the present model has analyzed independent particles and does not include these processes, we can wonder if better understanding fluctuations from single-particle sources will improve our understanding of more complex collective sources. An attempt to subtract the signature of individual particle dynamics from spectra of bedload transport may be a useful

step to understand more complex morphological sources of sediment transport variability in channels. A comprehensive understanding of the linkage between individual particle dynamics and sediment fluxes, as I have worked toward here, provides the foundation for such a subtraction process.

2.6 Summary

This chapter introduced a two-noise stochastic dynamical equation to describe individual bedload trajectories for particles alternating between motion and rest states. The motion state included velocity fluctuations, providing the first analytical model of this type.

The probability distribution of the bedload sediment flux was calculated from these particle dynamics, and the resulting flux distribution was demonstrated to adopt scale-dependence from the underlying dynamics of individual particles. The observation timescales over which sediment flux observations converge were expressed in terms of the mean particle movement velocity and the typical magnitude of its fluctuations, characterized by a Péclet number.

These results generalize the bedload trajectory models of *Einstein* (1937), *Lisle et al.* (1998), and *Lajeunesse et al.* (2017) to include fluctuating movement velocities. This work also builds a particle dynamics framework underneath earlier renewal models of the sediment flux probability distribution (*Ancey*, 2020a; *Lajeunesse et al.*, 2010).

This chapter further quantifies the dependence of the sediment flux on the observation scale and provides guidance as to the measurement times required to resolve sediment transport without ambiguity, at least under the idealized assumptions for which the model was developed. The next steps are to include interactions between particles to produce wider sediment transport fluctuations and to modify the description of velocity fluctuations to include temporal correlations.

Chapter 3

Analysis of bed elevation change and sediment transport fluctuations

The transport characteristics of coarse grains moving under a turbulent flow ultimately control a wide set processes within rivers, including the export of contaminants (*Macklin et al.*, 2006; *Malmon et al.*, 2005), the success of ecological restoration efforts (*Gaeuman et al.*, 2017), and the response of channel morphology to disturbances (*Hassan and Bradley*, 2017). Although the displacements of individual grains are a mechanical consequence of forces imparted from the flow, bed, and other grains (*González et al.*, 2017; *Vowinckel et al.*, 2014; *Wiberg and Smith*, 1985), accurately characterizing these forces within natural channels is practically impossible, especially considering the intense variability these forces display (*Celik et al.*, 2010; *Dwivedi et al.*, 2011; *Schmeeckle et al.*, 2007). In response, researchers have developed a stochastic concept of bedload transport (*Einstein*, 1937), wherein the erosion and deposition of individual grains are modeled as the random results of undetermined forces (*Ancey et al.*, 2006; *Einstein*, 1950; *Paintal*, 1971).

Essentially two types of bedload transport model have been developed from this concept. The first type provides the probabilistic dynamics of a

small population of tracer grains as they transport downstream (*Einstein*, 1937; *Hubbell and Sayre*, 1964; *Lajeunesse et al.*, 2017; *Martin et al.*, 2012; *Nakagawa and Tsujimoto*, 1976; *Wu et al.*, 2019a), while the second provides the statistics of the number of moving grains ("the particle activity") within a control volume (*Ancey et al.*, 2006; *Einstein*, 1950; *Furbish et al.*, 2012b). In the first type, individual displacements are considered to result from alternate step-rest sequences, where step lengths and resting times are random variables following statistical distributions (*Einstein*, 1937). Differences between the random-walk motions of one grain and the next imply a spreading apart (i.e., diffusion) of tracer grains as they transport downstream.

Resting time distributions have been carefully studied in relation to these models because the predicted diffusion characteristics are critically dependent on whether the distribution has a light or heavy tail (*Bradley*, 2017; *Martin et al.*, 2012; *Weeks and Swinney*, 1998). Resting times have puzzled researchers because early experiments showed exponential distributions (*Einstein*, 1937; *Hubbell and Sayre*, 1964; *Nakagawa and Tsujimoto*, 1976; *Yano*, 1969; *Yano et al.*, 1969), while later experiments showed heavy-tailed power-law distributions (*Bradley*, 2017; *Liu et al.*, 2019; *Martin et al.*, 2012; *Olinde and Johnson*, 2015; *Pretzlav*, 2016; *Voepel et al.*, 2013). A predominant hypothesis is that power-law distributed resting times originate from buried grains (*Martin et al.*, 2014; *Voepel et al.*, 2013). This permits surface grains to retain exponential resting times. Conceptually, when grains rest on the surface, material transported from upstream can deposit on top of them, preventing entrainment until its removal, driving up resting times and imparting a heavy tail to the distribution.

Martin et al. (2014) have provided the only direct support for this hypothesis by tracking grains through complete cycles of burial and exhumation in a narrow flume. They observed heavy-tailed resting times of buried grains and described their results with a mathematical model similar to an earlier effort by *Voepel et al.* (2013). Both of these models treat bed elevation changes as a random walk and interpret resting times as return periods from above in the bed elevation timeseries (*Redner*, 2007). Each describes resting time distributions from different experiments, but they rely on differ-

ent random walk models, and their treatment of bed elevations as a process independent of sediment transport is questionable at first glance, since bedload transport is the source of bed elevation changes (*Wong et al.*, 2007), yet neither model explicitly describes bedload transport. Models of sedimentary bed evolution incorporating sediment transport processes might enhance understanding of sediment resting times.

The second type of stochastic model prescribes rates (probabilities per unit time) to the erosion and deposition events of individual grains within a control volume to calculate the particle activity (*Einstein*, 1950). These approaches aim at a complete statistical characterization of the bedload flux (*Fathel et al.*, 2015; *Furbish et al.*, 2012b, 2017; *Heyman et al.*, 2016), including probability distributions (*Ancey et al.*, 2006, 2008), spatial and temporal characteristics of its fluctuations (*Dhont and Ancey*, 2018; *Heyman*, 2014; *Roseberry et al.*, 2012), and the dependence of these statistical characteristics on the length and timescales over which they are observed (*Saletti et al.*, 2015; *Singh et al.*, 2009, 2012). A recent surge in research activity has generated rapid progress in this area. For example, *Ancey et al.* (2006) demonstrated that a constant erosion rate as originally proposed by *Einstein* (1950) was insufficient to develop realistically large particle activity fluctuations, so they added a positive feedback between the particle activity and erosion rate they called "collective entrainment" (*Ancey et al.*, 2008; *Heyman et al.*, 2013, 2014; *Lee and Jerolmack*, 2018). While this feedback was deemed necessary to model realistic activity fluctuations, the implications of collective entrainment for the bed topography have not been fully explored.

In this work, I present the first stochastic model coupling the erosion and deposition of individual bedload grains to local bed elevation changes. This model extends the birth-death model approach reviewed in Sec. 1.1.13 to describe the interplay between the bedload flux and the bed elevation within a control volume. This new model evaluates the effect of collective entrainment on bed elevation change, and it allows for investigations of the residence times of particles buried under the bed surface. The model has two major assumptions: First, bedload erosion and deposition are characterized

by probabilistic rates (*Ancey et al.*, 2008; *Einstein*, 1950); and second, these rates are contingent on the local bed elevation, encoding the property that erosion of sediment is emphasized from regions of exposure, while deposition is emphasized in regions of shelter (*Sawai*, 1987; *Wong et al.*, 2007).

Below, Sec. 3.1 introduces the stochastic model and Sec. 3.2 presents solutions of the model from a mixture of numerical and analytical techniques. Model solutions illustrate several new features of particle activity and bed elevation statistics that result from feedbacks between the erosion and deposition rates with bed elevation change. Sec. 3.3 present these features, while Secs. 3.4 and 3.5 conclude with the implications of these features and the suggestions they raise for future research.

3.1 Stochastic model of bedload transport and bed elevations

The model in this chapter is formulated by considering a volume of downstream length L containing some number n of moving particles in the flow and some number m of stationary particles composing the bed at time t, as depicted in Fig. 3.1. The value m is defined relative to the mean number of grains within the control volume, so that it can be either positive or negative. n is always a positive integer including 0.

All particles are considered approximately spherical with the same radius a, so their mobility and packing characteristics are similar. Following *Ancey et al.* (2008), basically four events can occur at any instant to modify the populations n and m. These events are (1) migration of a moving particle into the volume from upstream ($n \to n+1$), (2) the entrainment (erosion) of a stationary particle into motion within the volume ($m \to m-1$ and $n \to n+1$), (3) the deposition of a moving particle to rest within the volume ($m \to m+1$ and $n \to n-1$), and (4) the migration of a moving particle out of the volume to downstream ($n \to n-1$). The four events are depicted as arrows in Fig. 3.1. As the events occur at random intervals, they set up a joint stochastic evolution of the populations n and m characterized by a joint probability distribution $P(n, m, t)$ for the number of particles in

motion and rest in the volume at t.

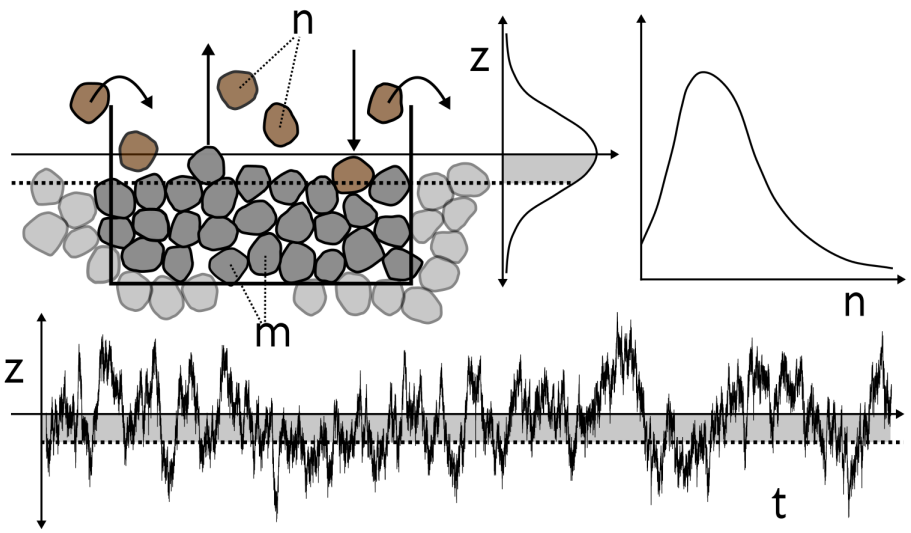

Figure 3.1: Definition sketch of a control volume containing n moving grains and m resting grains. Migration, entrainment, and deposition are represented by arrows, and the instantaneous bed elevation is depicted by dotted lines. The bed is displayed in a degraded state where $m < 0$. The marginal distributions of n and m are indicated in the upper right panel, while the bottom panel is a realized timeseries of bed elevations computed from m using Eq. 3.1.

The populations n and m provide the volumetric bedload flux Φ and the local bed elevation z. The mean transport rate is given by $\Phi = u_s\langle n\rangle/L$, where u_s is the characteristic velocity of moving bedload and $\langle n\rangle = \sum_{n,m} nP(n,m)$ is the mean number of grains in motion (*Ancey et al.*, 2008; *Charru et al.*, 2004; *Furbish et al.*, 2012b). The bed elevation is related to m through the packing geometry of the bed. This relationship depends on the packing fraction ϕ of grains in the bed (*Bennett*, 1972). Considering the bed as two-dimensional (*Einstein*, 1950; *Paintal*, 1971), the deviation

from the mean bed elevation can be expressed as

$$z(m) = \frac{\pi a^2}{\phi L} m = z_1 m. \tag{3.1}$$

The constant $z_1 = \pi a^2/(\phi L)$ is an important scale in the problem. z_1 is the magnitude of bed elevation change in an average sense across the control volume associated with the addition or removal of a single grain.

Bed elevation changes modify the likelihood of entrainment and deposition in a negative feedback (*Sawai*, 1987; *Wong et al.*, 2007). Aggradation increases the likelihood of entrainment, while degradation increases the likelihood of deposition. *Wong et al.* (2007) concluded that bed elevation changes induce an exponential variation in entrainment and deposition probabilities, while *Sawai* (1987) concluded that the variation is linear. For simplicity, this chapter utilizes the scaling of *Sawai* (1987). This scaling is equivalent to the *Wong et al.* (2007) scaling when bed elevation changes are small. Because experimental distributions of bed elevations are often symmetrical (e.g. *Crickmore and Lean*, 1962; *Martin et al.*, 2014; *Pender et al.*, 2001; *Wong et al.*, 2007), the erosion and deposition feedbacks are considered to have the same strength. As bed elevation changes drive up (down) erosion rates, so they drive down (up) deposition rates to the same degree.

Merging these ideas with those of *Ancey et al.* (2008) produces expressions for the four possible transitions with local bed elevation-dependent entrainment and deposition rates:

$$R_{MI}(n+1|n) = \nu \qquad \text{migration in,} \tag{3.2}$$

$$R_E(n+1, m-1|n, m) = (\lambda + \mu n)[1 + \kappa m], \qquad \text{entrainment,} \tag{3.3}$$

$$R_D(n-1, m+1|n, m) = \sigma n[1 - \kappa m], \qquad \text{deposition.} \tag{3.4}$$

$$R_{MO}(n-1|n) = \gamma n \qquad \text{migration out.} \tag{3.5}$$

In Eqs. 3.3 and 3.4, κ is a coupling constant between bed elevations and the entrainment and deposition rates. In terms of κ I will later demonstrate the

relationship

$$\kappa \approx \left(\frac{z_1}{2l}\right)^2 \tag{3.6}$$

where l is a characteristic length scale of bed elevation change that can be interpreted as the active layer depth (*Church and Haschenburger*, 2017; *Wong et al.*, 2007). In the rate equations 3.2-3.5, ν is the rate of migration into the control volume, λ is the conventional entrainment rate, μ is the collective entrainment rate, σ is the deposition rate, and γ is the rate of migration out of the control volume. At $m = 0$, these equations reduce to those of the *Ancey et al.* (2008) model. Away from this elevation, entrainment and deposition are alternatively suppressed or enhanced depending on the sign of m, constituting a feedback between bed elevations and entrainment and deposition.

All four rates are independent of the past history of the populations and depend only on the current populations (n, m). As a result, the model is Markovian (*Cox and Miller*, 1965; *Van Kampen*, 2007), meaning time intervals between any two subsequent transitions are exponentially distributed (*Gillespie*, 2007).

The master equation for the probability flow can be written using the Kolmogorov equation $\partial P(n,m;t)/\partial t = \sum_{n',m'}[R(n,m|n',m')P(n',m';t) - R(n',m'|n,m)P(n,m;t)]$ (*Ancey et al.*, 2008; *Cox and Miller*, 1965; *Gillespie*, 1992) as

$$\begin{aligned}\frac{\partial P}{\partial t}(n,m;t) = \nu P(n-1,m;t) + [\lambda(m+1)+\mu(n-1)][1+\kappa(m+1)]P(n-1,m+1;t) \\ + \sigma(n+1)[1-\kappa(m-1)]P(n+1,m-1;t) + \gamma(n+1)P(n+1,m;t) \\ - \{\nu + \lambda + \mu n(1+\kappa m) + \sigma n(1-\kappa m) + \gamma n\}P(n,m;t). \end{aligned} \tag{3.7}$$

The joint distribution $P(n, m; t)$ that solves this equation fully characterizes the statistics of n and m – proxies for the bedload flux and local bed elevation.

The average entrainment and deposition rates E and D over all bed elevations are $E = \lambda + \mu\langle n\rangle$ and $D = \sigma\langle n\rangle$. The solutions of Eq. 3.7 are expected to adjust from whatever initial conditions toward a steady-

state distribution $P_s(n, m)$ – independent of time – if the constant factors in the transition rates are representative of equilibrium transport conditions. Equilibrium requires $E = D$, meaning there is no net change in elevation, and $\nu = \gamma\langle n\rangle$, meaning mass is conserved in the control volume (inflow = outflow). This master equation describes a two-species stochastic birth-death model (*Cox and Miller*, 1965) of a type well known in population ecology (*Pielou*, 1977; *Swift*, 2002) and chemical physics (*Gardiner*, 1983). In context of this chapter, the two populations are the moving and stationary grains in the control volume.

3.2 Model solutions

Unfortunately, Eq. 3.7 does not admit an analytical solution unless $\kappa = 0$ (but see *Swift* (2002) for the generating function method which fails in this case). The difficulty originates from the product terms between n and m representing the bed elevation dependence of collective entrainment and deposition rates.

Because the model is Markovian, it is nevertheless possible to numerically simulate Eq. 3.7 with the Gillespie algorithm (*Gillespie*, 1977, 1992, 2007). In conditions when the coupling constant κ between the entrainment/deposition rates and the bed elevation is weak, it is also possible to solve the master equation approximately with mean field and Fokker-Planck approaches (*Gardiner*, 1983; *Haken*, 1978). The Gillespie simulation algorithm is described below in Sec. 3.2.1, while these analytical approximations are described in Sec. 3.2.2.

3.2.1 Numerical study of the joint model

The Gillespie algorithm takes advantage of the defining property of a Markov process: when transition rates are independent of history, time intervals between transitions are exponentially distributed (*Cox and Miller*, 1965).

As a result, to step the Markov process through a single transition, one can draw a first random value from the exponential distribution of transition intervals to determine the time of the next transition, then draw a second

flow	ν	λ	μ	σ	γ
(a)	5.45	6.59	3.74	4.67	0.77
(g)	7.74	8.42	4.34	4.95	0.56
(i)	15.56	22.07	3.56	4.52	0.68
(l)	15.52	14.64	4.32	4.77	0.48

Table 3.1: Migration, entrainment, and deposition rates at $z(m) = 0$ are tabulated from *Ancey et al.* (2008). Units are s^{-1} (probability/time). Bed elevation changes modulate these rates in accord with Eqs. 3.2-3.5.

random value to choose the type of transition that occurs using relative probabilities formed from Eqs. 3.2-3.5. The transition is enacted by shifting t, n, and m by the appropriate values to the type of transition (that is, entrainment is $m \to m - 1$ and $n \to n + 1$, and so on). This procedure can be iterated to form an exact realization of the stochastic process (*Gillespie*, 2007). The appendix Secs. B.1-B.1.3 provide additional background on the stochastic simulation method.

Using this method, I simulated 4 transport conditions with 13 different values of l taken across a range from $l = a$ (a single radius) to $l = 10a$ (10 radii). These values include the range exhibited by the available experimental data on bed elevation timeseries (*Martin et al.*, 2014; *Singh et al.*, 2009; *Wong et al.*, 2007).

For the migration, entrainment, and deposition parameters representing bedload transport at each flow condition $(\nu, \lambda, \mu, \sigma, \gamma)$, I used the values measured by *Ancey et al.* (2008) in a series of flume experiments: these are summarized in Tab. 3.1. Flow conditions are labeled (a), (g), (i), and (l), roughly in order of increasing bedload flux (see *Ancey et al.* (2008) for more details). In all simulations, I took the packing fraction $\phi = 0.6$ – a typical value for a pile of spheres (e.g. *Bennett*, 1972), and I set $L = 22.5$cm and $a = 0.3$cm, values from the original *Ancey et al.* (2008) experiments. Each simulation was run for 250hrs of virtual time, a period selected to ensure convergence of particle activity and bed elevation statistics.

3.2.2 Approximate solutions of the joint model

The n and m dynamics in Eq. 3.7 can be approximately decoupled using the inequality $l \gg z_1$ (equivalently $\kappa \ll 1$) which holds for large values of the active layer depth l. These inequalities imply that many individual entrainment or deposition events are required for an appreciable change in the entrainment and deposition rates. Concentrating on steady-state conditions $\partial P/\partial t = 0$, one can introduce the exact decomposition $P(n,m) = A(n|m)M(m)$ to Eq. 3.7, with the new distributions normalized as $\sum_m M(m) = 1$ and $\sum_n A(n|m) = 1$ (e.g. *Haken*, 1978). This provides the steady-state equation

$$\begin{aligned} 0 = \nu A(n-1|m)M(m) + [\lambda+\mu(n-1)][1+\kappa(m+1)]A(n-1|m+1)M(m+1) \\ +\sigma(n+1)[1-\kappa(m-1)]A(n+1,m-1)M(m-1) + \gamma(n+1)A(n+1|m)M(m) \\ -\{\nu + [\lambda+\mu n](1+\kappa m) + \sigma n(1-\kappa m) + \gamma n\}A(n,m)M(m). \quad (3.8) \end{aligned}$$

Summing this equation over n provides a still exact description of the distribution of bed elevations $M(m)$ in terms of the conditional mean particle activity $\langle n|m\rangle = \sum_n nA(n|m)$:

$$\begin{aligned} 0 = [\lambda + \mu\langle n|m+1\rangle][1+\kappa(m+1)]M(m+1) \\ +\sigma\langle n|m-1\rangle[1-\kappa(m-1)]M(m-1) \\ -\{[\lambda+\mu\langle n|m\rangle](1+\kappa m) + \sigma\langle n|m\rangle(1-\kappa m)\}M(m). \quad (3.9) \end{aligned}$$

Unfortunately, these two equations are no easier to solve than the original master equation, since the amount of coupling between n and m is not reduced in Eq. 3.8.

The simplest approximation to these equations holds that κ is so small that the dynamics of n are totally independent of m: $A(n|m) = A(n)$. Taking this limit in Eq. 3.8, summing over m, and using $\langle m\rangle = 0$ reproduces the *Ancey et al.* (2008) particle activity model. As shown in Sec. 1.1.13,

this has the solution

$$A(n) = \frac{\Gamma(r+n)}{\Gamma(r)n!}p^r(1-p)^n. \tag{3.10}$$

which is a negative binomial distribution for the particle activity with parameters $r = (\nu+\lambda)/\mu$ and $p = 1-\mu/(\sigma+\gamma)$. This result implies $\langle n|m\rangle = \langle n\rangle$, so with the definitions of E and D and the equilibrium condition $E = D$, Eq. 3.9 provides

$$0 \approx [1+\kappa(m+1)]M(m+1) + [1-\kappa(m-1)]M(m-1) - 2M(m). \tag{3.11}$$

This mean field equation matches the discrete Ornstein-Uhlenbeck model of bed elevation changes developed by *Martin et al.* (2014). The independent bed elevation and particle activity models of *Martin et al.* (2014) and *Ancey et al.* (2008) derive from the model Eq. 3.7 in a mean field approximation when κ is insignificant.

In the appendix Sec. B.2.2 I show that the Fokker-Planck approximation (*Gardiner*, 1983) formed by expanding $M(m \pm 1)$ to second order in m within Eq. 3.11 provides the solution $M(m) \propto \exp(-\kappa m^2)$: this is a normal distribution of bed elevations with variance $\sigma_m^2 \propto \frac{1}{2\kappa}$. As I will demonstrate in Sec. 3.3, and as I have already suggested with Eq. (3.6), this is a poor approximation to the bed elevation variance. Nevertheless, this approximation does capture the Gaussian shape of the bed elevation distribution. The essential issue with this mean field approach is that in actuality, the conditional mean particle activity $\langle n|m\rangle$ varies significantly with m, especially when collective entrainment contributes to the mean entrainment rate E.

A more careful approximate solution to Eq. 3.9 can be obtained by prescribing a phenomenological equation for $\langle n|m\rangle$ into Eq. 3.9 in order to close the equation for m without solving Eq. 3.8. As explained in appendix Sec. B.2.3, comparison with the numerical simulations determines that the relationship

$$\langle n|m\rangle \approx \langle n\rangle\Big(1 - \frac{2\kappa m}{1-\mu/\sigma}\Big) \tag{3.12}$$

captures the general features of the conditional mean particle activity. In-

troducing this closure relation to Eq. 3.9, making the Fokker-Planck approximation, and neglecting terms of $O(\kappa^2)$ provides

$$M(m) \approx \sqrt{\frac{2\kappa}{\pi}} e^{-2\kappa m^2}, \tag{3.13}$$

representing a Gaussian distribution with variance $\sigma_m^2 = \frac{1}{4\kappa}$ – smaller than the former mean field theory by a factor of two and in agreement with the result of Eq. 3.6. This closure equation approach shows good correspondence with numerical solutions of Eq. 3.7, at least for the flow parameters in Tab. 3.1.

3.3 Results

From the initial conditions, all simulations show a rapid attainment of steady-state stochastic dynamics of n and m which support a time-independent joint distribution $P(n, m)$. The bottom panel of Fig. 3.1 shows an example elevation timeseries. In order to describe the implications of coupling bedload transport to bed elevation changes, the numerical and analytical results for the probability distributions of bedload transport and bed elevations are presented in Sec. 3.3.1 and the statistical moments of these quantities are presented in Sec. 3.3.2. The effects of collective entrainment on bed elevation changes are studied in Sec. 3.3.3, and the resting times of sediment undergoing burial are evaluated in Sec. 3.3.4.

3.3.1 Probability distributions of bedload transport and bed elevations

The joint distribution is computed numerically by counting occurrences of the states (n, m) in the simulated timeseries. From this joint distribution the marginal distributions $P(n)$ and $P(m)$ are obtained by summing over m and n respectively. A representative subset of these marginal distributions is displayed in Fig. 3.2 alongside the approximate results of Eqs. 3.10 and 3.13. The mean field equation 3.10 for the particle activity n closely represents the numerical results, and while there are small differences between numerical

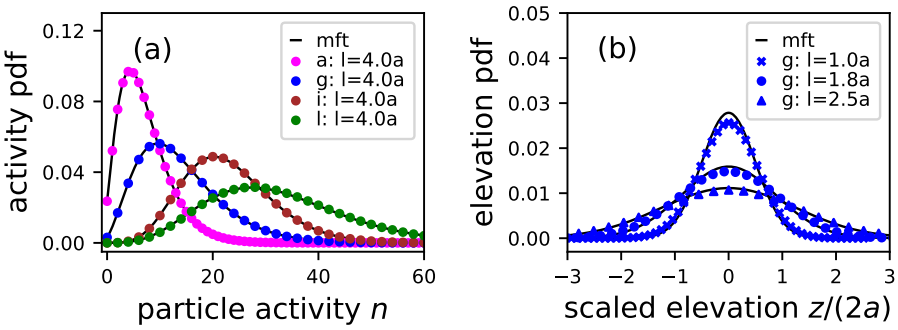

Figure 3.2: Panel (a) presents the probability distribution of particle activity n and panel (b) presents the probability distribution of the relative number of particles m for a representative subset of simulations. These distributions represent different flows from Tab. 3.1, distinguished by color, and different values of the active layer depth l (equivalently the coupling constant κ), distinguished by the marker style. The mean field theories (mft) of Eqs. 3.10 and 3.13 are displayed as solid black lines.

and analytical results for the relative number m of resting particles, the numerical solutions approximately match Eq. 3.13, having Gaussian profiles consistent with the assumption of a symmetric scaling between erosion and deposition rates and bed elevation changes.

3.3.2 Statistical moments of bed elevation and the particle activity

The moments of n and m are calculated by summing over $P(n, m)$. The jth order unconditional moment of the particle activity n is defined as

$$\langle n^j \rangle = \sum_n n^j P(n), \tag{3.14}$$

while the jth order moment of n held conditional on m is

$$\langle n^j | m \rangle = \sum_n n^j P(n, m). \tag{3.15}$$

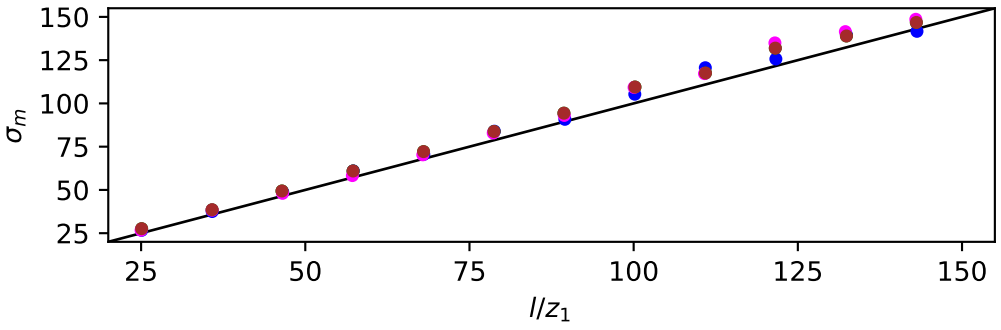

Figure 3.3: Data from all simulations demonstrates that the active layer depth l characterizes bed elevation changes as described by Eq. 3.6: $\sigma_m^2 \approx (l/z_1)^2$.

The moments of m show no dependence on the value of n. The mean elevation is always $\langle m \rangle = 0$ due to the initial assumption of symmetry in the entrainment and deposition rate scaling with m.

Fig. 3.3 demonstrates that the variance of bed elevations is approximately $\sigma_z^2 = z_1^2 \sigma_m^2 = \frac{1}{4\kappa} = l^2$, agreeing with the approximation in Eq. 3.13; this result indicates that l is a characteristic length scale of bed elevation fluctuations. The close correspondence between the mean field approximation and the numerical simulations in Fig. 3.2 panel (a) suggests the unconditional moments of n correspond closely with the *Ancey et al.* (2008) result. They appear identical within numerical uncertainty.

The coupling between bed elevation changes and the erosion and deposition rates develop a strong dependence of the particle activity on m. Fig. 3.4 displays the mean shift $[\langle n|m \rangle - \langle n \rangle]/\langle n \rangle$ and the variance shift $[\mathrm{var}(n|m) - \mathrm{var}(n)]/\mathrm{var}(n)$ of the particle activity due to departures of the bed elevation from its mean position. Fig. 3.4 panel (a) demonstrates that the flow conditions in Tab. 3.1 support departures of the mean particle activity by as much as 60% from the overall mean value when the bed is in a degraded state $z \approx -3l$, and the activity can be decreased by 20% when the bed is in an aggraded state. The closure model 3.12 used to derive the approximate bed elevation distribution 3.13 is plotted behind the conditional

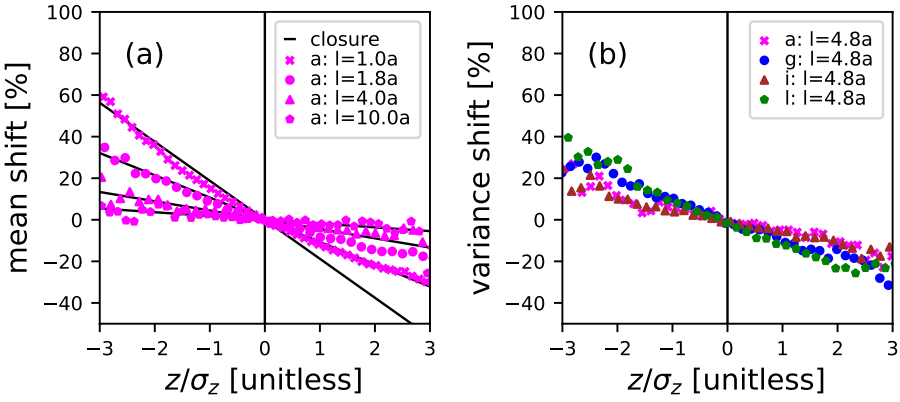

Figure 3.4: The particle activity moments conditioned on instantaneous bed elevations shift from their over-all mean values. Panel (a) indicates the mean particle activity shift versus the bed elevation measured in units of $\sigma_z = l$. This shift displays asymmetric dependence on m at the flow conditions of the *Ancey et al.* (2008) experiments, and departures of the bedload transport mean can be as much as 60% when the bed is in a severely degraded state with $z \approx -3l$. The closure equation 3.12 is plotted in panel (a). Panel (b) demonstrates a more symmetrical variance shift with some dependence on flow conditions displaying variations of up to 20% with bed elevation changes. These results indicate that bedload statistics measurements on short timescales could be severely biased by departures from the mean bed elevation.

mean profiles in Fig. 3.4 panel (a), where it appears as a crude approximation since it does not capture the asymmetry. Nevertheless, Fig. 3.3 demonstrates the variance $1/(4\kappa)$ derived from this closure equation is representative of the numerical relationship. For the parameters of the *Ancey et al.* (2008) experiments, Fig. 3.4 panel (b) displays a variance shift with bed elevation changes that is less severe than the mean shift but is nevertheless appreciable, with bed elevations changing the magnitude of bedload activity fluctuations by as much as 20%. These results indicate that bed elevation changes regulate the first and second particle activity moments,

with a moment suppression effect when the bed is aggraded, and a moment enhancement effect when the bed is degraded.

3.3.3 Collective entrainment and bedload activity fluctuations

Noting that bed elevations affect the particle activity moments, the next step is to study the influence of collective entrainment on this effect by modifying the relative proportion of the individual to collective contributions in the mean entrainment rate $E = \lambda + \sigma\langle n \rangle$. The equilibrium condition $E = D$ implies that the fraction of entrainment due to the collective process is $f = \mu\langle n \rangle / E = \mu/\sigma$. This fraction can be used to hold E constant and modify the prevalence of the collective entrainment process by setting $\lambda = E(1 - f)$ and $\mu = \sigma f$. Interpolating f between zero and one interpolates the particle activity component of the master equation 3.7 from a purely Poissonian model to a negative binomial model, isolating the effect of collective entrainment on the particle activity statistics over a dynamic sedimentary bed. Fig. 3.5 depicts the modification of the particle activity mean and variance as the importance of collective entrainment is tuned (through λ and μ) with all other parameters fixed. When $f = 0$, the bed elevation ceases to influence the particle activity mean or variance, while larger fractions increasingly enable the moment regulation effect identified in Sec. 3.3.2.

3.3.4 Resting times of sediment undergoing burial

Resting times for sediment undergoing burial are obtained from analyzing the return times from above in the timeseries of m (e.g. *Redner*, 2007). Following *Voepel et al.* (2013) and *Martin et al.* (2014), I concentrate on a particular bed elevation m', and find all time intervals separating deposition events at $m = m'$ from erosion events at $m = m' + 1$. These are the return times from above of the sedimentary bed conditional to the elevation m'. Binning these conditional return times (using logarithmically-spaced bins to reduce computational load) and counting the occurrences in each bin

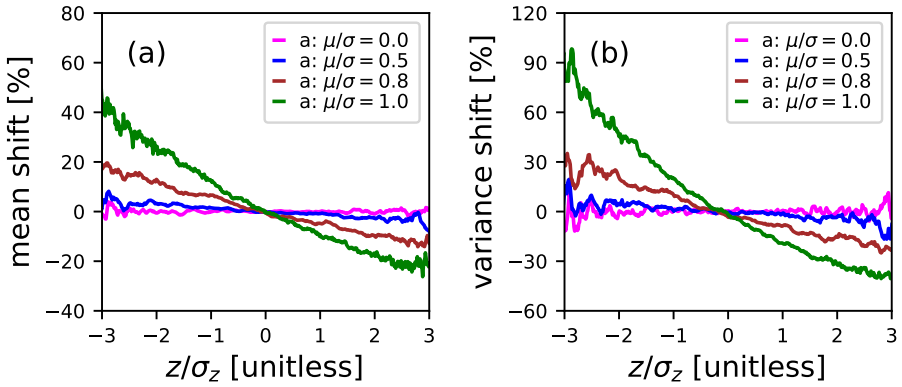

Figure 3.5: Panel (a) displays the shift of the mean particle activity with departures of the bed elevation from its mean value, while panel (b) displays the shift of the particle activity fluctuations. All simulations are conducted with flow condition (g) from Tab. 3.1, except that λ and μ are modified to shift the fraction $f = \mu/\sigma$ of the over-all entrainment rate E due to collective entrainment. Collective entrainment drives strong departures of the bedload statistics away from the mean field model (Eq. 3.10) at large departures from the mean bed elevation. Panel (b) shows particle activity fluctuations suppressed by 90% when $z \approx -3l$ and collective entrainment is the dominant process. When collective entrainment is absent, meaning $\mu/\sigma = 0$, this moment regulation effect vanishes, as it is a consequence of collective entrainment.

obtains the exceedance distribution of return times t_r held conditional to the elevation m': $P(T > t_r|m')$. The marginal probability distribution of bed elevations $P(m)$ displayed in Fig. 3.2 panel (b) derives the unconditional exceedance distribution of resting times as a sum over all elevations (*Martin et al.*, 2014; *Nakagawa and Tsujimoto*, 1980; *Voepel et al.*, 2013; *Yang and Sayre*, 1971):

$$P(T > t_r) = \sum_{m'} P(m')P(T > t_r|m'). \tag{3.16}$$

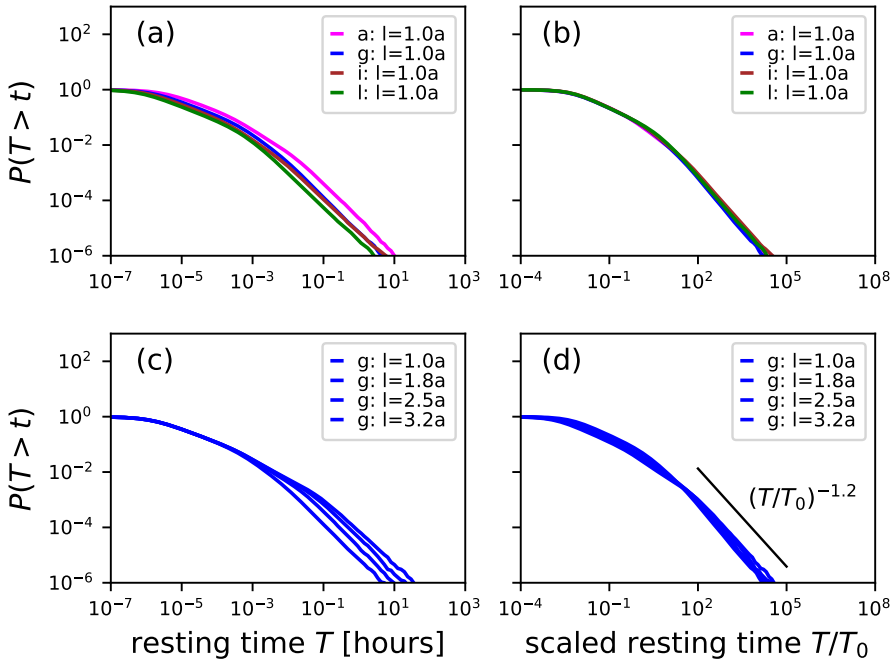

Figure 3.6: Resting time statistics scale differently with transport conditions and the bed elevation variance. Panel (a) shows different flow conditions at a fixed l value, while panel (c) shows fixed flow conditions at different l. When scaled by T_0 (Eq. 3.17), both types of difference collapse in the tails of the distributions, as shown in panels (b) and (d), where the black dotted lines indicate a power law decay of the collapsed tails having parameter $\alpha \approx 1.18$.

Fig. 3.6 displays a representative subset of these results. Comparing panels (a) and (c) in this figure shows two separate variations with input parameters: first, the distributions vary with the flow conditions, and second, they vary with the standard deviation of bed elevations (l). However, as shown in panels (b) and (d), a characteristic timescale T_0 is found to collapse away both variations. This T_0 can be obtained heuristically by considering the characteristic speed of bed elevation change. Because the mean number of

grains leaving the bed per unit time is E and the removal of a single grain changes the bed elevation by z_1 (Eq. 3.1), bed elevations change with a characteristic speed $v = z_1 E$. Since the range of elevation deviations is l (Fig. 3.3), the time required for the bed to shift through this characteristic distance is l/v, or equivalently

$$T_0 = \frac{l}{z_1 E}. \tag{3.17}$$

Scaling the resting time by this T_0 obtains the collapse shown in Fig. 3.6. Using the log-likelihood estimation technique described by *Newman* (2005), the scaled resting time non-exceedance distributions are estimated to decay as a heavy tailed power law with parameter $\alpha = 1.18 \pm 0.32$ for all return times satisfying $T/T_0 > 10^3$. These distributions are sufficiently heavy tailed to violate the central limit theorem and drive anomalous super-diffusion of bedload, a result which supports the earlier conclusions of *Voepel et al.* (2013) and *Martin et al.* (2014).

3.4 Discussion

3.4.1 Context of the research

Einstein developed the first stochastic models of bedload tracer diffusion (*Einstein*, 1937) and the bedload flux (*Einstein*, 1950), and his ideas can be viewed as the nexus of an entire paradigm of research that extends into the present day (e.g. *Ancey et al.*, 2008; *Hassan et al.*, 1991; *Hubbell and Sayre*, 1964; *Nakagawa and Tsujimoto*, 1976; *Wu et al.*, 2019a). These approaches aim to predict bedload transport characteristics from stochastic concepts of individual particle motions. With some exceptions (*Nakagawa and Tsujimoto*, 1980; *Pelosi et al.*, 2016; *Wu et al.*, 2019a,b; *Yang and Sayre*, 1971), existing descriptions are spatially one-dimensional, concentrating on the motion of grains in the downstream direction without including the vertical dimension wherein local bed elevation changes imply sediment burial (*Martin et al.*, 2014; *Voepel et al.*, 2013) and change the mobility of surface

grains (*Nakagawa and Tsujimoto*, 1980; *Yang and Sayre*, 1971).

3.4.2 New contributions

This chapter has modified the birth-death approach to describe sediment transport in a control volume. This model was applied to study the interplay between bedload transport and bed elevation fluctuations and to investigate resting time distributions of sediment undergoing burial. This model is the first description of bedload transport and bed elevations as a coupled stochastic population model based on individual grains. Numerical solutions and analytical approximations provided negative binomial distributions of bedload activity and normal distributions of bed elevations. Although experiments under more natural conditions with segregation processes, migrating bedforms, or sediment supply perturbations have shown particle activity distributions with heavier tails (*Dhont and Ancey*, 2018; *Saletti et al.*, 2015) and non-Gaussian bed elevations (*Aberle and Nikora*, 2006; *Singh et al.*, 2012), the results of this chapter reproduce the key features of the most controlled bed elevation (*Martin et al.*, 2014; *Wong et al.*, 2007) and bedload transport (*Ancey et al.*, 2008; *Heyman et al.*, 2016) experiments.

The inclusion of coupling between the bed elevation and entrainment and deposition rates revealed a novel dependence of particle activity on bed elevation changes, highlighting a new consequence of the collective entrainment process (*Ancey et al.*, 2008; *Lee and Jerolmack*, 2018). This coupling develops a significant variation of the particle activity moments with deviations of the bed from its mean elevation. These particle activity variations with bed elevation changes disappear in the absence of collective entrainment.

Finally, the model allowed resolution of resting times for sediment undergoing burial within the sedimentary bed. These timescales were obtained by analyzing return times from above in the bed elevation timeseries. This analysis produces heavy-tailed power-law resting times with tail parameters sufficient to drive anomalous diffusion of bedload at long timescales. The power-law tails were found to collapse across flow conditions using a

timescale formed from the mean erosion rate and the active layer depth.

As the model in this chapter builds on earlier works describing particle activity and bed elevation changes independently, it also reduces to these works in simplified limits when the coupling between the particle activity and the local bed elevation vanishes. With the mean field approach in Sec. 3.2.2, the *Martin et al.* (2014) Ornstein-Uhlenbeck model for bed elevations and the *Ancey et al.* (2008) birth-death model for the particle activity were derived as simplified limits of the coupled model developed in this chapter. While the mean field description of bed elevations over-predicts the bed elevation variance by approximately a factor of two, it does capture the Gaussian shape of the bed elevation distribution, and its conclusions on the tail characteristics of resting time distributions for sediment undergoing burial are identical to the model in this chapter within the numerical uncertainty. *Martin et al.* (2014) described a power-law distribution with tail parameter $\alpha \approx 1$ which falls neatly within the estimation $\alpha = 1.18 \pm 0.32$ presented here.

3.4.3 Next steps for research

The model presented in this chapter computes statistical characteristics of the bedload particle activity and bed elevation within a control volume by assuming all particles on the bed surface have similar mobility characteristics while sediment transport and bed topography are in equilibrium. In actuality, particles span a range of sizes, and spatial organization occurs both in the forces imparted to particles by the flow (*Amir et al.*, 2014; *Shih et al.*, 2017) and in the mobility characteristics of particles on the bed surface (*Charru et al.*, 2004; *Hassan et al.*, 2008; *Nelson et al.*, 2014). Together, these factors may generate spatial correlations in particle activities that models concentrating on a single control volume will be unable to capture. Models chaining multiple control volumes together have shown spatial correlations in the particle activity as a result of collective entrainment (*Ancey et al.*, 2015; *Heyman et al.*, 2014), and similar approaches have also been applied to study correlations in turbulent flows (*Gardiner*, 1983). In light

of this work, the model presented in this chapter is considered a preliminary step toward a multiple-cell model of particle activities and bed elevation changes with potential to express spatial correlations between longitudinal profile and particle activity statistics.

Like the theory developed by *Martin et al.* (2014), the model 3.7 produces heavy-tailed power-law resting times for sediment undergoing burial by treating bed elevation changes as an unbounded random walk with a mean reverting tendency. This result suggests sediment burial can explain the heavy-tailed rests seen in field data (*Bradley*, 2017; *Olinde and Johnson*, 2015; *Pretzlav*, 2016). The resting time distributions derived in Sec. 3.3.4 show a divergent variance and possibly a divergent mean, since this occurs for $\alpha < 1$ (*Sornette*, 2006) which is within range of the results.

Divergent mean resting time distributions present a paradox, since they imply all particles should eventually be immobile, violating the equilibrium transport assumption. *Voepel et al.* (2013) demonstrated that a bounded random walk for bed elevations provides a power-law distribution that eventually transitions to a faster thin-tailed decay, allowing for power-law scaling like the result in this chapter and *Martin et al.* (2014) without this divergent mean paradox. One resolution to this issue could come from a spatially distributed model with multiple cells. Neighboring locations might bound excessive local elevation changes through granular relaxations from gradients above the angle of repose. In this interpretation, divergent mean power law resting time distributions may be relics of single cell models for bed elevation changes. We should always expect a maximum depth to which the bed can degrade relative to neighboring locations; this could temper the power law tail without required the reflecting boundaries used by *Voepel et al.* (2013).

Finally, this chapter presented the probability distribution functions and first and second moments of the particle activity and bed elevation, indicating novel coordination between the statistical characteristics of these quantities which deserve experimental testing. Some relatively recent particle tracking experiments have demonstrated joint resolution of bed elevations and bedload transport (*Heyman et al.*, 2016; *Martin et al.*, 2014). A suitably

designed experiment using this methodology could test the prediction that bed elevations regulate particle activity statistics, as essentially represented in Figs. 3.4 and 3.5.

Many other statistical characteristics of bedload transport have been left for future studies. For example, the dependence of bedload transport (*Saletti et al.*, 2015; *Singh et al.*, 2009) and bed elevation statistics (*Aberle and Nikora*, 2006; *Singh et al.*, 2009, 2012) on the spatial and temporal scales over which they are observed is an emerging research topic which was previously referenced in Sec. 1.1.14. Whether bed elevation distributions are also scale-dependent like the sediment flux distribution of Ch. 2 is an interesting question for future research.

3.5 Summary

This chapter presented a stochastic model for particle activity and local bed elevations including feedbacks between elevation changes and sediment transport. This model includes collective entrainment, whereby moving particles tend to destabilize stationary ones. The model was analyzed using a mixture of numerical and analytical methods, and two key results were presented:

1. Resting times for sediment undergoing burial lie on a heavy-tailed power law distributions with tail parameter $\alpha \approx 1.2$;

2. Collective entrainment generates a statistical regulation effect, whereby bed elevation changes modify the mean and variance of the particle activity by as much as 90%: this effect vanishes when collective entrainment is absent.

These results imply measurements of bedload transport statistics could be biased at observation timescales smaller than adjustments of the bed elevation timeseries when collective entrainment occurs. The next step is to generalize the model in this chapter to a multi-cell framework to study channel morphodynamics in a stochastic framework.

Chapter 4

Burial-induced three-range diffusion in sediment transport

Many environmental problems including channel morphology (*Hassan and Bradley*, 2017), contaminant transport (*Macklin et al.*, 2006), and aquatic habitat restoration (*Gaeuman et al.*, 2017) rely on our ability to predict the diffusion characteristics of coarse sediment tracers in river channels. Diffusion is quantified by the time dependence of the positional variance σ_x^2 of a group of tracers. With the scaling $\sigma_x^2 \propto t$, the diffusion is said to be normal, since this is found in the classic problems (*Einstein*, 1905). However, with the scaling $\sigma_x^2 \propto t^\gamma$ with $\gamma \neq 1$, the diffusion is said to be anomalous (*Sokolov*, 2012), with $\gamma > 1$ defining super-diffusion and $\gamma < 1$ defining sub-diffusion (*Metzler and Klafter*, 2000). *Einstein* (1937) developed one of the earliest models of bedload diffusion to describe a series of flume experiments (*Ettema and Mutel*, 2004). Interpreting individual bedload trajectories as a sequence of random steps and rests, Einstein originally concluded that a group of bedload tracers undergoes normal diffusion.

More recently, Nikora et al. realized coarse sediment tracers can show either normal or anomalous diffusion depending on the length of time they have been tracked (*Nikora et al.*, 2001b, 2002). From numerical simulations

and experimental data, Nikora et al. discerned "at least three" scaling ranges $\sigma_x^2 \propto t^\gamma$ as the observation time increased. They associated the first range with "local" timescales less than the interval between subsequent collisions of moving grains with the bed, the second with "intermediate" timescales less than the interval between successive resting periods of grains, and the third with "global" timescales composed of many intermediate timescales. Nikora et al. proposed super-diffusion in the local range, anomalous or normal diffusion in the intermediate range, and sub-diffusion in the global range. They attributed these ranges to "differences in the physical processes which govern the local, intermediate, and global trajectories" of grains (*Nikora et al.*, 2001b), and they called for a physically based model to explain the diffusion characteristics (*Nikora et al.*, 2002).

Experiments support the Nikora et al. conclusion of multiple scaling ranges (*Fathel et al.*, 2016; *Martin et al.*, 2012), but they do not provide consensus on the expected number of ranges or their scaling properties. This lack of consensus probably stems from resolution issues. For example, experiments have tracked only moving grains, resolving the local range (*Fathel et al.*, 2016; *Furbish et al.*, 2012a, 2017); grains resting on the bed surface between movements, resolving the intermediate range (*Einstein*, 1937; *Nakagawa and Tsujimoto*, 1976; *Yano*, 1969); grains either moving or resting on the bed surface, likely resolving local and intermediate ranges (*Martin et al.*, 2012); or grains resting on the surface after floods, likely resolving the global range (*Bradley*, 2017; *Phillips et al.*, 2013). At long timescales, a significant fraction of tracers become buried under the bed surface (*Ferguson et al.*, 2002; *Haschenburger*, 2013; *Hassan et al.*, 1991, 2013; *Papangelakis and Hassan*, 2016), meaning burial dominates long term diffusion characteristics (*Bradley*, 2017; *Martin et al.*, 2014; *Voepel et al.*, 2013), possibly at global or even longer "geomorphic" timescales (*Hassan and Bradley*, 2017) than Nikora et al. originally considered. As a result, three diffusion ranges can be identified by patching together multiple datasets (*Nikora et al.*, 2002; *Zhang et al.*, 2012), but they are not resolved by any one dataset.

Newtonian bedload trajectory models also show multiple diffusion ranges, although they also do not provide consensus on the expected number of

ranges or their scaling properties. The majority of these models predict two ranges of diffusion (local and intermediate) without predicting a global range. Among these, *Nikora et al.* (2001b) used synthetic turbulence (*Kraichnan*, 1970) with a discrete element method for the granular phase (*Cundall and Strack*, 1979); *Bialik et al.* (2012) used synthetic turbulence with a random collision model (*Sekine and Kikkawa*, 1992); and *Fan et al.* (2016) used a Langevin equation with probabilistic rests. To my knowledge, only *Bialik et al.* (2015) have claimed to capture all three ranges from a Newtonian approach. They incorporated a second resting mechanism into their earlier model (*Bialik et al.*, 2012), implicitly suggesting that three diffusion ranges could result from two distinct timescales of sediment rest. However, Newtonian approaches have not evaluated the effect of sediment burial on tracer diffusion, probably due to the long simulation timescales required.

Random walk bedload diffusion models constructed in the spirit of *Einstein* (1937) provide an alternative to the Newtonian approach and can include a second timescale of rest by incorporating sediment burial. Einstein originally modeled bedload trajectories as instantaneous steps interrupted by durations of rest lying on statistical distributions (*Hassan et al.*, 1991), but this generates only one range of normal diffusion (*Einstein*, 1937; *Hubbell and Sayre*, 1964; *Nakagawa and Tsujimoto*, 1976). Recently, researchers have generalized Einstein's model in a few different ways to describe multiple diffusion ranges. *Lisle et al.* (1998) and *Lajeunesse et al.* (2017) promoted Einstein's instantaneous steps to motion intervals with random durations and a constant velocity, providing two diffusion ranges – local and intermediate. *Wu et al.* (2019a) retained Einstein's instantaneous steps but included the possibility that grains can become permanently buried as they rest on the bed, also providing two diffusion ranges – intermediate and global. These earlier works suggest the minimal required components to model three bedload diffusion ranges are (1) exchange between motion and rest intervals and (2) the sediment burial process.

In this study, I incorporate these two components into Einstein's original approach to describe three diffusion ranges with a physically based model, as called for by *Nikora et al.* (2002). Einstein was a giant in river geophysics

and fostered an entire paradigm of research leveraging and generalizing his stochastic methods (*Gordon et al.*, 1972; *Hubbell and Sayre*, 1964; *Nakagawa and Tsujimoto*, 1976; *Paintal*, 1971; *Yang and Sayre*, 1971; *Yano*, 1969). Einstein's model can be viewed as a pioneering application of the continuous time random walk (CTRW) developed by *Montroll* (1964) in condensed matter physics to describe the diffusion of charge carriers in solids. To incorporate motion intervals and sediment burial, I utilize the multi-state CTRW formalism developed by *Weiss* (1976, 1994) that extends the CTRW of *Montroll* (1964). Below, I develop and solve the model in Sec. 4.1. Then, I discuss the predictions of this model, present its implications for local, intermediate, and global ranges of bedload diffusion, and suggest next steps for bedload diffusion research in Secs. 4.2 and 4.3.

4.1 Bedload trajectories as a multi-state random walk

4.1.1 Assumptions of the burial model

Particle trajectories are formulated as a three-state random walk where the states are motion, surface rest, and burial. These states are labeled as $i = 2$ (motion), $i = 1$ (rest), and $i = 0$ (burial). The target is the probability distribution $p(x, t)$ to find a grain at position x and time t if it is known to have started with the initial distribution $p(x, 0) = \delta(x)$. Times spent moving or resting on the surface are characterized by exponential distributions $\psi_M(t) = k_2 e^{-k_2 t}$ and $\psi_1(t) = k_1 e^{-k_1 t}$, since numerous experiments show thin-tailed distributions for these quantities (*Ancey et al.*, 2006; *Einstein*, 1937; *Fathel et al.*, 2015; *Martin et al.*, 2012; *Roseberry et al.*, 2012). The end results will not be contingent on the specific distributions chosen, since all thin-tailed distributions provide similar diffusion characteristics in random walks (*Weeks and Swinney*, 1998; *Weiss*, 1994). Grains in motion are considered to have a characteristic velocity v (*Lajeunesse et al.*, 2017; *Lisle et al.*, 1998), and burial is modeled as long lasting enough to be effectively permanent (*Wu et al.*, 2019a), with grains resting on the surface having

a probability per unit time κ to become buried. This means $\Phi(t) = e^{-\kappa t}$ represents the probability that a grain is not buried after resting for a time t, while $1 - \Phi(t)$ represents the probability that it is buried. The initial conditions are specified with probabilities θ_1 and θ_2 to be in rest or motion at $t = 0$. Normalization requires $\theta_1 + \theta_2 = 1$.

4.1.2 Governing equations

With these assumptions, the governing equations for the set of probabilities $\omega_{ij}(x,t)$ that a transition occurs from state i to state j at position x and time t can be derived using the statistical physics approach to multi-state random walks (*Schmidt et al.*, 2007; *Weeks and Swinney*, 1998; *Weiss*, 1994). Denoting by $g_{ij}(x,t)$ the probability for a particle to move a distance x in a time t within the state i before it transitions to the state j, the transition probabilities $\omega_{ij}(x,t)$ sum over all possible paths to the state i from previous locations and times:

$$\omega_{ij}(x,t) = \theta_i g_{ij}(x,t) + \sum_{k=0}^{2} \int_0^x dx' \int_0^t dt' \omega_{ki}(x',t') g_{ij}(x-x', t-t'). \quad (4.1)$$

Defining another set of probabilities $G_i(x,t)$ that a particle moves by a distance x in a time t within the state i and possibly remains within the state, a similar sums over paths for the probabilities to be in the state i at x, t produces:

$$p_i(x,t) = \theta_i G_i(x,t) + \sum_{k=0}^{2} \int_0^x dx' \int_0^t dt' \omega_{ki}(x',t') G_i(x-x', t-t'). \quad (4.2)$$

Finally, the overall probability to be at position x at time t is

$$p(x,t) = \sum_{k=0}^{2} p_k(x,t). \quad (4.3)$$

This joint density is completely determined from the solutions of Eqs. 4.1 and 4.2 given specification of the distributions g_{ij} and G_i.

4.1.3 Probability distribution of particle position with burial

These distributions can be constructed from the assumptions described in Sec. 4.1.1. Since particles resting on the bed surface become buried in a time t with probability $\Phi(t)$, and resting times are distributed as $\psi_1(t)$, these assumptions obtain $g_{12}(x,t) = \delta(x)k_1e^{-k_1t}e^{-\kappa t}$ and $g_{10}(x,t) = \delta(x)k_1e^{-k_1t}(1-e^{-\kappa t})$. Since motions have velocity v for times distributed as $\psi_2(t)$, the assumptions provide $g_{21}(x,t) = \delta(x-vt)k_2e^{-k_2t}$. Since burial is quasi-permanent, all other $g_{ij} = 0$. The G_i are constructed in the same way except using the cumulative probabilities $\int_t^\infty dt'\psi_i(t) = e^{-k_it}$, since these characterize motions and rests that are ongoing (*Weiss*, 1994). Using the cumulative probabilities provides $G_1(x,t) = \delta(x)e^{-k_1t}$ and $G_2(x,t) = \delta(x-vt)e^{-k_2t}$.

Eqs. 4.1 and 4.2 with these g_{ij} and G_i are solved using Laplace transforms in space and time ($x,t \to \eta,s$). This method, similar to *Weeks and Swinney* (1998), unravels the convolution structure of these equations, eventually producing

$$\tilde{p}(\eta,s) = \frac{1}{s}\frac{(s+\kappa+k')s + \theta_1(s+\kappa)\eta v + \kappa k_2}{(s+\kappa+k_1)\eta v + (s+\kappa+k')s + \kappa k_2}, \tag{4.4}$$

where $k' = k_1 + k_2$. As explained in appendix Sec. C.1, inverting this result using known Laplace transforms (*Arfken*, 1985; *Prudnikov et al.*, 1992) obtains

$$\begin{aligned} p(x,t) = \theta_1\Big[1 - \frac{k_1}{\kappa+k_1}\Big(1-e^{-(\kappa+k_1)t}\Big)\Big]\delta(x) \\ + \frac{1}{v}e^{-\Omega\tau-\xi}\Big(\theta_1\Big[k_1\mathcal{I}_0\big(2\sqrt{\xi\tau}\big) + k_2\sqrt{\frac{\tau}{\xi}}\mathcal{I}_1\big(2\sqrt{\xi\tau}\big)\Big] \\ + \theta_2\Big[k_1\delta(\tau) + k_2\mathcal{I}_0\big(2\sqrt{\xi\tau}\big) + k_1\sqrt{\frac{\xi}{\tau}}\mathcal{I}_1\big(2\sqrt{\xi\tau}\big)\Big]\Big) \\ + \frac{1}{v}\frac{\kappa k_2}{\kappa+k_1}e^{-\kappa\xi/(\kappa+k_1)}\Big[(\theta_1/\Omega)\mathcal{Q}_2(\xi/\Omega,\Omega\tau) + \theta_2\mathcal{Q}_1(\xi/\Omega,\Omega\tau)\Big] \end{aligned} \tag{4.5}$$

for the joint distribution that a tracer is found at position x at time t. This

result generalizes the earlier results of *Lisle et al.* (1998) and *Einstein* (1937) to include sediment burial. This equation uses the shorthand notations $\xi = k_2 x/v$, $\tau = k_1(t - x/v)$, and $\Omega = (\kappa + k_1)/k_1$ (cf. *Lisle et al.*, 1998). The $\mathcal{I}_\nu$ are modified Bessel functions of the first kind and the $\mathcal{Q}_\mu$ are generalized Marcum Q-functions defined by $\mathcal{Q}_\mu(x, y) = \int_0^y e^{-z-x}(z/x)^{(\mu-1)/2}\mathcal{I}_{\mu-1}(2\sqrt{xz})dz$ and originally devised for radar detection theory (*Marcum*, 1960; *Temme*, 1996). The Marcum Q-functions derive from the burial process. Because resting grains can become buried with an exponential probability, while the probability that particles rest follows a modified Bessel distribution (*Einstein*, 1937; *Lisle et al.*, 1998), evaluating the probability that particles rest and become buried generates the Q-function convolution structure.

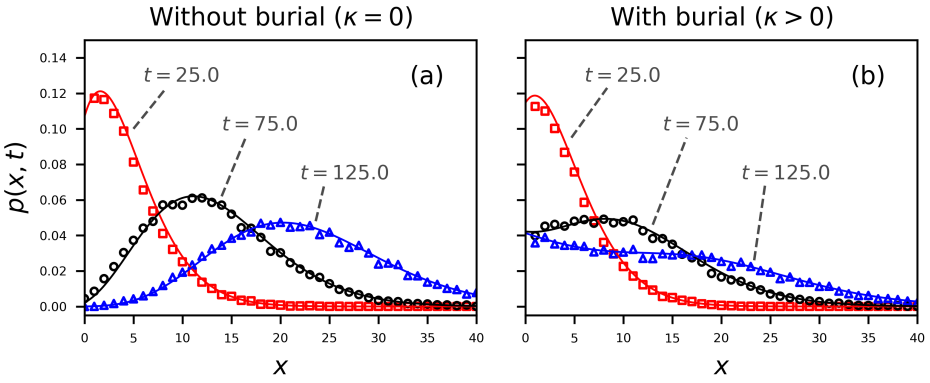

Figure 4.1: Joint distributions for a grain to be at position x at time t are displayed for the choice $k_1 = 0.1$, $k_2 = 1.0$, $v = 2.0$. Grains are initially at rest ($\theta_1 = 1$, $\theta_2 = 0$). The solid lines are the analytical distribution in Eq. 4.5, while the points are numerically simulated, showing the correctness of the mathematical derivations. Colors pertain to different times. Units are unspecified, since the aim is to demonstrate the general characteristics of $p(x, t)$. Panel (a) shows the case $\kappa = 0$ – no burial. In this case, the joint distribution tends toward Gaussian at large times (*Einstein*, 1937; *Lisle et al.*, 1998). Panel (b) shows the case when grains have rate $\kappa = 0.01$ to become buried while resting on the bed surface. Because of burial, the joint distribution tends toward a more uniform distribution than Gaussian.

Fig. 4.1 depicts the distribution Eq. 4.5 alongside simulations generated by a direct method based on evaluating the cumulative transition probabilities between states on a small timestep (*Barik et al.*, 2006). When grains do not become buried, as in panel (a) of Fig. 4.1, the distribution becomes Gaussian-like at relatively large observation times, exemplifying normal diffusion and satisfying the central limit theorem. When grains become buried, as in panel (b) of Fig. 4.1, the Q-function terms prevent the distribution from approaching a Gaussian at large timescales, exemplifying anomalous diffusion (*Weeks and Swinney*, 1998) and violating the central limit theorem (*Metzler and Klafter*, 2000; *Schumer et al.*, 2009).

4.1.4 Downstream diffusion

To obtain an analytical formula for tracers diffusing downstream while they gradually become buried, the first two moments of position are derived by taking derivatives with respect to η of the Laplace space distribution 4.4 using an approach similar to *Shlesinger* (1974) and *Weeks and Swinney* (1998). These moments produce the positional variance $\sigma_x^2 = \langle x^2 \rangle - \langle x \rangle^2$. The first two moments are

$$\langle x(t) \rangle = A_1 e^{(b-a)t} + B_1 e^{-(a+b)t} + C_1, \tag{4.6}$$

$$\langle x^2(t) \rangle = A_2(t) e^{(b-a)t} + B_2(t) e^{-(a+b)t} + C_2, \tag{4.7}$$

so the variance is

$$\sigma_x^2(t) = A(t) e^{(b-a)t} + B(t) e^{-(a+b)t} + C(t). \tag{4.8}$$

In these equations, $a = (\kappa + k_1 + k_2)/2$ and $b = \sqrt{a^2 - \kappa k_2}$ are effective rates having dimensions of inverse time, while the A, B, and C factors are provided in Tab. 4.1.

The positional variance Eq. 4.8 is plotted in Fig. 4.2 for conditions $\theta_1 = 1$ and $k_2 \gg k_1 \gg \kappa$. The notation "$\gg$" is interpreted in this context to mean "of at least an order of magnitude greater". These conditions are most relevant to tracers in gravel-bed rivers, since they represent that

Table 4.1: Abbreviations used in the expressions of the mean (Eq. 4.6), second moment (Eq. 4.7) and variance (Eq. 4.8) of bedload tracers are defined.

$$A_1 = \frac{v}{2b}\Big[\theta_2 + \frac{k_1 + \theta_2\kappa}{b-a}\Big]$$

$$B_1 = -\frac{v}{2b}\Big[\theta_2 - \frac{k_1 + \theta_2\kappa}{a+b}\Big]$$

$$C_1 = -\frac{v}{2b}\Big[\frac{k_1 + \theta_2\kappa}{b-a} + \frac{k_1 + \theta_2\kappa}{a+b}\Big]$$

$$A_2(t) = \frac{v^2}{2b^3}\Big[(bt-1)[k_1 + \theta_2(2\kappa + k_1 + b - a)] + \theta_2 b + \frac{(\kappa + k_1)(\theta_2\kappa + k_1)}{(b-a)^2}[(bt-1)(b-a) - b]\Big]$$

$$B_2(t) = \frac{v^2}{2b^3}\Big[(bt+1)[k_1 + \theta_2(2\kappa + k_1 - a - b)] + \theta_2 b - \frac{(\kappa + k_1)(\theta_2\kappa + k_1)}{(a+b)^2}[(bt+1)(a+b) + b]\Big]$$

$$C_2 = \frac{v^2}{2b^3}(\kappa + k_1)(\theta_2\kappa + k_1)\Big[\frac{2b-a}{(b-a)^2} + \frac{a+2b}{(a+b)^2}\Big]$$

$$A(t) = A_2(t) - 2A_1C_1 - A_1^2\exp[(b-a)t]$$

$$B(t) = B_2(t) - 2B_1C_1 - B_1^2\exp[-(a+b)t]$$

$$C(t) = C_2 - C_1^2 - 2A_1B_1\exp[-2at]$$

grains are initially at rest (*Hassan et al.*, 1991; *Wu et al.*, 2019a), motions are typically much shorter than rests (*Einstein*, 1937; *Hubbell and Sayre*, 1964), and burial requires a much longer time than typical rests (*Ferguson and Hoey*, 2002; *Haschenburger*, 2013; *Hassan and Church*, 1994). Fig. 4.2 demonstrates that under these conditions the variance 4.8 shows three diffusion ranges with approximate power law scaling ($\sigma_x^2 \propto t^\gamma$) that are identified as the local, intermediate, and global ranges proposed by Nikora et al., followed by a fourth range of no diffusion ($\sigma_x^2 = \text{const}$) stemming from the burial of all tracers. Following *Hassan and Bradley* (2017) I suggest to call the fourth range "geomorphic", since any further transport in this range can occur only if scour re-exposes buried grains to the flow (*Martin et al.*, 2014; *Nakagawa and Tsujimoto*, 1980; *Voepel et al.*, 2013; *Wu et al.*, 2019b).

4.1.5 Diffusion exponents and three-range scaling

Two limiting cases of Eq. 4.8 provide the scaling exponents γ of the diffusion $\sigma_x^2 \propto t^\gamma$ in each range. Limit (1) represents times so short that a negligible amount of sediment burial has occurred, $t \ll 1/\kappa$, while limit (2) represents

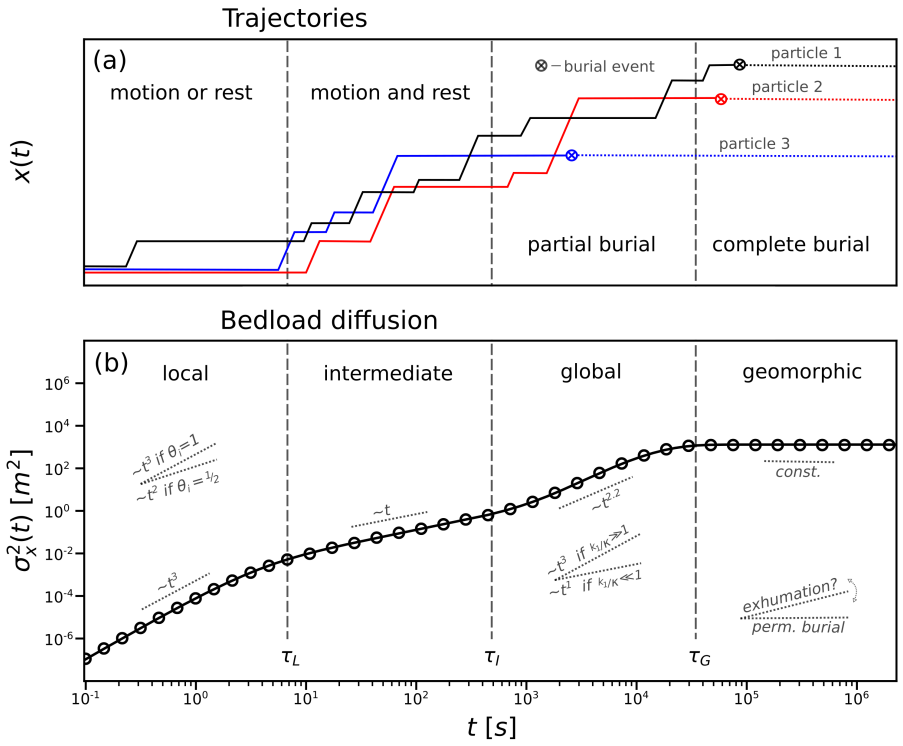

Figure 4.2: Panel (a) sketches conceptual trajectories of grains, while panel (b) depicts Eq. 4.8 with mean motion time 1.5s, rest time 30.0s, and velocity 0.1m/s. The burial timescale is 7200s (two hours), and grains start from rest ($\theta_1 = 1$). The solid line is Eq. 4.8 and the points are numerically simulated. Panel (b) demonstrates four distinct scaling ranges of σ_x^2: local, intermediate, global, and geomorphic. The first three are diffusive. Crossover times τ_L, τ_I, and τ_G divide the ranges. Slope keys demonstrate the scaling $\sigma_x^2 \propto t^\gamma$ in each range. Panel (a) demonstrates that different mixtures of motion, rest, and burial states generate the ranges. At local timescales, grains usually either rest or move; at intermediate timescales, they transition between rest and motion; at global timescales, they transition between rest, motion, and burial; and at geomorphic timescales, all grains become buried.

times so long motion intervals appear as instantaneous steps of mean length $l = v/k_2$, $1/k_2 \to 0$ while $v/k_2 =$ constant. Limit (1) provides local exponent $2 \leq \gamma \leq 3$ depending on the initial conditions θ_i, and intermediate exponent $\gamma = 1$. If grains start in motion or rest exclusively, meaning one $\theta_i = 0$, the local exponent is $\gamma = 3$, while if grains start in a mixture of motion and rest states, meaning neither θ_i is zero, the local exponent is $\gamma = 2$. Limit (2) provides global exponent $1 \leq \gamma \leq 3$ depending on the relative importance of κ and k_1. The extreme $k_1/\kappa \ll 1$ produces $\gamma = 1$ in the global range, while the opposite extreme $k_1/\kappa \to \infty$ produces $\gamma = 3$. To summarize, when $k_2 \gg k_1 \gg \kappa$ so all three diffusion ranges exist, Eq. 4.8 implies:

1. local range super-diffusion with $2 < \gamma < 3$ depending on whether grains start from purely motion or rest ($\gamma = 3$) or from a mixture of both states ($\gamma = 2$),

2. intermediate range normal diffusion $\gamma = 1$ independent of model parameters, and

3. global range super-diffusion $1 < \gamma < 3$ depending on whether burial happens relatively slowly ($\gamma \to 1$) or quickly ($\gamma \to 3$) compared to surface resting times.

Finally, the burial of all tracers generates a geomorphic range of no diffusion.

4.2 Discussion

4.2.1 Local and intermediate ranges with comparison to earlier work

This chapter has extended *Einstein* (1937) by including motion, rest, and burial processes in a multi-state random walk (*Weeks and Swinney*, 1998; *Weiss*, 1994) to demonstrate that a group of bedload tracers moving downstream while gradually becoming buried will generate a super-diffusive local range (*Fathel et al.*, 2016; *Martin et al.*, 2012; *Witz et al.*, 2019), a normal-diffusive intermediate range (*Nakagawa and Tsujimoto*, 1976; *Yano*, 1969),

and a super-diffusive global range (*Bradley*, 2017; *Bradley et al.*, 2010) before the diffusion eventually terminates in a geomorphic range (*Hassan and Bradley*, 2017). *Nikora et al.* (2002) highlighted the need for such a physical description, although they suggested to use a two-state random walk between motion and rest states with heavy-tailed resting times, and they did not discuss sediment burial. However, other works have demonstrated that a two-state walk with heavy-tailed rests provides two diffusion ranges – not three (*Fan et al.*, 2016; *Weeks et al.*, 1996), and although heavy-tailed resting times have been documented for surface particles (*Fraccarollo and Hassan*, 2019; *Liu et al.*, 2019), they are more often associated with buried particles (*Martin et al.*, 2012, 2014; *Olinde and Johnson*, 2015; *Pelosi et al.*, 2016; *Pierce and Hassan*, 2020a; *Voepel et al.*, 2013), while surface particles retain light-tailed resting times (*Ancey et al.*, 2006; *Einstein*, 1937; *Nakagawa and Tsujimoto*, 1976; *Yano*, 1969). Accordingly, I developed a random walk model of bedload trajectories with light-tailed surface resting times that incorporates sediment burial.

The local and intermediate range diffusion characteristics resulting from this model correspond closely to the original Nikora et al. concepts, while the global range has a different origin than Nikora et al. envisioned. *Nikora et al.* (2001b) explained that local diffusion results from the non-fractal (smooth) characteristics of bedload trajectories between subsequent interactions with the bed, while intermediate diffusion results from the fractal (rough) characteristics of bedload trajectories after many interactions with the bed. This chapter represents these conclusions: non-fractal (and super-diffusive) bedload trajectories exist on timescales short enough that each grain is either resting or moving, while fractal (and normal-diffusive) bedload trajectories exist on timescales when grains are actively switching between motion and rest states. I conclude that local and intermediate ranges stem from the interplay between motion and rest timescales, as demonstrated by earlier two-state random walk models (*Lajeunesse et al.*, 2017; *Lisle et al.*, 1998) and by all Newtonian models that develop sequences of motions and rests (*Bialik et al.*, 2012; *Nikora et al.*, 2001b), even those including heavy-tailed rests (*Fan et al.*, 2016).

4.2.2 Global and geomorphic ranges with next steps for research

Nikora et al. explained that divergent resting times generate a sub-diffusive global range. However, studies have demonstrated that divergent resting times can generate super-diffusion in asymmetric random walks (*Weeks and Swinney*, 1998; *Weeks et al.*, 1996), and both experiments (*Bradley*, 2017; *Bradley et al.*, 2010) and models (*Pelosi et al.*, 2016; *Wu et al.*, 2019a,b) of bedload tracers undergoing burial have demonstrated global range super-diffusion. While my own results also show global range super-diffusion, they do not necessarily refute the Nikora et al. conclusion of sub-diffusion at long timescales. I assumed sediment burial was a permanent condition which developed a non-diffusive geomorphic range. In actuality, burial is a temporary condition, because bed scour can exhume buried sediment back into transport (*Wu et al.*, 2019b), probably after heavy-tailed intervals (*Martin et al.*, 2014; *Voepel et al.*, 2013). A generalization of the model in this chapter to include heavy-tailed timescales between burial and exhumation might develop four ranges of diffusion, where the long-time decay of the exhumation time distribution would dictate the geomorphic range diffusion characteristics as depicted in Fig. 4.2. If cumulative exhumation times decay faster than $T^{-1/2}$, as suggested in Ch. 3, other equilibrium transport models (*Martin et al.*, 2014; *Voepel et al.*, 2013), and laboratory experiments (*Martin et al.*, 2012, 2014), the geomorphic range is expected to be super-diffusive (*Weeks and Swinney*, 1998). However, if they decay slower than $T^{-1/2}$, as implicitly suggested by the data of *Olinde and Johnson* (2015), the geomorphic range is expected to be genuinely sub-diffusive (*Weeks and Swinney*, 1998), leaving Nikora et al. with the final word on long-time sub-diffusion.

The analytical solution of bedload diffusion in Eq. 4.8 reduces exactly to the analytical solutions of the *Lisle et al.* (1998) and *Lajeunesse et al.* (2017) models in the limit without burial ($\kappa \to 0$), the *Wu et al.* (2019a) model in the limit of instantaneous steps ($k_2 \to \infty$ and $l = v/k_2$), and the original *Einstein* (1937) model in the limit of instantaneous steps without burial. These reductions demonstrate that the majority of recent bedload diffusion models, whether developed from Exner-type equations (*Pelosi and Parker*,

2014; *Pelosi et al.*, 2016; *Wu et al.*, 2019a) or advection-diffusion equations (*Lajeunesse et al.*, 2017; *Lisle et al.*, 1998), can be viewed equivalently as continuous-time random walks applied to individual bedload trajectories. Within random walk theory, sophisticated descriptions of transport with variable velocities (*Masoliver and Weiss*, 1994; *Zaburdaev et al.*, 2008), correlated motions (*Escaff et al.*, 2018; *Vicsek and Zafeiris*, 2012), and anomalous diffusion (*Fa*, 2014; *Masoliver*, 2016; *Metzler et al.*, 2014) have been developed. Meanwhile, in bedload transport research, variable velocities (*Furbish et al.*, 2012a; *Heyman et al.*, 2016; *Lajeunesse et al.*, 2010), correlated motions (*Heyman et al.*, 2014; *Lee and Jerolmack*, 2018; *Saletti and Hassan*, 2020), and anomalous diffusion (*Bradley*, 2017; *Fathel et al.*, 2016; *Schumer et al.*, 2009) constitute open research issues. Further developing the linkage between existing bedload models and random walk concepts could rapidly progress our understanding.

4.3 Summary

In this chapter, I developed a random walk model to describe sediment tracers transporting through a river channel as they gradually become buried, providing a physical description of the local, intermediate, and global diffusion ranges identified by *Nikora et al.* (2002). Pushing their ideas somewhat further, I followed *Hassan and Bradley* (2017) to propose a geomorphic range describing particle diffusion characteristics at timescales larger than the global range when burial and exhumation both moderate downstream transport. At base level, this work demonstrates that (1) durations of sediment motions, (2) durations of sediment rest, and (3) the sediment burial process are sufficient to develop three diffusion ranges that terminate when all tracers become buried. A next step is to incorporate exhumation to better understand the geomorphic range. Ultimately, the multi-state random walk formalism used in this chapter has been demonstrated to implicitly underlie most existing bedload diffusion models. The random walk formalism is an alternative perspective on the Langevin approaches used elsewhere in this thesis, and it provides a powerful tool for researchers targeting landscape-

scale understanding from statistical concepts of the underlying grain-scale dynamics.

Chapter 5

Collisional Langevin model of bedload sediment velocity distributions

5.1 Introduction

Bedload transport rates show wide and frequent fluctuations which originate from coupling between the fluid and granular phases. Owing to these fluctuations, measured transport rates often show slow convergence through time (*Dhont and Ancey*, 2018; *Turowski*, 2010), and predicted rates can deviate from measured values by several orders of magnitude (*Martin*, 2003; *Recking et al.*, 2012). These challenges limit numerous ecological and engineering applications that rely on sediment transport predictions (*Gaeuman et al.*, 2017; *Malmon et al.*, 2005).

In recent decades, stochastic formulations of the bedload flux have become increasingly popular for their potential to predict the mean transport rates required by applications while also predicting the magnitude of transport fluctuations and quantifying the dependence of measurements on the observation scale (Secs. 1.1.13 and 1.1.14). Recent indications that sediment transport fluctuations might explain longstanding open problems in alluvial

channel stability, such as channel width maintenance (*Abramian et al.*, 2019, 2020) and bedform initiation (*Bohorquez and Ancey*, 2016; *Jerolmack and Mohrig*, 2005) provide additional motivation to develop these stochastic approaches.

One subset of stochastic methods expresses downstream transport rates as a sum over the instantaneous streamwise velocities of all particles in motion within a control volume (Sec. 1.1.13). This formulation requires the instantaneous velocity distributions of sediment particles (e.g. *Ancey and Pascal*, 2020), yet our understanding of these distributions remains limited. There is as of yet no consensus on the shape of the bedload velocity distribution, and although the models described in Sec. 1.1.5 describe some extreme end-member distributions (e.g. *Ancey and Heyman*, 2014; *Fan et al.*, 2014), no models have been developed that describe all experimental observations reported to date (*Fathel et al.*, 2015; *Heyman et al.*, 2016; *Houssais and Lajeunesse*, 2012; *Lajeunesse et al.*, 2010; *Liu et al.*, 2019). In this chapter, I develop a stochastic model of particle velocities which addresses this shortcoming.

High-speed video experiments have measured different streamwise particle velocity distributions without indicating why one distribution or another appears in a given set of hydraulic and sedimentary conditions. One set of studies has shown exponential particle velocity distributions (*Charru et al.*, 2004; *Fathel et al.*, 2016, 2015; *Lajeunesse et al.*, 2010; *Roseberry et al.*, 2012; *Seizilles et al.*, 2014). These experiments involve uniformly-sized small sands or glass beads ($0.05-2$mm) in turbulent and subcritical flows, but not always; the experiments of *Lajeunesse et al.* (2010) were turbulent and supercritical, while the experiments of *Charru et al.* (2004) and *Seizilles et al.* (2014) were laminar and likely subcritical. A second set of studies show Gaussian particle velocity distributions (*Ancey and Heyman*, 2014; *Heyman et al.*, 2016; *Martin et al.*, 2012). In these experiments, particles are typically larger ($2-8$mm) uniformly-sized gravels or glass beads, and flows are generally turbulent and supercritical. Other experiments display velocity distributions that are intermediate between exponential and Gaussian that appear visually more like a Gamma distribution (*Houssais and Lajeunesse*,

2012; *Liu et al.*, 2019). *Houssais and Lajeunesse* (2012) used a bimodal distribution of glass beads with diameters 0.7mm and 2.2mm in turbulent and supercritical flow conditions, while *Liu et al.* (2019) used sand having median diameter 1.1mm in turbulent and subcritical flow. From this experimental record, the velocity distribution shape apparently does not consistently relate to the flow conditions. There is however a loose trend within the particle size. Smaller particles tend to show more exponential-like distributions (e.g. *Fathel et al.*, 2015), while larger ones show Gaussian distributions (e.g. *Heyman et al.*, 2016). This summary suggests that streamwise bedload velocity distributions could be controlled by the particle size.

Existing models of streamwise bedload velocities can be divided into computational and stochastic physics categories. Computational models numerically integrate some approximate coupled dynamics for individual grains and the fluid, generally modeling particles as spheres interacting through repulsive forces and numerically integrating the Navier-Stokes equations (or some approximation of them) to describe the flow forces on grains. When streamwise particle velocities have been analyzed in such simulations, they show exponential tails (*Furbish and Schmeeckle*, 2013; *González et al.*, 2017) that agree with one subset of the experimental data.

Stochastic models have incorporated fluctuating driving and resisting terms into Newtonian equations of individual grains to develop Langevin-like descriptions of bedload particle motions (Sec. 1.1.5). *Fan et al.* (2014) represented turbulent drag as Gaussian white noise and included a static Coulomb friction term to model particle-bed collisions, while *Ancey and Heyman* (2014) applied an Ornstein-Uhlenbeck process which combines the fluid and driving forces into a simplified velocity-dependent force, again modeling fluctuations with Gaussian white noise. Each of these models derives one end-member distribution from among the range of distributions reported in experiments. A physical description for the full range of experimentally-observed bedload velocity distributions remains an elusive target.

In this chapter I explore the possibility that the particle velocity distribution is controlled by momentum dissipation from particle-bed collisions by incorporating ideas from the physics of granular media. A major paradigm

in granular dynamics is to describe particles as a continuum or "granular liquid" having an effective rheology (e.g. *Andreotti et al.*, 2013; *Jenkins and Hanes*, 1998), but as discussed in Ch. 1 such a continuum assumption is unlikely to be satisfied for weak bedload transport conditions.

Instead, particles in these conditions are better characterized as a rarefied granular gas (e.g. *Furbish et al.*, 2021). In granular gases, dissipative collisions are known to cause departures toward an exponential velocity distribution from the Gaussian form expected for perfectly elastic collisions (*Brilliantov and Poschel*, 2004). Gas theory formulates particle-particle collisions as a nonlocal integral within the master equation for the probability distribution of particle velocity called the Boltzmann equation (*Brilliantov and Poschel*, 2004; *Chapman and Cowling*, 1970; *Landau and Lifshitz*, 1969). Collisions in these models involve episodic kicks to the particle momenta at random times, usually parameterized by billiard ball-like models of the underlying rigid body dynamics (e.g. *Brach*, 1989). Such episodic forcing is distinct from the smooth friction terms included in the current stochastic models describing bedload particle velocities.

I develop in this chapter an improved model for sediment grains in transport which replaces the smooth friction terms of earlier models by episodic particle-bed collisions. I present the model and explain its key assumptions in Sec. 5.2. Then I explain the analytical solution of the model and other major results in Sec. 5.3. Finally I discuss the implications of these results, summarize key findings, and suggest ideas for further research in Secs. 5.4 and 5.5.

5.2 Mechanistic description of particle velocities

Fig. 5.1 indicates the configuration of the model in this chapter. Nearly spherical particles of diameter d and mass m move as bedload over a granular bed. The flow is just strong enough to drive grains into the rarefied transport often typical in gravel-bed rivers (e.g. *Ashworth and Ferguson*, 1989; *Warburton*, 1992). Particles saltate downstream through a sequence of particle-bed collisions, and moving particles collide often with stationary

particles but rarely with other moving particles (cf. *Williams and Furbish*, 2021).

Particles respond to turbulent flow forces and episodic particle-bed collision forces. In contrast to the computational physics approach, I do not aim to characterize the exact timeseries of the forces on an individual particle. Instead, I model the ensemble of possible force timeseries that particles could conceivably experience. Each force timeseries realization implies a different velocity timeseries $u(t)$ in the downstream direction. The objective is to calculate the probability distribution $P(u,t)$ of this downstream velocity by averaging over the ensemble of forces.

The description of bedload particle velocity fluctuations will be more detailed than the simple white noise model Ch. 2, but alternation between motion and rest will be neglected, meaning the model of this chapter is only applicable to moving particles. In analyzing the velocities of moving particles, I include the most realistic particle-bed collision and fluid forces possible while still allowing for analytical solutions.

5.2.1 Episodic collision forces

Collisions between bedload particles dissipate translational momentum, partly by converting it to vertical, lateral, or angular momentum, partly by deforming particles and the bed and generating heat (*Schmeeckle*, 2014; *Williams and Furbish*, 2021), and partly by pressurizing the fluid between approaching particles (*Joseph et al.*, 2001; *Schmeeckle et al.*, 2001). The microscopic details of particle-particle collisions have been thoroughly studied (*Brach*, 1989; *Lorenz et al.*, 1997; *Montaine et al.*, 2011), although in bedload transport the coefficient of restitution may be less relevant than other factors such as collision geometry and bed deformation (*Pähtz et al.*, 2021). Here, I introduce a simple elasticity parameter ε as a first attempt at modeling dissipation by episodic collisions, as indicated in Fig. 5.1. This elasticity characterizes the fraction of downstream momentum lost in a collision. If the streamwise velocity just prior to a collision is u, just after the collision it becomes εu. The elasticity ranges from $\varepsilon = 0$, representing a completely

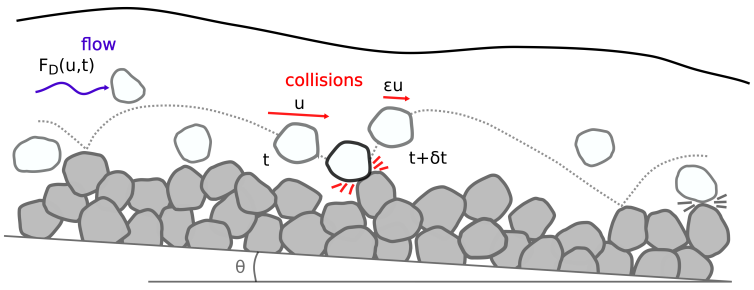

Figure 5.1: Rarefied sediment transport involves turbulent fluid drag and episodic particle-bed collisions. In the collision model developed in this chapter, pre-collisional streamwise velocities u are transformed instantaneously to post-collisional velocities ε. The parameter ε is an "elasticity" with $0 \leq \varepsilon \leq 1$.

inelastic collision, to $\varepsilon = 1$, representing a completely elastic collision.

Since the elasticity combines effects of particle shape and collision geometry and should vary from one collision to the next, the elasticity ε is interpreted as a random variable, characterized by a statistical distribution $\rho(\varepsilon)$. Some granular gas models have also included random elasticity (e.g. *Serero et al.*, 2015), but this topic has not been completely explored in the literature.

Assuming that the average number of collisions per unit time is ν (the collision rate) and that the time intervals between subsequent particle-bed collisions are exponentially distributed (e.g. *Gordon et al.*, 1972), the collision force in the downstream direction can be written as a Poisson pulse noise (Sec. 1.1.8):

$$F_C(u,t) = -mu \sum_{k=1}^{N_\nu(t)} (1-\varepsilon_k)\delta(t-\tau_k). \tag{5.1}$$

Here, $N_\nu(t)$ is the number of collisions in time t (a Poisson random variable),

the τ_k ($k = 1, 2, \dots$) are times at which collisions occur, and the ε_k are the elasticity coefficients, drawn from the distribution $\rho(\varepsilon)$ characterizing the fraction of momentum lost in each particle-bed collision. The time intervals $\Delta\tau = \tau_k - \tau_{k-1}$ between collisions are distributed as $P(\Delta\tau) = \nu \exp(-\nu\Delta\tau)$, so the number of collisions $n = N_\nu(t)$ in time t is distributed as $P(n) = (\nu t)^n \exp(-\nu t)/n!$. This collision force is a sequence of random impulses which are proportional to the pre-collisional streamwise momenta. This collision model should be adequate when the contact times between moving and resting particles are small compared to the times between collisions. These conditions should be satisfied for typical saltation trajectories as in Fig. 5.1.

5.2.2 Turbulent fluid forces

Fluid forces on coarse particles are parameterized by the particle Reynolds number $Re_p = Vd/\lambda$, involving the particle size d, slip velocity V between particle and fluid, and kinematic viscosity λ. These forces have been calculated from the Navier-Stokes equations for spherical particles at small (or vanishing) Re_p and include drag, virtual mass, buoyancy, fluid pressure gradient, Basset history integral, Saffman lift, and Magnus lift terms (*Auton*, 1987; *Hjelmfelt and Mockros*, 1966; *Maxey and Riley*, 1983). At realistic Re_p, analytical results for the fluid forces on a particle remain inaccessible, so it is standard practice to introduce empirical corrections to the small Re_p formulas (e.g. *Clift et al.*, 1978; *Schmeeckle et al.*, 2007).

Our understanding of the fluid forces remains incomplete. Existing formulas were derived in the absence of boundaries, so it is unclear how these formulas should be modified near the bed. Even ignoring this complication, the added mass and Basset forces are difficult to compute and therefore impractical to include in analytical models. These challenges require us to adopt the most complex expressions of the fluid forces that are compatible with our modeling goals (e.g. *Armenio and Fiorotto*, 2001; *Michaelides*, 1997). From this same requirement, a majority of bedload transport models include fluid drag (and possibly pressure gradient) terms as the only

force(s) driving the downstream movement of bedload particles (*Ancey and Heyman*, 2014; *Elghannay and Tafti*, 2018; *Fan et al.*, 2014; *González et al.*, 2017; *Schmeeckle*, 2014).

The downstream drag force with an Re_p correction is usually written

$$F_D = \frac{\pi}{8}\rho_f d^2 C_D(Re_p)|V|V, \tag{5.2}$$

where ρ_f is the fluid density, d is the particle diameter, $C_D(Re_p)$ is an empirical drag coefficient, and $V = U - u$ is the slip velocity calculated as the difference of fluid (U) and particle (u) velocities (*Coleman*, 1967; *Dwivedi et al.*, 2012; *Schmeeckle et al.*, 2007). Experiments on stationary particles indicate that drag forces fluctuate rapidly and lie on wide Gaussian-like distributions (*Celik et al.*, 2014; *Dwivedi et al.*, 2010; *Hofland and Battjes*, 2006; *Schmeeckle et al.*, 2007). Drag forces on moving particles have not been experimentally measured, but even in globally steady flow conditions, slip velocities are expected to fluctuate due to particle acceleration, fluid turbulence, passage of other moving particles, and vertical movement of particles within the flow profile. The nonlinearity in Eq. 5.2 will amplify slip velocity fluctuations, generating large and erratic drag force variations that only add to the undetermined contributions of the neglected fluid forces.

Here I assume with earlier computational (*Elghannay and Tafti*, 2018; *González et al.*, 2017; *Schmeeckle*, 2014) and analytical (e.g. *Ancey and Heyman*, 2014; *Fan et al.*, 2014) models of bedload transport that fluid drag is the primary force driving sediment particles downstream. I further assume with *Fan et al.* (2014) and *Ancey and Heyman* (2014) that the fluctuating component of this force can be represented by a Gaussian white noise. This latter assumption is justified insofar as drag forces fluctuate rapidly compared to the inertial response times of particles and the timescales over which particles change height within the flow profile. Defining $\bar{C}_D$ as the empirical drag coefficient evaluated at $\bar{V}$ and $\xi(t)$ as a Gaussian white noise of mean 0 and variance 1 (e.g. *Gardiner*, 1983), the fluid drag force considered in this chapter is

$$F_D(t) = \Gamma + \sqrt{2D}\eta(t), \tag{5.3}$$

where $\Gamma = \frac{\pi}{8}\rho_f d^2 \bar{C}_D \bar{V}^2$ is the steady component of the drag. Although this representation of the fluid forces is a simplified approximation, it is similar to the representations used in earlier stochastic models in that it has no dependence on the vertical structure of the flow (e.g. *Ancey and Heyman*, 2014; *Fan et al.*, 2014). This level of simplification is required for an analytically tractable model of bedload particle velocities (e.g. *Michaelides*, 1997).

5.2.3 Langevin equation for collisional bedload transport

With the above forces, the Langevin equation $m\dot{u}(t) = F_D(t) + F_C(t)$ for the sediment dynamics in the downstream direction becomes

$$m\dot{u}(t) = \Gamma + \sqrt{2D}\eta(t) - mu(t)\xi_{\nu,\varepsilon}(t). \tag{5.4}$$

This equation replaces the steady friction terms of earlier models with an episodic term, designed to provide a more realistic representation of particle-bed collisions. Mathematically, Eq. 5.4 is a Langevin-like equation representing a jump-diffusion process (*Daly and Porporato*, 2006) with multiplicative Poisson noise (*Denisov et al.*, 2009; *Dubkov et al.*, 2016). Collisions introduce velocity jumps while turbulence generates velocity diffusion. The collision term is multiplicative in the sense that u multiplies the Poisson noise $\xi_{\nu,\varepsilon}(t)$.

Models like Eq. 5.4 have long been studied in the stochastic physics literature (*Hänggi*, 1978; *Van Den Broeck*, 1983), but solving such equations remains extremely challenging (*Daly and Porporato*, 2010; *Dubkov and Kharcheva*, 2019; *Mau et al.*, 2014). One issue is that multiplicative white noises imply the prescription dilemma of stochastic calculus (*Gardiner*, 1983; *Risken*, 1984), meaning Eq. 5.4 is not defined without further specifying an integration rule (*Suweis et al.*, 2011). Here, the Itô interpretation (lower endpoint integration rule) is the physical choice the energy dissipated by collisions depends strictly on pre-collisional velocities, not post-collisional (e.g. *Gardiner*, 1983). Given this integration rule, the remaining issues are to obtain the master equation characterizing the ensemble of velocities de-

fined by Eq. 5.4, and then to solve this equation for the velocity distribution $P(u,t)$.

5.2.4 Master equation and particle-bed collision integral

The equation governing the streamwise velocity distribution $P(u,t)$ is derived in the appendix Sec. D.1 with a limiting procedure, providing

$$\nu^{-1}\partial_t P(u,t) = -\tilde{\Gamma}\partial_u P(u,t) + \tilde{D}\partial_u^2 P(u,t) + I_c(u,t). \tag{5.5}$$

The parameters $\tilde{\Gamma} = \Gamma/(\nu m)$ and $\tilde{D} = D/(\nu m)$ scale the steady and fluctuating components of the fluid force against the collision rate ν. The term

$$I_c(u,t) = -P(u,t) + \int_0^1 \frac{d\varepsilon}{\varepsilon} P\big(\frac{u}{\varepsilon},t\big)\rho(\varepsilon) \tag{5.6}$$

is a "collision integral" term representing particle-bed collisions.

Eq. 5.5 is a nonlocal extension of the Fokker-Planck equation used in earlier bedload models (*Ancey and Heyman*, 2014; *Fan et al.*, 2014). Nonlocality is introduced by the collision integral of Eq. 5.6 which transfers probability from higher pre-collisional velocities u/ε to lower post-collisional velocities u. This term is analogous to the collision integral within the Boltzmann equation of kinetic theory (*Brilliantov and Poschel*, 2004; *Duderstadt and Martin*, 1979). Physically, it corresponds to binary collisions between particles having different masses and random restitution coefficients (cf. *Serero et al.*, 2015) in the limit that the mass of one particle (here, the particle resting on the bed) diverges to infinity. Mathematically, the collision integral represents the probability distribution of the product between the elasticity ε and the downstream momentum ($p = mu$), considering them as uncorrelated random variables (cf. *Feller*, 1967).

Owing to its nonlocality, Eq. 5.5 does not admit analytical solutions as is, so further approximation is necessary. To make progress, I assume the distribution of elasticity $\rho(\varepsilon)$ is sharply peaked at some most common (mode) value ε' to allow for a Kramers-Moyal type expansion of the particle-bed collision integral (e.g. *Gardiner*, 1983). Such a mode value in the colli-

sion elasticity distribution is present in experiments on rigid body collisions (*Glielmo et al.*, 2014). For particle-bed collisions of bedload, a modal elasticity is also expected since experiments indicate a most common collision geometry (e.g. *Gordon et al.*, 1972; *Martin*, 2013).

Expanding all terms in the integrand except $\rho(\varepsilon)$ provides

$$I_c(u,t) = -P(u,t) + \frac{1}{\varepsilon'}P\big(\frac{u}{\varepsilon'},t\big) + \sum_{k=1}^{\infty}\frac{\alpha_k}{k!}(\varepsilon-\varepsilon')^k\Big[\frac{1}{\varepsilon}P\big(\frac{u}{\varepsilon}\big)\Big]^{(k)}\Big|_{\varepsilon=\varepsilon'}, \quad (5.7)$$

where the $\alpha_k = \int_0^1 d\varepsilon\rho(\varepsilon)(\varepsilon-\varepsilon')^k$ are the central moments of ε around the modal elasticity ε' and the superscript (k) denotes the kth derivative.

In what follows, I drop all but the first two terms in this expansion to obtain the leading order contribution of particle-bed collisions to the velocity distribution. Higher orders could always be included later by perturbation theory (*Morse and Feshbach*, 1953b). I solve the resulting approximate equation in steady-state, when $\partial P(u,t)/\partial t = 0$. Eq. 5.5 indicates that this solution will be a good approximation to the time-dependent problem when particle motions generally survive multiple collisions ($t \gg \nu^{-1}$).

5.3 Results

5.3.1 Derivation of the bedload velocity distribution

Hereafter I drop the prime on the most common streamwise restitution coefficient ε'. With the truncation to two terms, Eq. 5.5 gives

$$0 = -\tilde{\Gamma}\partial_u P(u) + \tilde{D}\partial_u^2 P(u) - P(u) + \frac{1}{\varepsilon}P\big(\frac{u}{\varepsilon}\big), \quad (5.8)$$

which is an advanced functional differential equation. This equation is "functional" in the sense that it is nonlocal in velocity due to the last term on the right hand side, and it is "advanced" in that u/ε is advanced beyond the argument u involved in the rest of this equation (since $0 < \varepsilon < 1$). Such equations have seen some attention in the mathematics literature, where they are sometimes called pantograph equations (*Hall and Wake*, 1989; *Kim*, 1998;

Zaidi et al., 2015).

In the appendix Sec. D.2 Eq. 5.8 is solved with Laplace transforms, providing

$$P(u) = \frac{\theta(-u)}{K_+} \sum_{l=0}^{\infty} \frac{\varepsilon^{-l} e^{\lambda_+ \varepsilon^{-l} u}}{\prod_{m=1}^{l} (-\tilde{D}\lambda_+^2 \varepsilon^{-2m} + \tilde{\Gamma}\lambda_+ \varepsilon^{-m} + 1)} + \frac{\theta(u)}{K_-} \sum_{l=0}^{\infty} \frac{\varepsilon^{-l} e^{\lambda_- \varepsilon^{-l} u}}{\prod_{m=1}^{l} (-\tilde{D}\lambda_-^2 \varepsilon^{-2m} + \tilde{\Gamma}\lambda_- \varepsilon^{-m} + 1)}. \quad (5.9)$$

The factors $\lambda_\pm$ are defined in appendix Eq. D.7. They are proportional to $\tilde{\Gamma}/\tilde{D}$. The normalization factors $K_\pm$ are

$$K_\pm = \tilde{D}(\lambda_+ - \lambda_-) \prod_{l=1}^{\infty} (-\tilde{D}\lambda_\pm^2 \varepsilon^{2l} + \tilde{\Gamma}\lambda_\pm \varepsilon^l + 1). \quad (5.10)$$

Although this velocity distribution has a complex mathematical structure, one can verify that this is a normalized probability distribution ($\int du P(u) = 1$) which has very simple limiting behaviors as the mode elasticity ε approaches fully elastic ($\varepsilon = 1$) and inelastic ($\varepsilon = 0$) values.

It is possible to derive the moments of this probability distribution by multiplying Eq. 5.8 by u, integrating, and then solving the resulting moment evolution equations (e.g. *Cox and Miller*, 1965). These calculations are provided in the appendix Sec. D.3, where the mean bedload velocity is derived as

$$\langle u \rangle = \frac{\Gamma}{\nu(1-\varepsilon)} = \frac{\tilde{\Gamma}}{1-\varepsilon}. \quad (5.11)$$

This result scales linearly with the mean fluid drag and nonlinearly with the rate and typical elasticity of collisions, indicating a strong influence of particle collisions on bedload velocities. The second moment is

$$\langle u^2 \rangle = 2\frac{\tilde{D} + \tilde{\Gamma}\langle u \rangle}{1-\varepsilon^2}, \quad (5.12)$$

leading to the velocity variance ($\sigma_u^2 = \langle u^2 \rangle - \langle u \rangle^2$)

$$\sigma_u^2 = \frac{2\tilde{D} + \tilde{\Gamma}^2}{1 - \varepsilon^2}. \tag{5.13}$$

This result demonstrates that within the model, velocity fluctuations originate from both the steady and fluctuating components of the flow forces, yet the variance is linear in these factors and is therefore relatively insensitive to the fluid flow. This is consistent with the similarities apparent between viscous and turbulent flow experiments (e.g. *Charru et al.*, 2004; *Lajeunesse et al.*, 2010). In contrast, particle velocity fluctuations in Eq. 5.13 depend sharply on the parameters representing particle-bed collisions, suggesting collisions could be the leading control on particle velocity fluctuations.

Fig. 5.2 depicts the velocity characteristics of particles for different realizations of the fluid and collisional forces. Fig. 5.2 reveals an apparent transition from exponential to Gaussian-like velocity distributions as collisions vary from more inelastic ($\varepsilon \to 0$) to more elastic ($\varepsilon \to 1$). In between, the full distribution Eq. 5.9 resembles a Gamma distribution, although it is represented by Eq. 5.9, not a Gamma distribution.

5.3.2 Exponential and Gaussian regimes: Limits to earlier work

In fact, the apparent transition from exponential to Gaussian in Fig. 5.2 can be demonstrated analytically from Eq. 5.9. Despite its complex appearance, simple Gaussian and exponential forms derive from this equation as exact mathematical limits. When particle-bed collisions are completely inelastic ($\varepsilon = 0$), Eq. 5.9 becomes an exponential distribution, and when they are completely elastic ($\varepsilon = 1$), Eq. 5.9 becomes Gaussian. Fig. 5.3 demonstrates in detail the approach of the distribution toward these limits.

The exponential limit of Eq. 5.9 as $\varepsilon \to 0$ is easy to see. Taking $\varepsilon \to 0$ in Eq. 5.9, all terms in the series except for the one at $l = 0$ become exponentially small, leaving behind the same two-sided exponential distribution

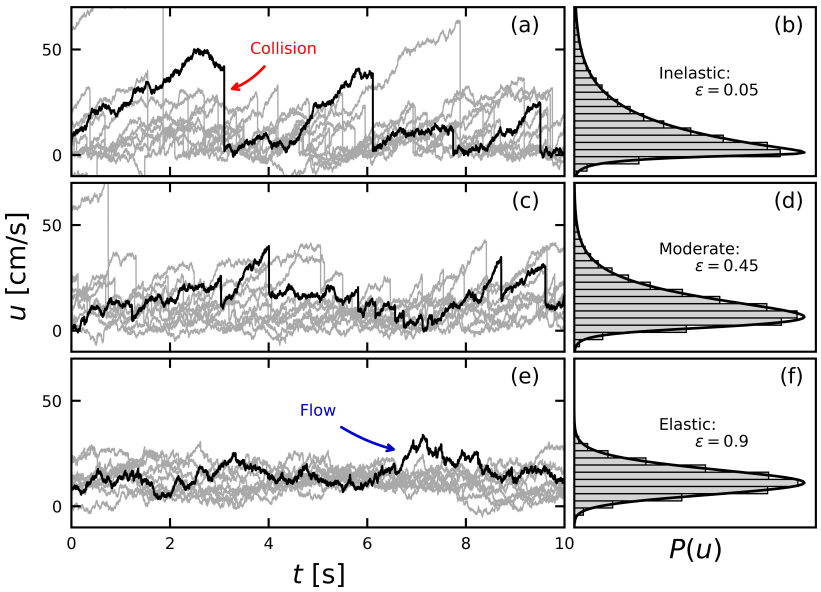

Figure 5.2: Left and right panels are paired. Left panels show velocity realizations as gray traces. Velocities are calculated from Monte Carlo simulations. Individual realizations are singled out as black traces. Particle-bed collisions imply sudden downward-velocity jumps. Flow forces generate fluctuating positive accelerations between collisions. Right panels show simulated histograms of particle velocities and exact solutions from Eq. 5.9. As the elasticity ε varies, the particle velocity distributions interpolate between exponential (inelastic) and Gaussian (elastic) forms.

derived by *Fan et al.* (2014) up to differences in notation:

$$P(u) = \frac{\tilde{D}}{\sqrt{\tilde{\Gamma}^2 + 4\tilde{D}}} e^{\frac{\tilde{\Gamma} u}{2\tilde{D}} - \frac{\sqrt{\tilde{\Gamma}^2 + 4\tilde{D}}|u|}{2\tilde{D}}}. \tag{5.14}$$

Thus, for bedload transport conditions with typically very inelastic particle-bed collisions, we can expect exponential-like velocities and large deviations from a Gaussian behavior.

The Gaussian limit as $\varepsilon \to 1$ of Eq. 5.9 is more difficult to evaluate. The

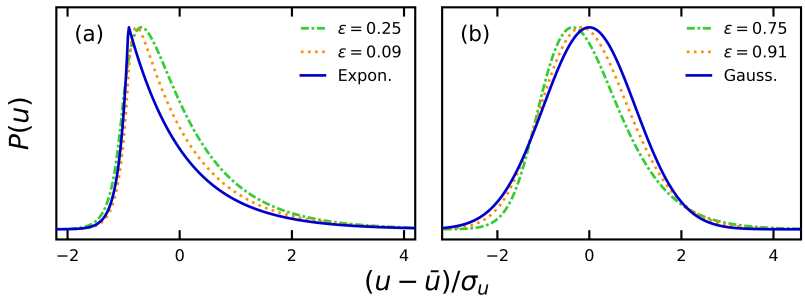

Figure 5.3: The particle velocity distribution approaches an exponential distribution in panel (a) as particle-bed collisions become extremely elastic ($\varepsilon \to 1$), and it approaches a Gaussian in panel (b) as they become extremely inelastic ($\varepsilon \to 0$). On the abscissa, the mean sediment velocity is standardized by its mean $\bar{u}$ and standard deviation σ_u.

challenge is that the statistical moments (Eqs. 5.11 and 5.13) diverge at the same time as the denominator factors of the distribution Eq. 5.9. In the appendix Sec. D.4 I return instead to the original equation 5.8 to evaluate the completely elastic limit, obtaining

$$P(u) = \frac{1}{\sqrt{2\pi\sigma_u^2}} e^{-\frac{(u-\bar{u})^2}{2\sigma_u^2}}. \tag{5.15}$$

This result is identical to the velocity distribution derived by *Ancey and Heyman* (2014), up to notation.

5.3.3 Comparison with experimental data

A variety of velocity distributions have been observed in bedload transport experiments, ranging from exponential to Gaussian in shape. This section compares Eq. 5.9 with the results of six different experiments. Comparing Eq. 5.9 with experimental data requires values for the steady component of the drag force Γ, the particle mass m, the magnitude of turbulent drag fluctuations D, the rate of particle-bed collisions ν, and the modal elasticity of collisions ε.

In each case, the particle mass is computed from experimental parameters assuming spherical sediment as $m = \pi\rho_s d^3/6$, where ρ_s is the sediment density and d is the particle diameter. The characteristic slip velocity entering the steady component of the drag force in Eq. 5.3 is not obviously related to any one velocity scale of the fluid flow. It should really be calculated as an average over different particle heights, particle velocities, and fluid velocities within the flow profile. For lack of a better option I simply assume the typical slip velocity scales with the shear velocity of the flow, as it would for a small particle resting on the bed. Using this assumption, the steady component of the drag force is estimated as

$$\Gamma = \frac{\pi}{8}\rho C_D(Re_p)d^2u_*^2, \tag{5.16}$$

where ρ is the fluid density and $C_D(Re_p)$ is the drag coefficient, given as (*Clift et al.*, 1978; *González et al.*, 2017)

$$C_D = \frac{24}{Re_p}(1 + 0.194Re_p^{0.631}). \tag{5.17}$$

Particle Reynolds numbers are estimated using the shear velocity: $Re_p = u_*d/\lambda$. The magnitude D of turbulent fluctuations, collision elasticity ε, and collision rate ν are treated as calibration parameters and are tuned to provide best fit between the distribution 5.9 and the experimental data.

The parameters for each experiment and the best-fit calibration parameters are collected in Tab. 5.1, while the results of fitting the model to the available experimental data are shown in Fig. 5.4. In each case, good agreement is obtained between the theoretical and empirical velocity distributions, suggesting that the Langevin model Eq. 5.4 captures the essential physics.

5.4 Discussion

In this final chapter I developed a Langevin description of bedload sediment transport which includes episodic collisions between particles and the bed. The model relates the shape of the instantaneous streamwise particle

Experiment	d $[mm]$	u_* $[cm/s]$	Re_p [-]	St [-]	Fr [-]	ε [-]	ν $[s^{-1}]$
(a) Fathel et al	0.5	2.0	9.97	2.9	0.3	0.08	24.
(b) Lajeu. et al	2.2	4.4	99.	29.	1.5	0.21	2.6
(c) Liu et al	1.1	8.6	94.	29.	0.3	0.28	34.
(d) Heyman et al	6.4	9.7	620.	180.	1.3	0.96	13.
(e) Ancey et al	8.0	7.4	590.	170.	2.1	0.92	4.8
(f) Martin et al	7.1	5.8	410.	120.	3.7	0.89	2.1

Table 5.1: Parameters used to fit the distributions in Fig. 5.4. The first five columns involve data from the experiments for particle diameter d, shear velocity u_*, particle Reynolds number Re_p, Stokes number St, and Froude number Fr. The final two columns involve values that were tuned to fit Eq. 5.9, the elasticity ε and the collision rate ν. Units are indicated in square brackets. One can see a generally increasing relationship between particle size and elasticity, and likewise a decreasing relationship between particle size and collision frequency.

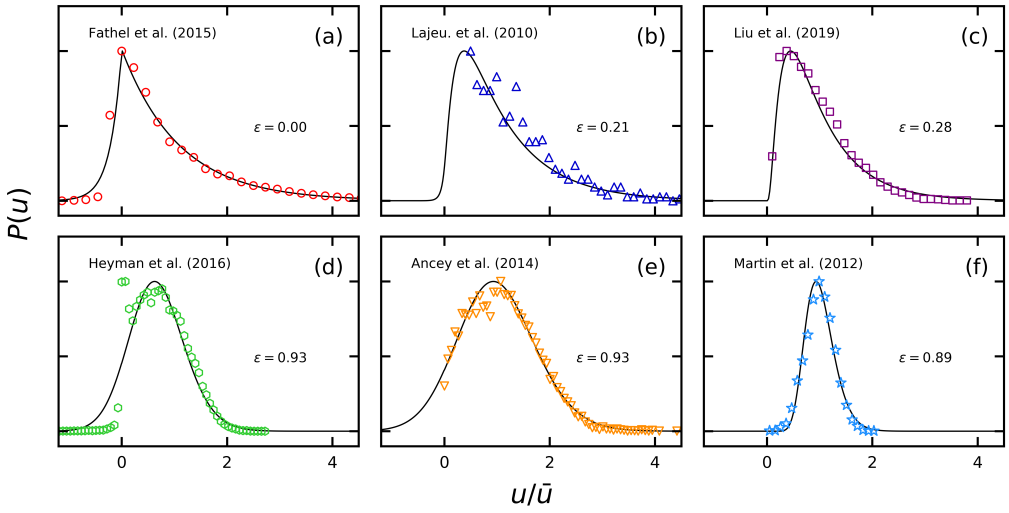

Figure 5.4: The available experimental data on velocity distributions is compared to Eq. 5.9 with calibration parameters ν, ε, and D. In all cases there is good agreement, indicating that the model produces the range of distributions seen in the experimental data.

velocity distribution to the elasticity of particle-bed collisions. This work generalizes earlier approaches available in the literature which did not include episodic collisions (*Ancey and Heyman*, 2014; *Fan et al.*, 2014), and provides a new physical explanation for the different streamwise sediment velocity distributions resolved in experiments.

Although in reality, the turbulent forces on moving sediment particles vary in a complex spatio-temporal way, I have approximated the fluid forces on bedload particles as spatially-uniform Gaussian white noise for reasons of analytical tractability (e.g. *Michaelides*, 1997). Even though the non-Gaussian, space- and time-varying, and history-dependent aspects of fluid turbulence certainly do impact sediment movement (*Cameron et al.*, 2020; *Celik et al.*, 2014), this flow model appears more or less justified since sediment transport experiments provide similar velocity distributions regardless of whether the flow is laminar or turbulent (*Charru et al.*, 2004; *Lajeunesse et al.*, 2010), and since particle relaxation times are typically large compared to the timescales of turbulent fluctuations (*Hofland and Battjes*, 2006; *Nakagawa and Tsujimoto*, 1981; *Schmeeckle et al.*, 2007). Nevertheless, it is possible that the vertical flow structure, and in particular the size of particles in comparison to the thickness of the laminar sub-layer, may be explanatory of the different velocity distributions resolved in bedload transport experiments, and future studies should investigate this possibility.

The model developed in this chapter described particle-bed collision forces as a sequence of instantaneous impulses in an approach that is reminiscent of the kinetic theory of gases (*Brilliantov and Poschel*, 2004; *Landau and Lifshitz*, 1969). The effect of each collision on the streamwise particle velocity was described by a simple elasticity-like coefficient. Although such approximate descriptions of particle-particle collisions are common in the theory of granular gases, the elasticity coefficient introduced here is not equivalent to the "coefficient of restitution" typically applied in granular gas theory. The coefficient of restitution is defined normal to the contact plane of two particles during a collision, and it characterizes energy loss due to deformation of the colliding particles in the absence of a viscous fluid (*Brach and Dunn*, 1992; *Ismail and Stronge*, 2008).

In bedload transport, colliding particles are submerged in a viscous fluid, and this introduces additional damping processes besides particle deformation (*Joseph et al.*, 2001; *Schmeeckle et al.*, 2001; *Yang and Hunt*, 2006). The model developed here does not consider these viscous forces, nor does it explicitly model the geometry of collisions, as ε was defined as a parameter applying to the downstream velocity only. Thus, although I have included episodic particle-bed collisions in a stochastic sediment transport model for the first time, the key parameter ε in this formulation has a rather heuristic character and is not clearly related to the coefficient of restitution from granular gas theory. Future studies should formulate particle-bed collisions in stochastic sediment transport models considering more details of collision geometry (*Sekine and Kikkawa*, 1992), fluid-particle interactions (*Marshall*, 2011), and traditional restitution (*Brach*, 1989) using the stochastic methods in the present study as a starting point.

5.4.1 Does the velocity distribution depend on particle size?

Several researchers have considered why particle velocity distributions differ from one experiment to the next. A prevailing view is that it relates to flow hydraulics (*Wu et al.*, 2020). Many of the experiments producing Gaussian velocity distributions were conducted in supercritical flows (e.g. *Ancey and Heyman*, 2014; *Heyman et al.*, 2016; *Martin et al.*, 2012), whereas many producing exponential distributions were conducted in subcritical flows (e.g. *Charru et al.*, 2004; *Fathel et al.*, 2015; *Seizilles et al.*, 2014). However several experiments run counter to this hypothesis. The experiments of *Lajeunesse et al.* (2010) produced distinctly exponential velocity distributions in flows well within the supercritical regime ($Fr = 1.5$), whereas *Liu et al.* (2019) produced Gamma-like distributions in the subcritical regime ($Fr = 0.3$).

An alternative viewpoint, formulated in this chapter, is that the shape of the velocity distribution originates mainly from granular interactions. Particle size enters the Langevin model Eq. 5.4 explicitly within the steady component of the drag, but it may also enter implicitly through the elasticity parameter ε. The analytical velocity distribution Eq. 5.9 was fit to six

different experimental datasets in Fig. 5.4, and the best fit parameters were presented in Tab. 5.1. These fit parameters suggest collisions are generally less elastic for smaller particle sizes, whereas they are more elastic for larger particle sizes. This suggests that the amount of momentum dissipated by collisions may depend on particle size.

Because the elasticity ε lumps together collision geometry and dissipation effects, it is challenging to attribute the increasing relationship between elasticity and particle size evident in Tab. 5.1 directly to particle size. Yet this would be consistent with experiments of idealized particle collisions in viscous fluids. These demonstrate that momentum dissipation varies sharply with particle size, being more elastic for large particles, and less elastic for small particles (*Joseph et al.*, 2001; *Schmeeckle et al.*, 2001; *Yang and Hunt*, 2006), exactly like the trend in the table. A definite conclusion that particle size controls the shape of the bedload velocity distribution requires additional experimental and theoretical study. This work nevertheless produces suggestive ideas.

5.5 Summary

This chapter has presented a Langevin description of individual bedload particles saltating downstream through episodic collisions. The model suggests that episodic particle-bed collisions control the shape of the particle velocity distribution, and it is the first model to describe the range of bedload velocity distributions which have to date been reported in experimental studies.

This work suggests that particle-bed collisions may be a leading order control over the velocity distributions of bedload particles, although future study is required for a definite conclusion. The next steps are to build up the episodic collision model presented in this chapter to include the geometric details of particle-bed collisions and to introduce slip velocity dependence and vertical structure into the flow forces acting on moving particles. These efforts would produce additional insight into the controls of fluid turbulence and transverse, vertical, and rotational movements on the downstream ve-

locities of individual bedload grains.

Chapter 6

Summary and future work

This thesis has described bedload transport from the statistical physics of individual grains. This work describes the movements of grains along a wider range of timescales than before, highlights Langevin equations, master equations, and random walks as the common threads of stochastic sediment transport modeling, and provides more realistic descriptions of bedload transport. In particular, within the thesis I have

1. developed the linkage between sediment flux probability distributions and individual particle trajectories (Ch. 2),
2. described particle trajectories alternating through motion and rest with fluctuating velocities (Ch. 2),
3. evaluated the control of bed elevation changes over sediment transport rates (Ch. 3),
4. characterized how long particles can remain buried within the sedimentary bed (Ch. 3),
5. incorporated the process of sediment burial in a description of downstream particle movement (Ch. 4), and
6. formulated the velocity distributions of sediment particles including episodic particle-bed collisions (Ch. 5).

These developments bring us closer to a comprehensive mathematical description of sediment transport in streams and bring powerful physics and mathematics tools to longstanding problems in river science.

6.1 Overall methodology of the thesis

6.1.1 Langevin and master equations

The overarching strategy in all of these developments has been to identify control and response variables, represent control variables by idealized noises (entrainment and deposition events, particle burial events, turbulent forces, or particle-bed collisions), and then formulate dynamical equations relating the response variables to these stochastic control variables. This strategy phrases sedimentary dynamics in terms of Langevin-like equations, stochastic and phenomenological analogues of Newton's $F = ma$, where the acceleration a is swapped for the response variable of interest in the problem and the force F is a stochastic combination of the control variables.

Once the stochastic dynamical equations were written for a given problem, its solutions were averaged over realizations of the control variables to produce a master equation for the problem, an integro-differential equation governing the probability distributions of the response variables.

The solutions of the master equation in a given problem provide the probability distribution for the response variable of interest, which in the thesis has included at different points the bedload particle position (Chs. 2 and 4), the particle velocity (Ch. 5), the bed elevation (Ch. 3), and the sediment transport rate (Ch. 2). The same stochastic strategy should be applicable to a wide range of problems in geomorphology where phenomena can be built up from component parts with apparently noisy characteristics.

6.1.2 Idealized noises and their combinations

A major challenge in this research is that only a handful of noises in statistical physics are comprehensively understood (*Horsthemke and Lefever*, 1984), so the available options in stochastic modeling are constrained. The

noises used in this thesis include Gaussian white noise, Poisson pulse noise, and dichotomous noise, representing erratic fluctuations, sequences of spikes, and random switches respectively (*Van Den Broeck*, 1983). Turbulence was described using Gaussian white noise, while instantaneous steps, particle arrivals to a control surface, and particle-bed collisions were described with Poisson noise. Alternation between motion and rest was represented by dichotomous noise. Whenever these processes acted in combination, the dynamical equations describing the response variable included multiple sources of idealized noise as required. This inclusion of multiple noise sources has not yet to my knowledge been pursued in any earlier stochastic models of sediment transport.

River science offers no guarantee that these idealized noise sources which we happen to understand best are sufficient to describe its phenomena. White noises in particular are an idealization which is probably never realized in nature (*Gardiner*, 1983; *Kubo et al.*, 1978). In contrast, colored noises in which fluctuations have favored frequencies are well-known to occur in many fluid and granular physics phenomena, most famously in fluid turbulence (*Kolmogorov*, 1941; *Nikora and Goring*, 2002) and granular collapse (*Bak et al.*, 1987; *Jensen*, 1998). In river science, many phenomena exhibit colored spectra, including the size distributions of bedforms (*Guala et al.*, 2014; *Nikora et al.*, 1997), the fluid forces on bed particles (*Amir et al.*, 2014; *Dwivedi et al.*, 2011), the roughness characteristics of gravel beds (*Aberle and Nikora*, 2006; *Singh et al.*, 2012), and sediment flux timeseries (*Chartrand and Furbish*, 2021; *Dhont and Ancey*, 2018). Unfortunately, dynamical equations driven by colored noise are extremely challenging to solve, so progress has been mainly limited to dichotomous and Ornstein-Uhlenbeck noises (*Hänggi*, 1978; *Hänggi and Jung*, 1995; *Łuczka*, 2005). In this context, even if the idealized noise models developed in this thesis are not exactly accurate, their development remains necessary as a basis for comparison when formulating and solving more challenging colored noise models (e.g. *Fox*, 1986; *Moss and McClintock*, 1989).

6.2 Key contributions

6.2.1 Calculation of the probability distribution of the sediment flux from individual particle trajectories

The first major contribution of this thesis is in Ch. 2. Here, I formulated the probability distribution of the sediment flux from the trajectories of individual particles moving downstream. This work unifies the sediment trajectory models originating from Einstein (Secs. 1.1.2 and 1.1.3) with the renewal approach to calculate the sediment flux (Sec. 1.1.14). The striking feature of this formulation is that, as a result of the particle dynamics, the mean bedload flux becomes scale-dependent, whereby the expected magnitude of the flux depends on the timescale over which it is observed.

Ballio et al. (2018) explained that scale-dependence originates from individual particle trajectories, but this had not been described in a mathematical model until now. Descriptions of the mean sediment flux from the movement characteristics of individual grains have existed now for a long time (Sec. 1.1.8), and an emerging body of research has produced the full probability distribution of the flux without referencing individual movement characteristics (Secs. 1.1.13 and 1.1.14). This work unifies these two research themes and provides a statistical mechanics formulation of the bed load sediment flux probability distribution based on individual particle trajectories.

6.2.2 Inclusion of velocity fluctuations into Einstein's model of individual particle trajectories

Second, in Ch. 2 I developed the first analytical description of sediment trajectories through motion and rest including velocity fluctuations within the motion state. Einstein originally formulated sediment transport as a sequence of instantaneous steps and rests (Sec. 1.1.2), and this was later improved to include the duration of motion (Sec. 1.1.3). Until this thesis, movement velocities in analytical models were considered constant, an unrealistic assumption. Although some numerical models have described

motion/rest cycles with velocity fluctuations (*Bialik et al.*, 2012; *Fan et al.*, 2016; *Schmeeckle*, 2014), they had not resolved the novel three-range diffusion characteristics these dynamics imply.

This description predicts multiple-range diffusion across local, intermediate, and global scales as a result of particle velocity fluctuations within the motion state; it introduces a dimensionless Péclet number as an important characteristic of bedload sediment transport; and it relates the timescales at which transitions between local, intermediate, and global timescales occur to the movement characteristics of individual grains. These developments constitute new understanding of bedload movement across its timescales and invite generalizations that include interactions between particles and temporal correlations to bedload movement velocities.

6.2.3 Quantification of the control of bed elevation fluctuations over sediment transport fluctuations

Third, Ch. 3 modified the birth-death description of bedload transport (Sec. 1.1.13) to include feedbacks between the local bed elevation and the entrainment and deposition rates. This allowed for a mathematical investigation of (1) how bed elevation changes affect sediment transport rates and (2) how bed elevation changes control the residence times of particles buried in the bed.

Sediment transport fluctuations have come under increasing scrutiny with the resurgence of stochastic modeling in sediment transport, while the burial times of particles are crucial for using sediment tracers to predict sediment transport. Earlier birth-death models had generally considered that entrainment and deposition rates of particles remain constant even though these processes imply bed degradation and aggradation respectively, which are known to modify the entrainment and deposition rates in a negative feedback.

This work demonstrates that this negative feedback buffers bedload transport fluctuations whenever collective entrainment occurs, meaning the magnitude of bedload transport fluctuations depends on the relative bed elevation. The residence times of buried particles are random variables that

lie on heavy-tailed power-law distributions. These distributions allow for arbitrarily long resting times, which poses challenging implications for researchers attempting to determine downstream sediment fluxes from sediment tracer data.

6.2.4 Characterization of sediment burial controls on the downstream transport of sediment particles

Fourth, Ch. 4 presents a model of sediment trajectories through motion, rest, and burial, describing sediment transport across local, intermediate, global, and geomorphic ranges (Sec. 1.1), and producing new understanding of how exactly the distinct spreading characteristics of particles within each of these ranges arise (e.g *Pretzlav et al.*, 2021).

Until this work, the mechanisms which produce the different spreading rates of particles across the scaling ranges identified by Nikora and coworkers had been uncertain for several decades, and earlier works had included what were believed to be the required features without describing three or more scaling ranges. Ch. 4 brings some closure to these studies and demonstrates that many approaches to describe individual particle motions are particular adaptations of the continuous time random walk formalism from physics, indicating unity within a diverse body of research and bringing powerful tools from statistical physics to the sediment transport problem.

6.2.5 Description of how particle-bed collisions control movement velocities of grains

Finally, Ch. 5 displayed a new theoretical model of individual grains saltating downstream in a turbulent flow through a sequence of particle-bed collisions. This work provides the first comprehensive description of all bedload velocity distributions sar far observed in experiments (Sec. 5.3.3), while earlier works had described only particular end-member distributions (Sec. 1.1.5). This work incorporates ideas from the kinetic theory of granular gases into the description of weak bedload transport and invites generalizations that explicitly include the geometry of particle-particle collisions and

more realistic particle height and slip velocity-dependent fluid forces.

6.3 Limitations and future research directions

This thesis has produced new understanding of how to describe bedload transport using statistical physics, but the developments introduce many limitations deserving of future research attention. In some cases these are specific to the models produced in the thesis, but in others, they are shared in common with a majority of models in the stochastic sediment transport research paradigm (e.g. *Ancey*, 2020a; *Furbish and Doane*, 2021).

6.3.1 Channel morphodynamics

The first limitation concerns the assumption, implicit in every chapter of this thesis, that sediment transport characteristics are steady and uniform in time and space. This assumption contrasts with conditions in real gravel-bed rivers, where riffles, bars, and steps coordinate the movements of individual grains (*Ashmore and Church*, 1998; *McDowell and Hassan*, 2020), sediment is supplied in episodic bursts from mass movements (*Benda*, 1990; *Müller and Hassan*, 2018), woody debris directs sediment accumulation (*Eaton et al.*, 2012; *Reid et al.*, 2019), and variable flow conditions modify bed texture and sediment availability (*Mao*, 2012; *Phillips et al.*, 2018).

To date, very little work has concentrated on developing stochastic sediment transport models for unsteady conditions (e.g. *Bohorquez and Ancey*, 2016). The most obvious scheme to address unsteadiness is to introduce time and space dependence to movement velocities, diffusivities, or entrainment and deposition rates, but how exactly one should express these rates in terms of time and space is a matter for speculation. These expressions would be contingent on a given context, given our limited understanding of how these parameters relate to the flow hydraulics and granular physics (e.g. *Heyman et al.*, 2016).

Future studies might investigate in more depth the linkage between flow hydraulics, the geometric arrangement of grains on the bed, and the bed topography with the entrainment and deposition rates of individual particles

to develop our foundational knowledge to later incorporate temporally or spatially variable flow and sedimentary conditions into stochastic models of sediment transport.

6.3.2 Grain size distributions

The second limitation of this work concerns grain size. Sediments in rivers span a range of sizes, and differential mobility based on particle size produces spatial sorting, both vertically as in bed armoring (*Aberle and Nikora*, 2006; *Parker and Klingeman*, 1982; *Wilcock and Southard*, 1989), and laterally as patch, particle cluster, or riffle development (*Nelson et al.*, 2014; *Venditti et al.*, 2017).

Only a few works on stochastic modeling of sediment transport involve multiple grain sizes (*Parker et al.*, 2000; *Sun and Donahue*, 2000), but these approaches are not spatially distributed, so there is as yet no stochastic method to understand sorting processes (cf. *Ancey*, 2020b).

Future studies should revisit the stochastic framework applied to multiple grain sizes. Simplified experimental geometries based on bimodal sediment beds (e.g. *Houssais and Lajeunesse*, 2012) would be a great context to revisit these issues. Extending the motion-rest model of Ch. 3 to two grain sizes with a matrix formulation, then calibrating its parameters to experiments would be a nice starting point.

6.3.3 The full range of geophysical flows

The final limitation I will mention is that all of the efforts in this thesis were concentrated on weak bedload transport, where densities of moving particles are low enough that they may interact with the static bed but never with each other. This assumption is justified insofar as weak bedload transport conditions are common within gravel-bed rivers (*Ashworth and Ferguson*, 1989; *Warburton*, 1992), but it is nonetheless a limitation given the diversity of processes which move sediment over Earth's surface.

Earth's landforms are shaped by numerous transport phenomena from catastrophic debris flows (*Iverson*, 1997) to barely perceptible hillslope creep

(*Deshpande et al.*, 2021). Different transport phenomena are basically distinguished by the relative importance of fluid, granular, and gravitational forces in sustaining them (*Jerolmack and Daniels*, 2019).

Weak bedload transport is characterized by fluid forces small in comparison to gravity, and collision forces comparable to gravity. Viewed in this way, the work in this thesis targets a minute region of the vast parameter space spanned by Earth's geophysical flows, and geomorphology requires characterization of them all. Future studies should continue the effort (e.g. *Furbish and Doane*, 2021) to describe these processes as different expressions of the same basic statistical mechanics building blocks.

6.4 Conclusion

This thesis has described the movements of individual grains along streambeds using probabilistic methods. The research relates the overall sediment transport rate to the movements of individual grains. At base level, the thesis embraces variability as an intrinsic part of Earth surface dynamics, and it produces descriptions of sediment transport which predict mean values as well as the magnitude of their fluctuations.

The founders of process geomorphology always acknowledged the role of variability in landscape evolution (*Horton*, 1945; *Langbein and Leopold*, 1964; *Strahler*, 1952), although their main efforts were to develop strategies to describe landscapes without including variability, like averaged shear stresses to avoid fluid turbulence (*Bagnold*, 1954; *Meyer-Peter and Müller*, 1948), competent conditions to replace climatic fluctuations (*Wolman and Gerson*, 1978; *Wolman and Miller*, 1960), and representative grain sizes to avoid evolving surface grain size distributions (*Andrews*, 1983; *Parker and Klingeman*, 1982).

The stochastic descriptions of sediment transport developed in this thesis show a methodology we can use to step beyond averaged descriptions of geomorphic change, propagate noises through the equations governing landscape change, and revisit the old question in geomorphology: How does variability shape Earth's surface?

Bibliography

Abbott, J. E., and J. R. Francis, Saltation and suspension trajectories of solid grains in a water stream, *Proc. Roy. Soc. London, Series A.*, *284*, 225–254, 1977. → page 9

Aberle, J., and V. Nikora, Statistical properties of armored gravel bed surfaces, *Water Resources Research*, *42*, 1–11, 2006. → pages 73, 76, 115, 120

Abramian, A., O. Devauchelle, G. Seizilles, and E. Lajeunesse, Boltzmann distribution of sediment transport, *Physical Review Letters*, *123*, 14,501, 2019. → page 93

Abramian, A., O. Devauchelle, and E. Lajeunesse, Laboratory rivers adjust their shape to sediment transport, *Physical Review E*, *102*, 2020. → page 93

Allen, B., and A. Kudrolli, Granular bed consolidation, creep, and armoring under subcritical fluid flow, *Physical Review Fluids*, *7*, 1–13, 2018. → pages 2, 17

Amir, M., V. I. Nikora, and M. T. Stewart, Pressure forces on sediment particles in turbulent open-channel flow: A laboratory study, *Journal of Fluid Mechanics*, *757*, 458–497, 2014. → pages 2, 74, 115

Ancey, C., Bedload transport: A walk between randomness and determinism. Part 1. The state of the art, *Journal of Hydraulic Research*, *58*, 1–17, 2020a. → pages 2, 27, 34, 48, 49, 53, 119

Ancey, C., Bedload transport: A walk between randomness and determinism. Part 2. Challenges and prospects, *Journal of Hydraulic Research*, *58*, 18–33, 2020b. → pages 3, 120

Ancey, C., and J. Heyman, A microstructural approach to bed load transport: Mean behaviour and fluctuations of particle transport rates, *Journal of Fluid Mechanics*, *744*, 129–168, 2014. → pages 12, 13, 25, 30, 31, 34, 35, 49, 93, 94, 99, 100, 101, 106, 109, 110

Ancey, C., and I. Pascal, Estimating mean bedload transport rates and their uncertainty, *Journal of Geophysical Research: Earth Surface*, *125*, 1–29, 2020. → pages 25, 27, 30, 35, 93

Ancey, C., T. Böhm, M. Jodeau, and P. Frey, Statistical description of sediment transport experiments, *Physical Review E*, *74*, 1–14, 2006. → pages 10, 11, 18, 24, 25, 26, 34, 48, 54, 55, 56, 80, 88

Ancey, C., A. C. Davison, T. Böhm, M. Jodeau, and P. Frey, Entrainment and motion of coarse particles in a shallow water stream down a steep slope, *Journal of Fluid Mechanics*, *595*, 83–114, 2008. → pages xiii, xix, 17, 25, 31, 35, 49, 56, 57, 58, 59, 60, 62, 63, 64, 67, 68, 72, 73, 74, 169

Ancey, C., P. Bohorquez, and J. Heyman, Stochastic interpretation of the advection-diffusion, *Journal of Geophysical Research : Earth Surface*, *120*, 325–345, 2015. → page 74

Andreotti, B., Y. Forterre, and O. Pouliquen, *Granular Media: Between Fluid and Solid*, 1st ed., Cambridge University Press, New York, 2013. → page 95

Andrews, E. D., Entrainment of gravel from naturally sorted riverbed material., *Geological Society of America Bulletin*, *94*, 1225–1231, 1983. → page 121

Arfken, G., *Mathematical Methods for Physicists*, Academic Press, Inc., San Diego, 1985. → pages 8, 82, 159, 160, 161, 163, 172, 174, 175

Armanini, A., *Principles of River Hydraulics*, Springer, Cham, 2017. → page 19

Armanini, A., V. Cavedon, and M. Righetti, A probabilistic/deterministic approach for the prediction of the sediment transport rate, *Advances in Water Resources*, *81*, 10–18, 2015. → page 19

Armenio, V., and V. Fiorotto, The importance of the forces acting on particles in turbulent flows, *Physics of Fluids*, *13*, 2437–2440, 2001. → page 98

Ashley, T. C., S. Naqshband, and B. McElroy, Lower-stage plane bed topography is an outcome of rarefied, intermittent sediment transport, *Journal of Geophysical Research: Earth Surface*, *126*, 1–21, 2021. → page 35

Ashmore, P. E., and M. Church, Sediment transport and river morphology: A paradigm for study, in *Gravel-bed Rivers in the Environment*, pp. 115–148, Water Resources Publications, Highlands Ranch, CO, 1998. → page 119

Ashworth, P. J., and R. I. Ferguson, Size-selective entrainment of bed load in gravel bed streams, *Water Resources Research*, *25*, 627–634, 1989. → pages 95, 120

Auton, T. R., The lift force on a spherical body in a rotational flow, *Journal of Fluid Mechanics*, *183*, 199–218, 1987. → page 98

Azéma, E., and F. Radjaï, Force chains and contact network topology in sheared packings of elongated particles, *Physical Review E*, *85*, 1–12, 2012. → page 49

Bagnold, R. A., Experiments on a gravity-free dispersion of large solid spheres in a Newtonian fluid under shear, *Proc. Roy. Soc. London, Series A.*, *225*, 49–63, 1954. → pages 16, 121

Bagnold, R. A., The flow of cohesionless grains in fluids, *Proc. Roy. Soc. London, Series A.*, *249*, 235–297, 1956. → pages 2, 16

Bagnold, R. A., An approach to the sediment transport problem from general physics, *Tech. Rep. 4*, U.S. Geological Survey, Washington, DC, 1966. → page 16

Bagnold, R. A., The nature of saltation and of 'bed-load' transport in water, *Proc. Roy. Soc. London, Series A.*, *332*, 473–504, 1973. → page 16

Bak, P., C. Tang, and K. Wiesenfeld, Self-organized criticality: An explanation of the 1/f noise, *Physical Review Letters*, *59*, 381–384, 1987. → page 115

Balakrishnan, V., On a simple derivation of master equations for diffusion processes driven by white noise and dichotomic Markov noise, *Pramana*, *40*, 259–265, 1993. → pages 7, 10, 157, 158

Ballio, F., V. Nikora, and S. E. Coleman, On the definition of solid discharge in hydro-environment research and applications, *Journal of Hydraulic Research*, *52*, 173–184, 2014. → pages 14, 16

Ballio, F., D. Pokrajac, A. Radice, and S. A. Hosseini Sadabadi, Lagrangian and Eulerian description of bed load transport, *Journal of Geophysical Research: Earth Surface*, *123*, 384–408, 2018. → pages 14, 24, 116

Banerjee, T., S. N. Majumdar, A. Rosso, and G. Schehr, Current fluctuations in noninteracting run-and-tumble particles in one dimension, *Physical Review E*, *101*, 1–16, 2020. → page 39

Barabasi, A.-L., and H. E. Stanley, *Fractal Concepts in Surface Growth*, 1st ed., Cambridge University Press, Cambridge, 1995. → page 52

Barik, D., P. K. Ghosh, and D. S. Ray, Langevin dynamics with dichotomous noise; Direct simulation and applications, *Journal of Statistical Mechanics: Theory and Experiment*, 2006. → pages xvii, 43, 84

Barry, J. J., J. M. Buffington, and J. G. King, A general power equation for predicting bed load transport rates in gravel bed rivers, *Water Resources Research*, *40*, 1–22, 2004. → page 2

Bateman, H., and A. Erdelyi, *Higher Transcendental Functions*, McGraw-Hill, New York, 1953. → page 161

Bathurst, J. C., Effect of coarse surface layer on bed-load transport, *Journal of Hydraulic Engineering*, *133*, 1192–1205, 2007. → page 2

Bena, I., Dichotomous Markov noise: Exact results for out-of-equilibrium systems, *International Journal of Modern Physics B*, *20*, 2825–2888, 2006. → pages 9, 50

Benavides, S. J., E. A. Deal, M. Rushlow, J. G. Venditti, K. Kamrin, and J. T. Perron, The impact of intermittency on bed load sediment transport, *Unpublished*, 2021. → page 49

Benda, L., The influence of debris flows on channels and valley floors in the Oregon coast range, USA, *Earth Surface Processes and Landforms*, *15*, 457–466, 1990. → page 119

Bennett, C. H., Serially deposited amorphous aggregates of hard spheres, *Journal of Applied Physics*, *43*, 2727–2734, 1972. → pages 58, 62

Berezhkovskii, A. M., and G. H. Weiss, Detailed description of a two-state non-Markov system, *Physica A: Statistical Mechanics and its Applications*, *303*, 1–12, 2002. → page 172

Berkowitz, B., A. Cortis, M. Dentz, and H. Scher, Modeling non-Fickian transport in geological formations as a continuous time random walk, *Reviews of Geophysics*, *44*, 1–49, 2006. → page 6

Bialik, R. J., V. I. Nikora, and P. M. Rowiński, 3D Lagrangian modelling of saltating particles diffusion in turbulent water flow, *Acta Geophysica*, *60*, 1639–1660, 2012. → pages 79, 88, 117

Bialik, R. J., V. I. Nikora, M. Karpiński, and P. M. Rowiński, Diffusion of bedload particles in open-channel flows: Distribution of travel times and second-order statistics of particle trajectories, *Environmental Fluid Mechanics*, *15*, 1281–1292, 2015. → pages 37, 79

Böhm, T., C. Ancey, P. Frey, J. L. Reboud, and C. Ducottet, Fluctuations of the solid discharge of gravity-driven particle flows in a turbulent stream, *Physical Review E*, *69*, 13, 2004. → page 24

Böhm, T., C. Ancey, P. Frey, M. Jodeau, and J. L. Reboud, Experiments on gravity-driven particle flows in a turbulent stream, *Powders and Grains 2005 - Proceedings of the 5th International Conference on Micromechanics of Granular Media*, *2*, 1001–1004, 2005. → page 34

Bohorquez, P., and C. Ancey, Particle diffusion in non-equilibrium bedload transport simulations, *Applied Mathematical Modelling*, *40*, 7474–7492, 2016. → pages 93, 119

Brach, R. M., Rigid body collisions, *American Society of Mechanical Engineers*, *56*, 133–138, 1989. → pages 95, 96, 110

Brach, R. M., and P. F. Dunn, A mathematical model of the impact and adhesion of microsphers, *Aerosol Science and Technology*, *16*, 51–64, 1992. → page 109

Bradley, D. N., Direct observation of heavy-tailed storage times of bed load tracer particles causing anomalous superdiffusion, *Geophysical Research Letters*, *44*, 12,227–12,235, 2017. → pages 5, 31, 55, 75, 78, 88, 89, 90

Bradley, D. N., G. E. Tucker, and D. A. Benson, Fractional dispersion in a sand bed river, *Journal of Geophysical Research: Earth Surface*, *115*, F00A09, 2010. → pages 88, 89

Brilliantov, N. V., and T. Poschel, *Kinetic Theory of Granular Gases*, 1st ed., Oxford University Press, Oxford, 2004. → pages 32, 50, 95, 101, 109

Bunte, K., S. R. Abt, J. P. Potyondy, and S. E. Ryan, Measurement of coarse gravel and cobble transport using portable bedload traps, *Journal of Hydraulic Engineering*, *130*, 879–893, 2004. → page 25

Cameron, S. M., V. I. Nikora, and M. J. Witz, Entrainment of sediment particles by very large-scale motions, *Journal of Fluid Mechanics*, *888*, 2020. → pages 4, 49, 109

Campagnol, J., A. Radice, and F. Ballio, Scale-based statistical analysis of sediment fluxes, *Acta Geophysica*, *60*, 1744–1777, 2012. → page 25

Campagnol, J., A. Radice, F. Ballio, and V. Nikora, Particle motion and diffusion at weak bed load: Accounting for unsteadiness effects of entrainment and disentrainment, *Journal of Hydraulic Research*, *53*, 633–648, 2015. → page 51

Cardy, J., Reaction-diffusion processes, in *Non-Equilibrium Statistical Physics and Turbulence*, edited by S. Nazarenko and O. V. Zaboronski, pp. 108–161, Cambridge University Press, Cambridge, 2008. → page 50

Celik, A. O., P. Diplas, C. L. Dancey, and M. Valyrakis, Impulse and particle dislodgement under turbulent flow conditions, *Physics of Fluids*, *22*, 1–13, 2010. → page 54

Celik, A. O., P. Diplas, and C. L. Dancey, Instantaneous pressure measurements on a spherical grain under threshold flow conditions, *Journal of Fluid Mechanics*, *741*, 60–97, 2014. → pages 2, 4, 33, 51, 99, 109

Chapman, S., and T. G. Cowling, *Mathematical Theory of Non-Uniform Gases*, Cambridge University Press, Cambridge, 1970. → page 95

Charru, F., Selection of the ripple length on a granular bed sheared by a liquid flow, *Physics of Fluids*, *18*, 1–9, 2006. → page 20

Charru, F., H. Mouilleron, and O. Eiff, Erosion and deposition of particles on a bed sheared by a viscous flow, *Journal of Fluid Mechanics*, *519*, 55–80, 2004. → pages 2, 4, 20, 33, 58, 74, 93, 104, 109, 110

Chartrand, S., and D. J. Furbish, The transport of sediment mixtures examined with a birth-death model for grain-size fractions, *Unpublished*, 2021. → page 115

Chartrand, S. M., A. M. Jellinek, M. A. Hassan, and C. Ferrer-Boix, Morphodynamics of a width-variable gravel bed stream: New insights on pool-riffle formation from physical experiments, *Journal of Geophysical Research: Earth Surface*, *123*, 2735–2766, 2018. → page 24

Cheng, N. S., Analysis of bedload transport in laminar flows, *Advances in Water Resources*, *27*, 937–942, 2004. → page 19

Church, M., Continental drift, *Earth Surface Processes and Landforms*, *30*, 129–130, 2005. → page 1

Church, M., Bed material transport and the morphology of alluvial river channels, *Annual Review of Earth and Planetary Sciences*, *34*, 325–354, 2006. → page 2

Church, M., The trajectory of geomorphology, *Progress in Physical Geography*, *34*, 265–286, 2010. → page 1

Church, M., and J. K. Haschenburger, What is the "active layer"?, *Water Resources Research*, *53*, 5–10, 2017. → page 60

Clark, A. H., M. D. Shattuck, N. T. Ouellette, and C. S. O'Hern, Onset and cessation of motion in hydrodynamically sheared granular beds, *Physical Review E*, *92*, 1–28, 2015. → page 12

Clark, A. H., M. D. Shattuck, N. T. Ouellette, and C. S. O'Hern, Role of grain dynamics in determining the onset of sediment transport, *Physical Review Fluids*, *2*, 2017. → pages 12, 17

Clift, R., J. R. Grace, and M. E. Weber, *Bubbles, Drops, and Particles*, Academic Press, Inc., New York, 1978. → pages 98, 107

Coleman, N. L., A theoretical and experimental study of drag and lift forces acting on a sphere resting on a hypothetical streambed, in *International Association for Hydraulic Research Congress*, pp. 185–192, Littleton, CO, 1967. → page 99

Coleman, S. E., and V. I. Nikora, Exner equation: A continuum approximation of a discrete granular system, *Water Resources Research*, *45*, 1–8, 2009. → pages 24, 52

Cox, D. R., *Renewal Theory*, Methuen, London, 1962. → page 27

Cox, D. R., and H. D. Miller, *The Theory of Stochastic Processes*, Wiley, New York, 1965. → pages 9, 19, 25, 26, 41, 44, 60, 61, 103, 165, 169

Crickmore, M., and G. Lean, The measurement of sand transport by the time-integration method with radioactive tracers, *Proc. Roy. Soc. London, Series A.*, *270*, 27–47, 1962. → page 59

Cudden, J. R., and T. B. Hoey, The causes of bedload pulses in a gravel channel: The implications of bedload grain-size distributions, *Earth Surface Processes and Landforms*, *28*, 1411–1428, 2003. → page 24

Cundall, P. A., and O. D. Strack, A discrete numerical model for granular assemblies, *Geotechnique*, *29*, 47–65, 1979. → pages 12, 79

Daly, E., and A. Porporato, Probabilistic dynamics of some jump-diffusion systems, *Physical Review E*, *73*, 1–7, 2006. → page 100

Daly, E., and A. Porporato, Effect of different jump distributions on the dynamics of jump processes, *Physical Review E*, *81*, 1–10, 2010. → page 100

De Gennes, P. G., Brownian motion with dry friction, *Journal of Statistical Physics*, *119*, 953–962, 2005. → page 13

Denisov, S. I., W. Horsthemke, and P. Hänggi, Generalized Fokker-Planck equation: Derivation and exact solutions, *European Physical Journal B*, *68*, 567–575, 2009. → page 100

Deshpande, N. S., D. J. Furbish, P. E. Arratia, and D. J. Jerolmack, The perpetual fragility of creeping hillslopes, *Nature Communications*, *12*, 1–7, 2021. → page 121

Dey, S., and S. Z. Ali, Advances in modeling of bed particle entrainment sheared by turbulent flow, *Physics of Fluids*, *30*, 2018. → page 20

Dhont, B., and C. Ancey, Are bedload transport pulses in gravel bed rivers created by bar migration or sediment waves?, *Geophysical Research Letters*, *45*, 5501–5508, 2018. → pages 24, 34, 49, 52, 56, 73, 92, 115

Drake, T. G., R. L. Shreve, W. E. Dietrich, P. J. Whiting, and L. B. Leopold, Bedload transport of fine gravel observed by motion-picture photography, *Journal of Fluid Mechanics*, *192*, 193–217, 1988. → page 9

Dubkov, A. A., and A. A. Kharcheva, Steady-state probability characteristics of Verhulst and Hongler models with multiplicative white Poisson noise, *European Physical Journal B*, *92*, 1–6, 2019. → page 100

Dubkov, A. A., O. V. Rudenko, and S. N. Gurbatov, Probability characteristics of nonlinear dynamical systems driven by δ -pulse noise, *Physical Review E*, *93*, 1–7, 2016. → page 100

Duderstadt, J. J., and W. R. Martin, *Transport Theory*, 1st ed., Wiley Interscience, New York, 1979. → page 101

Dwivedi, A., B. Melville, and A. Y. Shamseldin, Hydrodynamic forces generated on a spherical sediment particle during entrainment, *Journal of Hydraulic Engineering*, *136*, 756–769, 2010. → page 99

Dwivedi, A., B. W. Melville, A. Y. Shamseldin, and T. K. Guha, Analysis of hydrodynamic lift on a bed sediment particle, *Journal of Geophysical Research: Earth Surface*, *116*, 2011. → pages 54, 115

Dwivedi, A., B. Melville, A. J. Raudkivi, A. Y. Shamseldin, and Y. M. Chiew, Role of turbulence and particle exposure on entrainment of large spherical particles in flows with low relative submergence, *Journal of Hydraulic Engineering*, *138*, 1022–1030, 2012. → pages 2, 99

Eaton, B. C., M. A. Hassan, and S. L. Davidson, Modeling wood dynamics, jam formation, and sediment storage in a gravel-bed stream, *Journal of Geophysical Research: Earth Surface*, *117*, 1–18, 2012. → page 119

Eaton, B. C., L. G. MacKenzie, and W. H. Booker, Channel stability in steep gravel–cobble streams is controlled by the coarse tail of the bed material distribution, *Earth Surface Processes and Landforms*, *45*, 3639–3652, 2020. → page 2

Einstein, A., On the movement of small particles suspended in stationary liquids required by the molecular-kinetic theory of heat (In German), *Annalen der Physik (ser. 4)*, *17*, 549–560, 1905. → page 77

Einstein, H. A., Bed load transport as a probability problem, Ph.D. thesis, ETH Zurich, 1937. → pages xxi, 4, 5, 8, 9, 18, 30, 33, 42, 53, 54, 55, 72, 77, 78, 79, 80, 83, 85, 87, 88, 89

Einstein, H. A., Formulas for the transport of bed sediment, *Trans. Am. Soc. Civ. Eng.*, *107*, 561–574, 1942. → page 18

Einstein, H. A., The bedload function for sediment transportation in open channel flows, *Tech. rep.*, United States Department of Agriculture, Washington, DC, 1950. → pages 18, 20, 34, 54, 55, 56, 57, 58, 72

Elghannay, H., and D. Tafti, LES-DEM simulations of sediment transport, *International Journal of Sediment Research*, *33*, 137–148, 2018. → pages 12, 99

Elgueta-Astaburuaga, M. A., and M. A. Hassan, Sediment storage, partial transport, and the evolution of an experimental gravel bed under changing sediment supply regimes, *Geomorphology*, *330*, 1–12, 2019. → page 24

Engelund, F., and J. Fredsoe, A sediment transport model for straight alluvial channels., *Nordic Hydrology*, *7*, 293–306, 1976. → page 17

Escaff, D., R. Toral, C. Van Den Broeck, and K. Lindenberg, A continuous-time persistent random walk model for flocking, *Chaos*, *28*, 1–11, 2018. → pages 50, 90

Ettema, R., and C. F. Mutel, *Hans Albert Einstein: His Life as a Pioneering Engineer*, 1st ed., ASCE Press, Reston, Virginia, 2004. → pages 5, 77

Exner, F. M., About the interaction between water and bed load in rivers (In German), in *Sitzungsberichte der Akademie der Wissenschaften in Wien.*, pp. 165–207, Vienna, 1925. → page 23

Fa, K. S., Uncoupled continuous-time random walk model: Analytical and numerical solutions, *Physical Review E*, *89*, 1–9, 2014. → page 90

Fan, N., D. Zhong, B. Wu, E. Foufoula-Georgiou, and M. Guala, A mechanistic-stochastic formulation of bed load particle motions: From individual particle forces to the Fokker-Planck equation under low transport rates, *Journal of Geophysical Research: Earth Surface*, *119*, 464–482, 2014. → pages 12, 13, 31, 34, 93, 94, 99, 100, 101, 105, 109

Fan, N., A. Singh, M. Guala, E. Foufoula-Georgiou, and B. Wu, Exploring a semimechanistic episodic Langevin model for bed load transport: Emergence of normal and anomalous advection and diffusion regimes, *Water Resources Research*, *52*, 2789–2801, 2016. → pages 37, 79, 88, 117

Fathel, S., D. Furbish, and M. Schmeeckle, Parsing anomalous versus normal diffusive behavior of bedload sediment particles, *Earth Surface Processes and Landforms*, *41*, 1797–1803, 2016. → pages 78, 87, 90, 93

Fathel, S. L., D. J. Furbish, and M. W. Schmeeckle, Experimental evidence of statistical ensemble behavior in bed load sediment transport, *Journal of Geophysical Research: Earth Surface*, *120*, 2298–2317, 2015. → pages 9, 12, 33, 45, 56, 80, 93, 94, 110

Feller, W., *An Introduction to Probability Theory and its Applications*, 3rd ed., Wiley, New York, 1967. → page 101

Ferguson, R. I., and T. B. Hoey, Long-term slowdown of river tracer pebbles: Generic models and implications for interpreting short-term tracer studies, *Water Resources Research*, *38*, 17–1–17–11, 2002. → pages 4, 5, 31, 85

Ferguson, R. I., D. J. Bloomer, T. B. Hoey, and A. Werritty, Mobility of river tracer pebbles over different timescales, *Water Resources Research*, *38*, 3–1–3–8, 2002. → page 78

Ferreira, R. M. L., M. A. . Hassan, and C. Ferrer-Boix, Principles of bedload transport of non-cohesive sediment in open-channels, in *Rivers – Physical, Fluvial and Environmental Processes*, pp. 323–372, Springer, Cham, 2015. → page 2

Fox, R. F., Uniform convergence to an effective Fokker-Planck equation for weakly colored noise, *Physical Review A*, *34*, 4525–4527, 1986. → page 115

Fraccarollo, L., and M. A. Hassan, Einstein conjecture and resting-time statistics in the bed-load transport of monodispersed particles, *Journal of Fluid Mechanics*, *876*, 1077–1089, 2019. → page 88

Francis, J. R. D., Experiments on the motion of solitary grains along the bed of a water-stream, *Proc. Roy. Soc. London, Series A.*, *332*, 443–471, 1973. → page 9

Frey, P., Particle velocity and concentration profiles in bedload experiments on a steep slope, *Earth Surface Processes and Landforms*, *39*, 646–655, 2014. → page 4

Frey, P., and M. Church, Bedload: A granular phenomenon, *Earth Surface Processes and Landforms*, *36*, 58–69, 2011. → page 12

Furbish, D. J., and T. H. Doane, Rarefied particle motions on hillslopes – Part 4 : Philosophy, *Earth Surface Dynamics*, *9*, 629–664, 2021. → pages 119, 121

Furbish, D. J., and M. W. Schmeeckle, A probabilistic derivation of the exponential-like distribution of bed load particle velocities, *Water Resources Research*, *49*, 1537–1551, 2013. → page 94

Furbish, D. J., A. E. Ball, and M. W. Schmeeckle, A probabilistic description of the bed load sediment flux: 4. Fickian diffusion at low transport rates, *Journal of Geophysical Research: Earth Surface*, *117*, 1–13, 2012a. → pages 12, 14, 20, 22, 23, 78, 90

Furbish, D. J., P. K. Haff, J. C. Roseberry, and M. W. Schmeeckle, A probabilistic description of the bed load sediment flux: 1. Theory, *Journal of Geophysical Research: Earth Surface*, *117*, 2012b. → pages 15, 34, 55, 56, 58

Furbish, D. J., S. L. Fathel, and M. W. Schmeeckle, Particle motions and bedload theory: The entrainment forms of the flux and the Exner equation, in *Gravel-Bed Rivers: Process and Disasters*, edited by D. Tsutsumi and J. B. Laronne, 1st ed., chap. 4, pp. 97–120, John Wiley & Sons Ltd., 2017. → pages 22, 23, 36, 56, 78

Furbish, D. J., J. J. Roering, T. H. Doane, D. L. Roth, S. G. Williams, and A. M. Abbott, Rarefied particle motions on hillslopes - Part 1: Theory, *Earth Surface Dynamics*, *9*, 539–576, 2021. → page 95

Gaeuman, D., R. Stewart, B. Schmandt, and C. Pryor, Geomorphic response to gravel augmentation and high-flow dam release in the Trinity River, California, *Earth Surface Processes and Landforms*, *42*, 2523–2540, 2017. → pages 54, 77, 92

Gardiner, C. W., *Handbook of Stochastic Methods for Physics, Chemistry and the Natural Sciences*, Springer-Verlag, Berlin, 1983. → pages 13, 15, 61, 64, 74, 99, 100, 101, 115, 169, 183

Gilbert, G. K., The transportaton of debris by running water, *Tech. rep.*, U. S. Geological Survey, 1914. → page 2

Gillespie, D. T., Exact stochastic simulation of coupled chemical reactions, *Journal of Physical Chemistry*, *81*, 2340–2361, 1977. → pages 61, 165

Gillespie, D. T., *Markov Processes: An Introduction for Physical Scientists*, 1st ed., Academic Press, Inc., 1992. → pages 60, 61, 165

Gillespie, D. T., Stochastic simulation of chemical kinetics, *Annual Review of Physical Chemistry*, *58*, 35–55, 2007. → pages 60, 61, 62, 165

Glielmo, A., N. Gunkelmann, and T. Pöschel, Coefficient of restitution of aspherical particles, *Physical Review E*, *90*, 1–7, 2014. → page 102

Goh, K. I., and A. L. Barabási, Burstiness and memory in complex systems, *Europhysics Letters*, *81*, 2008. → page 49

Goldstein, H., *Classical Mechanics*, Addison-Wesley, Reading, 1997. → pages 7, 50

Gomez, B., and M. Church, An assessment of bed load sediment transport formulae for gravel bed rivers, *Water Resources Research*, *25*, 1161–1186, 1989. → page 2

González, C., D. H. Richter, D. Bolster, S. Bateman, J. Calantoni, and C. Escauriaza, Characterization of bedload intermittency near the threshold of motion using a Lagrangian sediment transport model, *Environmental Fluid Mechanics*, *17*, 111–137, 2017. → pages 12, 54, 94, 99, 107

Gordon, R., J. B. Carmichael, and F. J. Isackson, Saltation of plastic balls in a 'one-dimensional' flume, *Water Resources Research*, *8*, 444–459, 1972. → pages 3, 9, 33, 80, 97, 102

Gotoh, H., and T. Sakai, Numerical simulation of sheetflow as granular material, *Journal of Waterway, Port, Coastal and Ocean Engineering*, *123*, 329–336, 1997. → page 12

Grass, A., Initial instability of fine bed sand, *Journal of the Hydraulics Division*, *96*, 619–632, 1970. → page 20

Guala, M., A. Singh, N. Badheartbull, and E. Foufoula-Georgiou, Spectral description of migrating bed forms and sediment transport, *Journal of Geophysical Research: Earth Surface*, *119*, 123–137, 2014. → pages 24, 34, 52, 115

Haken, H., *Synergetics: An Introduction*, 2nd ed., Springer-Verlag, New York, 1978. → pages 61, 63

Hall, A. J., and G. C. Wake, A functional differential equation arising in modelling of cell growth, *The Journal of the Australian Mathematical Society. Series B. Applied Mathematics*, *30*, 424–435, 1989. → pages 102, 182

Hamamori, A., A theoretical investigation on the fluctuations of bed load transport. Technical Report No. R4., *Tech. rep.*, Delft Hydraulics Laboratory, 1962. → pages 24, 52

Hänggi, P., Correlation functions and masterequations of generalized (non-Markovian) Langevin equations, *Z. Physik B*, *31*, 407–416, 1978. → pages 7, 38, 100, 115

Hänggi, P., The functional derivative and its use in the description of noisy dynamical systems, in *International School on Stochastic Processes Applied to Physics*, edited by L. Pesquera and M. A. Rodriguez, pp. 69–94, World Scientific Publishing Company, Santander, Spain, 1984. → page 7

Hänggi, P., and P. Jung, Colored noise in dynamical systems, in *Advances in Chemical Physics, Volume LXXXIX*, edited by I. Prigogine and S. A. Rice, pp. 239–326, John Wiley & Sons Ltd., New York, 1995. → pages 51, 115

Haschenburger, J. K., Vertical mixing of gravel over a long flood series, *Earth Surface Processes and Landforms*, *36*, 1044–1058, 2011. → page 5

Haschenburger, J. K., Tracing river gravels: Insights into dispersion from a long-term field experiment, *Geomorphology*, *200*, 121–131, 2013. → pages 5, 78, 85

Hassan, M. A. ., and D. N. Bradley, Geomorphic controls on tracer particle dispersion in gravel-bed rivers, in *Gravel-Bed Rivers: Process and Disasters*, edited by D. Tsutsumi and J. B. Laronne, 1st ed., pp. 159–184, John Wiley & Sons Ltd., 2017. → pages 4, 5, 31, 54, 77, 78, 85, 88, 90

Hassan, M. A., and M. Church, Vertical mixing of coarse particles in gravel bed rivers: A kinematic model, *Water Resources Research*, *30*, 1173–1185, 1994. → pages 4, 85

Hassan, M. A., M. Church, and A. P. Schick, Distance of movement of coarse particles in gravel bed streams, *Water Resources Research*, *27*, 503–511, 1991. → pages 45, 72, 78, 79, 85

Hassan, M. A., B. J. Smith, D. L. Hogan, D. S. Luzi, A. E. Zimmermann, and B. C. Eaton, Sediment storage and transport in coarse bed streams: Scale considerations, in *Gravel-Bed Rivers VI: From Process Understanding to River Restoration*, edited by H. Habersack, H. Piegay, and M. Rinaldi, vol. 11, chap. 18, pp. 473–496, Elsevier B.V, 2008. → pages 2, 74

Hassan, M. A., H. Voepel, R. Schumer, G. Parker, and L. Fraccarollo, Displacement characteristics of coarse fluvial bed sediment, *Journal of Geophysical Research: Earth Surface*, *118*, 155–165, 2013. → page 78

Hernández-García, E., and C. López, Clustering, advection, and patterns in a model of population dynamics with neighborhood-dependent rates, *Physical Review E*, *70*, 11, 2004. → page 50

Heyman, J., A study of the spatio-temporal behaviour of bed load transport rate fluctuations, Ph.D. thesis, École Polytechnique Fédérale de Lausanne, 2014. → page 56

Heyman, J., F. Mettra, H. B. Ma, and C. Ancey, Statistics of bedload transport over steep slopes: Separation of time scales and collective motion, *Geophysical Research Letters*, *40*, 128–133, 2013. → pages 25, 27, 30, 49, 56

Heyman, J., H. B. Ma, F. Mettra, and C. Ancey, Spatial correlations in bed load transport : Evidence, importance, and modeling, *Journal of Geophysical Research: Earth Surface*, *119*, 1751–1767, 2014. → pages 24, 45, 49, 56, 74, 90

Heyman, J., P. Bohorquez, and C. Ancey, Entrainment, motion, and deposition of coarse particles transported by water over a sloping mobile bed, *Journal of Geophysical Research: Earth Surface*, *121*, 1931–1952, 2016. → pages 13, 14, 33, 56, 73, 75, 90, 93, 94, 110, 119

Hjelmfelt, A. T., and L. F. Mockros, Motion of discrete particles in a turbulent fluid, *Applied Scientific Research*, *16*, 149–161, 1966. → page 98

Hoey, T. B., Temporal variations in bedload transport in rates and sediment storage, *Progress in Physical Geography*, *16*, 319–338, 1992. → pages 24, 52

Hofland, B., and J. A. Battjes, Probability density function of instantaneous drag forces and shear stresses on a bed, *Journal of Hydraulic Engineering*, *132*, 1169–1175, 2006. → pages 99, 109

Hooke, R. L., On the history of humans as geomorphic agents, *Geology*, *28*, 843–846, 2000. → page 1

Horsthemke, W., and R. Lefever, *Noise-Induced Transitions: Theory and Applications in Physics, Chemistry and Biology*, 1st ed., Springer-Verlag, Berlin, 1984. → pages 9, 114

Horton, R. E., Erosional development of streams and their drainage basins; hydrophysical approach to quantitative morphology, *GSA Bulletin*, *56*, 275–370, 1945. → page 121

Houssais, M., and E. Lajeunesse, Bedload transport of a bimodal sediment bed, *Journal of Geophysical Research: Earth Surface*, *117*, 1–13, 2012. → pages 14, 93, 94, 120

Houssais, M., C. P. Ortiz, D. J. Durian, and D. J. Jerolmack, Onset of sediment transport is a continuous transition driven by fluid shear and granular creep, *Nature Communications*, *6*, 1–8, 2015. → page 17

Houssais, M., C. P. Ortiz, D. J. Durian, and D. J. Jerolmack, Rheology of sediment transported by a laminar flow, *Physical Review E*, *94*, 1–10, 2016. → page 4

Hubbell, D., and W. Sayre, Sand Transport Studies with Radioactive Tracers, *Journal of the Hydraulics Division*, *90*, 39–68, 1964. → pages 55, 72, 79, 80, 85

Iseya, F., and H. Ikeda, Pulsations in bedload transport rates induced by longitudinal sediment sorting: A flume study using sand and gravel mixtures, *Geografiska Annaler. Series A, Physical Geography*, *69*, 15, 1987. → page 24

Ismail, K. A., and W. J. Stronge, Impact of viscoplastic bodies: Dissipation and restitution, *Journal of Applied Mechanics, Transactions ASME*, *75*, 0610,111–0610,115, 2008. → page 109

Iverson, R. M., The physics of debris flows, *Reviews of Geophysics*, *35*, 245–296, 1997. → page 120

Jenkins, J. T., and D. M. Hanes, Collisional sheet flows of sediment driven by a turbulent fluid, *Journal of Fluid Mechanics*, *370*, 29–52, 1998. → page 95

Jensen, H. J., *Self-Organized Criticality*, Cambridge University Press, Cambridge, 1998. → page 115

Jerolmack, D. J., and K. E. Daniels, Viewing Earth's surface as a soft-matter landscape, *Nature Reviews Physics*, *1*, 716–730, 2019. → page 121

Jerolmack, D. J., and D. Mohrig, A unified model for subaqueous bed form dynamics, *Water Resources Research*, *41*, 1–10, 2005. → pages 3, 52, 93

Ji, C., A. Munjiza, E. Avital, J. Ma, and J. J. Williams, Direct numerical simulation of sediment entrainment in turbulent channel flow, *Physics of Fluids*, *25*, 2013. → page 12

Ji, C., A. Munjiza, E. Avital, D. Xu, and J. Williams, Saltation of particles in turbulent channel flow, *Physical Review E*, *89*, 1–14, 2014. → page 12

Jiang, Z., and P. K. Haff, Multiparticle simulation methods applied to the micromechanics of bed load transport, *Water Resources Research*, *29*, 399–412, 1993. → page 12

Joseph, G. G., R. Zenit, M. L. Hunt, and A. M. Rosenwinkel, Particle-wall collisions in a viscous fluid, *Journal of Fluid Mechanics*, *433*, 329–346, 2001. → pages 96, 110, 111

Kalinske, A. A., Movement of sediment as bed load in rivers, *EOS Transactions, American Geophysical Union*, *28*, 615–620, 1947. → page 2

Kanazawa, K., Statistical mechanics for athermal fluctuation, Ph.D. thesis, Kyoto University, 2017. → page 179

Kardar, M., *Statistical Physics of Fields*, Cambridge University Press, Cambridge, 2007. → page 52

Kawakatsu, T., *Statistical Physics of Polymers*, Springer-Verlag, New York, 2001. → page 52

Kim, H. K., Advanced second order functional differential equations, Ph.D. thesis, Massey University, 1998. → page 102

Kirchner, J. W., W. E. Dietrich, F. Iseya, and H. Ikeda, The variability of critical shear stress, friction angle, and grain protrusion in water-worked sediments, *Sedimentology*, *37*, 647–672, 1990. → pages 2, 17

Kolmogorov, A. N., The local structure of turbulence in incompressible viscous fluid for very large Reynolds numbers, *C. R. Acad. Sci. URSS*, *30*, 301–305, 1941. → page 115

Kraichnan, R. H., Diffusion by a random velocity field, *Physics of Fluids*, *13*, 22–31, 1970. → page 79

Kubo, R., M. Toda, and N. Hashitsume, *Statistical Physics II: Nonequilibrium Statistical Physics*, 1st ed., Springer-Verlag, Berlin, 1978. → pages 7, 12, 115

Kuhnle, R. A., and J. B. Southard, Bed load transport fluctuations in a gravel bed laboratory channel, *Water Resources Research*, *24*, 247–260, 1988. → page 24

Kumaran, V., Granular flow of rough particles in the high-Knudsen-number limit, *Journal of Fluid Mechanics*, *561*, 43–72, 2006. → page 36

Lajeunesse, E., L. Malverti, and F. Charru, Bed load transport in turbulent flow at the grain scale: Experiments and modeling, *Journal of Geophysical Research: Earth Surface*, *115*, 2010. → pages 9, 12, 20, 53, 90, 93, 104, 109, 110

Lajeunesse, E., O. Devauchelle, F. Lachaussée, and P. Claudin, Bedload transport in laboratory rivers: The erosion-deposition model, in *Gravel-Bed Rivers 8: Processes and Disasters*, edited by J. B. Laronne and D. Tsutsumi, pp. 415–438, Earth Surface Processes and Landforms, Kyoto and Takyama, Japan, 2015. → page 20

Lajeunesse, E., O. Devauchelle, and F. James, Advection and dispersion of bed load tracers, *Earth Surface Dynamics*, *6*, 389–399, 2017. → pages 9, 30, 31, 34, 37, 48, 53, 55, 79, 80, 88, 89, 90, 176

Landau, L. D., and E. M. Lifshitz, *Statistical Physics. Volume 5, Course of Theoretical Physics*, 6th ed., Pergamon Press, Oxford, 1969. → pages 95, 109

Langbein, W. B., and L. B. Leopold, Quasi-equilibrium states in channel morphology, *American Journal of Science*, *262*, 782–794, 1964. → page 121

Lee, D. B., and D. Jerolmack, Determining the scales of collective entrainment in collision-driven bed load, *Earth Surface Dynamics*, *6*, 1089–1099, 2018. → pages 49, 56, 73, 90

Li, T., T. K. Fuller, L. S. Sklar, K. B. Gran, and J. G. Venditti, A mechanistic model for lateral erosion of bedrock channel banks by bedload particle impacts, *Journal of Geophysical Research: Earth Surface*, *125*, 2020. → page 35

Lisle, I. G., C. W. Rose, W. L. Hogarth, P. B. Hairsine, G. C. Sander, and J. Y. Parlange, Stochastic sediment transport in soil erosion, *Journal of Hydrology*, *204*, 217–230, 1998. → pages xvii, xxi, 9, 10, 30, 31, 34, 37, 43, 48, 53, 79, 80, 83, 88, 89, 90, 176

Lisle, T. E., F. Iseya, and H. Ikeda, Response of a channel with alternate bars to a decrease in supply of mixed-size bed load: A flume experiment, *Water Resources Research*, *29*, 3623–3629, 1993. → page 24

Liu, D., X. Liu, X. Fu, and G. Wang, Quantification of the bed load effects on turbulent open-channel flows, *Journal of Geophysical Research : Earth Surface*, *121*, 767–789, 2016. → page 2

Liu, M. X., A. Pelosi, and M. Guala, A statistical description of particle motion and rest regimes in open-channel flows under low bedload transport, *Journal of Geophysical Research: Earth Surface*, *124*, 2666–2688, 2019. → pages 14, 55, 88, 93, 94, 110

Lorenz, A., C. Tuozzolo, and M. Y. Louge, Measurements of impact properties of small, nearly spherical particles, *Experimental Mechanics*, *37*, 292–298, 1997. → page 96

Łuczka, J., Non-Markovian stochastic processes: Colored noise, *Chaos*, *15*, 2005. → pages 51, 115

Łuczka, J., M. Niemiec, and E. Piotrowski, Randomly interrupted diffusion, *Physics Letters A*, *167*, 475–478, 1992. → page 37

Luczka, J., M. Niemiec, and E. Piotrowski, Linear systems with randomly interrupted Gaussian white noise, *Journal of Physics A: Mathematical and General*, *26*, 4849–4861, 1993. → page 37

Luczka, J., R. Bartussek, and P. Hänggi, White-noise-induced transport in periodic structures., *Europhysics Letters*, *31*, 431–436, 1995. → page 37

Luque, R. F., and R. van Beek, Erosion and transport of bed-load sediment, *Journal of Hydraulic Research*, *14*, 127–144, 1976. → page 17

Macklin, M. G., P. A. Brewer, K. A. Hudson-Edwards, G. Bird, T. J. Coulthard, I. A. Dennis, P. J. Lechler, J. R. Miller, and J. N. Turner, A geomorphological approach to the management of rivers contaminated by metal mining, *Geomorphology*, *79*, 423–447, 2006. → pages 54, 77

Madej, M. A., D. G. Sutherland, T. E. Lisle, and B. Pryor, Channel responses to varying sediment input: A flume experiment modeled after Redwood Creek, California, *Geomorphology*, *103*, 507–519, 2009. → page 24

Malmon, D. V., S. L. Reneau, T. Dunne, D. Katzman, and P. G. Drakos, Influence of sediment storage on downstream delivery of contaminated sediment, *Water Resources Research*, *41*, 1–17, 2005. → pages 54, 92

Mao, L., The effect of hydrographs on bed load transport and bed sediment spatial arrangement, *Journal of Geophysical Research: Earth Surface*, *117*, 1–16, 2012. → pages 24, 119

Marcum, J. I., A statistical theory of target detection by pulsed radar, *IRE Transactions on Information Theory*, *6*, 59–267, 1960. → page 83

Marshall, J. S., Viscous damping force during head-on collision of two spherical particles, *Physics of Fluids*, *23*, 2011. → page 110

Martin, R. L., Transient mechanics of bed load sediment transport, Ph.D. thesis, University of Pennsylvania, 2013. → pages 9, 102

Martin, R. L., D. J. Jerolmack, and R. Schumer, The physical basis for anomalous diffusion in bed load transport, *Journal of Geophysical Research: Earth Surface*, *117*, 1–18, 2012. → pages 13, 21, 55, 78, 80, 87, 88, 89, 93, 110

Martin, R. L., P. K. Purohit, and D. J. Jerolmack, Sedimentary bed evolution as a mean-reverting random walk: Implications for tracer statistics, *Geophysical Research Letters*, *41*, 6152–6159, 2014. → pages 55, 59, 62, 64, 69, 70, 72, 73, 74, 75, 78, 85, 88, 89

Martin, Y., Evaluation of bed load transport formulae using field evidence from the Vedder River, British Columbia, *Geomorphology*, *53*, 75–95, 2003. → page 92

Martin, Y., and M. Church, Re-examination of Bagnold's empirical bedload formulae, *Earth Surface Processes and Landforms*, *25*, 1011–1024, 2000. → page 17

Masoliver, J., Second-order dichotomous processes: Damped free motion, critical behavior, and anomalous superdiffusion, *Physical Review E*, *48*, 121–135, 1993. → page 51

Masoliver, J., Fractional telegrapher's equation from fractional persistent random walks, *Physical Review E*, *93*, 1–10, 2016. → page 90

Masoliver, J., and K. Lindenberg, Continuous time persistent random walk: A review and some generalizations, *European Physical Journal B*, *90*, 2017. → page 10

Masoliver, J., and G. H. Weiss, Transport equations in chromatography with a finite speed of signal propagation, *Separation Science and Technology*, *26*, 279–289, 1991. → page 9

Masoliver, J., and G. H. Weiss, Telegrapher's equations with variable propagation speeds, *Physical Review E*, *49*, 3852–3854, 1994. → page 90

Masoliver, J., G. H. Weiss, E. J. Phys, J. Masoliver, and G. H. Weiss, Finite-velocity diffusion, *European Journal of Physics*, *17*, 1996. → page 9

Masteller, C. C., N. J. Finnegan, J. M. Turowski, E. M. Yager, and D. Rickenmann, History-dependent threshold for motion revealed by continuous bedload transport measurements in a steep mountain stream, *Geophysical Research Letters*, *46*, 2583–2591, 2019. → page 2

Mau, Y., X. Feng, and A. Porporato, Multiplicative jump processes and applications to leaching of salt and contaminants in the soil, *Physical Review E - Statistical, Nonlinear, and Soft Matter Physics*, *90*, 1–8, 2014. → page 100

Maurin, R., J. Chauchat, B. Chareyre, and P. Frey, A minimal coupled fluid-discrete element model for bedload transport, *Physics of Fluids*, *27*, 2015. → page 12

Maxey, M. R., and J. J. Riley, Equation of motion for a small rigid sphere in a nonuniform flow, *Physics of Fluids*, *26*, 883–889, 1983. → page 98

McDowell, C., and M. A. Hassan, The influence of channel morphology on bedload path lengths: Insights from a survival process model, *Earth Surface Processes and Landforms*, *45*, 2982–2997, 2020. → page 119

Mendes, L., F. Antico, P. Sanches, F. Alegria, R. Aleixo, and R. M. Ferreira, A particle counting system for calculation of bedload fluxes, *Measurement Science and Technology*, *27*, 2016. → page 24

Menzel, A. M., and N. Goldenfeld, Effect of Coulombic friction on spatial displacement statistics, *Physical Review E*, *84*, 1–9, 2011. → page 13

Metzler, R., and J. Klafter, The random walk's guide to anomalous diffusion: A fractional dynamics approach, *Physics Report*, *339*, 1–77, 2000. → pages 77, 84

Metzler, R., J. H. Jeon, A. G. Cherstvy, and E. Barkai, Anomalous diffusion models and their properties: Non-stationarity, non-ergodicity, and ageing at the centenary of single particle tracking, *Phys. Chem. Chem. Phys.*, *16*, 24,128–24,164, 2014. → page 90

Meyer-Peter, E., and R. Müller, Formulas for bed-load transport, *Proceedings of the 2nd Meeting of the International Association of Hydraulic Research*, pp. 39–64, 1948. → pages 3, 17, 121

Michaelides, E. E., Review — The transient equation of motion for particles, bubbles, and droplets, *Journal of Fluids Engineering, Transactions of the ASME*, *119*, 233–247, 1997. → pages 3, 98, 100, 109

Miller, R. L., and R. J. Byrne, The angle of repose for a single grain on a fixed rough bed, *Sedimentology*, *6*, 303–314, 1966. → pages 2, 4

Montaine, M., M. Heckel, C. Kruelle, T. Schwager, and T. Pöschel, Coefficient of restitution as a fluctuating quantity, *Physical Review E*, *84*, 1–5, 2011. → page 96

Montroll, E. W., Random walks on lattices, *Journal of Mathematical Physics*, *6*, 193–220, 1964. → pages 6, 34, 80

Morse, P. M., and H. Feshbach, *Methods of Theoretical Physics, Vol I.*, McGraw-Hill, New York, 1953a. → page 42

Morse, P. M., and H. Feshbach, *Methods of Theoretical Physics, Vol. II*, McGraw-Hill, New York, 1953b. → page 102

Moss, F., and P. V. E. McClintock (Eds.), *Noise in Nonlinear Dynamical Systems*, vol. 1, Cambridge University Press, 1989. → pages 7, 115

Müller, T., and M. A. Hassan, Fluvial response to changes in the magnitude and frequency of sediment supply in a 1-D model, *Earth Surface Dynamics*, *6*, 1041–1057, 2018. → page 119

Nakagawa, H., and T. Tsujimoto, On probabilistic characteristics of motion of individual sediment particles on stream beds, in *Hydraulic Problems Solved by Stochastic Methods: Second International IAHR Symposium on Stochastic Hydraulics*, pp. 293–320, Water Resources Publications, Lund, Sweden, 1976. → pages 21, 23, 55, 72, 78, 79, 80, 87, 88

Nakagawa, H., and T. Tsujimoto, Sand bed instability due to bed load motion, *Journal of Hydraulic Engineering*, *106*, 2023–2051, 1980. → pages 70, 72, 73, 85

Nakagawa, H., and T. Tsujimoto, Hydrodynamic drag force acting upon a spherical particle on a rough bed composed of identical particles, *Bulletin of the Disaster Prevention Research Institute*, *31*, 115–130, 1981. → pages 4, 109

Nelson, P. A., D. Bellugi, and W. E. Dietrich, Delineation of river bed-surface patches by clustering high-resolution spatial grain size data, *Geomorphology*, *205*, 102–119, 2014. → pages 74, 120

Newman, M. E., Power laws, Pareto distributions and Zipf's law, *Contemporary Physics*, *46*, 323–351, 2005. → page 72

Nikora, V., and D. Goring, Flow turbulence over fixed and weakly mobile gravel beds, *Journal of Hydraulic Engineering*, *128*, 259–361, 2002. → page 115

Nikora, V., D. Goring, I. McEwan, and G. Griffith, Spatially averaged open-channel flow over rough bed, *Journal of Hydraulic Engineering*, *127*, 123–133, 2001a. → pages 4, 45

Nikora, V., J. Heald, D. Goring, and I. McEwan, Diffusion of saltating particles in unidirectional water flow over a rough granular bed, *Journal of Physics A: Mathematical and General*, *34*, 2001b. → pages 50, 77, 78, 79, 88

Nikora, V., H. Habersack, T. Huber, and I. McEwan, On bed particle diffusion in gravel bed flows under weak bed load transport, *Water Resources Research*, *38*, 17–1–17–9, 2002. → pages 4, 45, 50, 77, 78, 79, 88, 90

Nikora, V. I., A. N. Sukhodolov, and P. M. Rowinski, Statistical sand wave dynamics in one-directional water flows, *Journal of Fluid Mechanics*, *351*, 17–39, 1997. → pages 24, 115

Niño, Y., and M. García, Experiments on particle-turbulence interactions in the near-wall region of an open channel flow: Implications for sediment transport, *Journal of Fluid Mechanics*, *326*, 285–319, 1996. → page 17

Niño, Y., and M. García, Using Lagrangian particle saltation observations for bedload sediment transport modelling, *Hydrological Processes*, *12*, 1197–1218, 1998. → pages 3, 11, 17

Olinde, L., and J. P. L. Johnson, Using RFID and accelerometer-embedded tracers to measure probabilities of bed load transport, step lengths, and rest times in a mountain stream, *Water Resources Research*, *51*, 7525–7589, 2015. → pages 55, 75, 88, 89

Pähtz, T., A. H. Clark, M. Valyrakis, and O. Durán, The physics of sediment transport initiation, cessation, and entrainment across aeolian and fluvial environments, *Reviews of Geophysics*, *58*, 2020. → pages 17, 49

Pähtz, T., Y. Liu, Y. Xia, P. Hu, Z. He, and K. Tholen, Unified model of sediment transport threshold and rate across weak and intense subaqueous bedload, windblown sand, and windblown snow, *Journal of Geophysical Research: Earth Surface*, *126*, 1–36, 2021. → page 96

Paintal, A. S., A stochastic model of bed load transport, *Journal of Hydraulic Research*, *9*, 527–554, 1971. → pages 2, 17, 19, 20, 54, 58, 80

Papangelakis, E., and M. A. Hassan, The role of channel morphology on the mobility and dispersion of bed sediment in a small gravel-bed stream, *Earth Surface Processes and Landforms*, *41*, 2191–2206, 2016. → pages 25, 78

Papanicolaou, A. N., A. G. Tsakiris, M. A. Wyssmann, and C. M. Kramer, Boulder array effects on bedload pulses and depositional patches,

Journal of Geophysical Research: Earth Surface, *123*, 2925–2953, 2018. → pages 24, 52

Parker, G., Surface-based bedload transport relation for gravel rivers, *Journal of Hydraulic Research*, *28*, 417–436, 1990. → pages 3, 17

Parker, G., and P. C. Klingeman, On why gravel bed streams are paved, *Water Resources Research*, *18*, 1409–1423, 1982. → pages 120, 121

Parker, G., C. Paola, and S. Leclair, Probabilistic Exner sediment continuity equation for mixtures with no active layer, *Journal of Hydraulic Engineering*, *128*, 801, 2000. → pages 21, 23, 120

Parker, G., G. Seminara, and L. Solari, Bed load at low Shields stress on arbitrarily sloping beds: Alternative entrainment formulation, *Water Resources Research*, *39*, 1–11, 2003. → page 18

Pechenik, L., and H. Levine, Interfacial velocity corrections due to multiplicative noise, *Physical Review E*, *59*, 3893–3900, 1999. → page 50

Pelosi, A., and G. Parker, Morphodynamics of river bed variation with variable bedload step length, *Earth Surface Dynamics*, *2*, 243–253, 2014. → page 89

Pelosi, A., R. Schumer, G. Parker, and R. I. Ferguson, The cause of advective slowdown of tracer pebbles in rivers: Implementation of Exner-based master equation for coevolving streamwise and vertical dispersion, *Journal of Geophysical Research: Earth Surface*, *121*, 623–637, 2016. → pages 5, 72, 88, 89, 90

Pender, G., T. B. Hoey, C. Fuller, and I. K. McEwan, Selective bedload transport during the degradation of a well sorted graded sediment bed, *Journal of Hydraulic Research*, *39*, 269–277, 2001. → page 59

Phillips, C. B., R. L. Martin, and D. J. Jerolmack, Impulse framework for unsteady flows reveals superdiffusive bed load transport, *Geophysical Research Letters*, *40*, 1328–1333, 2013. → page 78

Phillips, C. B., K. M. Hill, C. Paola, M. B. Singer, and D. J. Jerolmack, Effect of flood hydrograph duration, magnitude, and shape on bed load transport dynamics, *Geophysical Research Letters*, *45*, 8264–8271, 2018. → page 119

Pielou, E. C., *Mathematical Ecology*, 1st ed., John Wiley & Sons Ltd., New York, NY, 1977. → pages 25, 61

Pierce, J. K., and M. A. Hassan, Joint stochastic bedload transport and bed elevation model: Variance regulation and power law rests, *Journal of Geophysical Research: Earth Surface*, *125*, 1–15, 2020a. → pages vi, 88

Pierce, J. K., and M. A. Hassan, Back to Einstein: Burial-induced three-range diffusion in fluvial sediment transport, *Geophysical Research Letters*, *47*, 2020b. → page vi

Pretzlav, K. L., J. P. Johnson, and D. N. Bradley, Smartrock transport from seconds to seasons: Shear stress controls on gravel diffusion inferred from hop and rest scaling, *Geophysical Research Letters*, *48*, 1–11, 2021. → pages 4, 5, 118

Pretzlav, K. L. G., Armor development and bedload transport processes during snowmelt and flash floods using laboratory experiments, numerical modeling, and field-based motion-sensor tracers, Ph.D. thesis, University of Texas, 2016. → pages 55, 75

Pretzlav, K. L. G., J. P. L. Johnson, and D. N. Bradley, Smartrock transport in a mountain stream: Bedload hysteresis and changing thresholds of motion, *Water Resources Research*, *56*, 1–20, 2020. → page 3

Prudnikov, A. P., I. A. Brychkov, O. I. Marichev, and G. G. Gould, *Integrals and Series Vol. 5: Inverse Laplace Transforms*, Gordon and Breach Science Publishers, Paris, 1992. → pages 8, 82, 162, 163, 174

Radjai, F., M. Jean, J. J. Moreau, and S. Roux, Force distributions in dense two-dimensional granular systems, *Physical Review Letters*, *77*, 274–277, 1996. → page 49

Recking, A., F. Liébault, C. Peteuil, and T. Jolimet, Testing bedload transport equations with consideration of time scales, *Earth Surface Processes and Landforms*, *37*, 774–789, 2012. → pages 2, 24, 34, 92

Recking, A., G. Piton, D. Vazquez-Tarrio, and G. Parker, Quantifying the morphological print of bedload transport, *Earth Surface Processes and Landforms*, *41*, 809–822, 2016. → page 2

Redner, S., *A Guide to First-Passage Processes*, 1st ed., Cambridge University Press, Cambridge, 2007. → pages 55, 69

Redolfi, M., W. Bertoldi, M. Tubino, and M. Welber, Bed load variability and morphology of gravel bed rivers subject to unsteady flow: A laboratory investigation, *Water Resources Research*, *54*, 842–862, 2018. → page 24

Reid, D. A., M. A. Hassan, S. Bird, and D. Hogan, Spatial and temporal patterns of sediment storage over 45 years in Carnation Creek, BC, a previously glaciated mountain catchment, *Earth Surface Processes and Landforms*, *44*, 1584–1601, 2019. → page 119

Rickenmann, D., and B. W. McArdell, Continuous measurement of sediment transport in the Erlenbach stream using piezoelectric bedload impact sensors, *Earth Surface Processes and Landforms*, *32*, 1362–1378, 2007. → page 24

Risken, H., *The Fokker-Planck Equation: Methods of Solution and Applications*, 2nd ed., Springer-Verlag, Ulm, 1984. → pages 7, 13, 100

Roseberry, J. C., M. W. Schmeeckle, and D. J. Furbish, A probabilistic description of the bed load sediment flux: 2. Particle activity and motions, *Journal of Geophysical Research: Earth Surface*, *117*, 2012. → pages 24, 25, 56, 80, 93

Rossetto, V., The one-dimensional asymmetric persistent random walk, *Journal of Statistical Mechanics: Theory and Experiment*, *2018*, 2018. → page 10

Saletti, M., and M. A. Hassan, Width variations control the development of grain structuring in steep step-pool dominated streams: insight from flume experiments, *Earth Surface Processes and Landforms*, *45*, 1430–1440, 2020. → page 90

Saletti, M., P. Molnar, A. Zimmermann, M. A. . Hassan, and M. Church, Temporal variability and memory in sediment transport in an experimental step-pool channel, *Water Resources Research*, *51*, 9325–3337, 2015. → pages 34, 49, 52, 56, 73, 76

Santos, B. O., M. J. Franca, and R. M. Ferreira, Coherent structures in open channel flows with bed load transport over an hydraulically rough bed, in *Proceedings of the International Conference on Fluvial Hydraulics, RIVER FLOW 2014*, pp. 883–890, Taylor & Francis, London, 2014. → page 2

Sawai, K., Dispersion of bed load particles, *Bulletin of the Disaster Prevention Research Institute*, *37*, 19–37, 1987. → pages 27, 57, 59

Schmeeckle, M. W., Numerical simulation of turbulence and sediment transport of medium sand, *Journal of Geophysical Research: Earth Surface*, *119*, 1240–1262, 2014. → pages 12, 96, 99, 117

Schmeeckle, M. W., and J. M. Nelson, Direct numerical simulation of bedload transport using a local, dynamic boundary condition, *Sedimentology*, *50*, 279–301, 2003. → page 12

Schmeeckle, M. W., J. M. Nelson, J. Pitlick, and J. P. Bennett, Interparticle collision of natural sediment grains in water, *Water Resources Research*, *37*, 2377–2391, 2001. → pages 96, 110, 111

Schmeeckle, M. W., J. M. Nelson, and R. L. Shreve, Forces on stationary particles in near-bed turbulent flows, *Journal of Geophysical Research: Earth Surface*, *112*, 1–21, 2007. → pages 3, 54, 98, 99, 109

Schmidt, M. G., F. Sagués, and I. M. Sokolov, Mesoscopic description of reactions for anomalous diffusion: A case study, *Journal of Physics Condensed Matter*, *19*, 2007. → page 81

Schumer, R., M. M. Meerschaert, and B. Baeumer, Fractional advection-dispersion equations for modeling transport at the Earth surface, *Journal of Geophysical Research: Earth Surface*, *114*, 1–15, 2009. → pages 6, 21, 84, 90

Seizilles, G., E. Lajeunesse, O. Devauchelle, and M. Bak, Cross-stream diffusion in bedload transport, *Physics of Fluids*, *26*, 2014. → pages 20, 93, 110

Sekine, M., and H. Kikkawa, Mechanics of saltating grains. II, *Journal of Hydraulic Engineering*, *118*, 536–558, 1992. → pages 4, 11, 79, 110

Seminara, G., L. Solari, and G. Parker, Bed load at low Shields stress on arbitrarily sloping beds: Failure of the Bagnold hypothesis, *Water Resources Research*, *38*, 31–1–31–16, 2002. → page 17

Serero, D., N. Gunkelmann, and T. Pöschel, Hydrodynamics of binary mixtures of granular gases with stochastic coefficient of restitution, *Journal of Fluid Mechanics*, *781*, 595–621, 2015. → pages 97, 101

Shapiro, V. E., and V. M. Loginov, "Formulae of differentiation" and their use for solving stochastic equations, *Physica A: Statistical Mechanics and its Applications*, *91*, 563–574, 1978. → page 158

Shih, W. R., P. Diplas, A. O. Celik, and C. Dancey, Accounting for the role of turbulent flow on particle dislodgement via a coupled quadrant analysis of velocity and pressure sequences, *Advances in Water Resources*, *101*, 37–48, 2017. → pages 2, 74

Shlesinger, M. F., Asymptotic solutions of continuous-time random walks, *Journal of Statistical Physics*, *10*, 421–434, 1974. → page 84

Shobe, C. M., J. M. Turowski, R. Nativ, R. C. Glade, G. L. Bennett, and B. Dini, The role of infrequently mobile boulders in modulating landscape evolution and geomorphic hazards, *Earth-Science Reviews*, *220*, 103,717, 2021. → page 24

Singh, A., K. Fienberg, D. J. Jerolmack, J. Marr, and E. Foufoula-Georgiou, Experimental evidence for statistical scaling and intermittency in sediment transport rates, *Journal of Geophysical Research: Earth Surface*, *114*, 1–16, 2009. → pages 34, 49, 52, 56, 62, 76

Singh, A., F. Porté-Agel, and E. Foufoula-georgiou, On the influence of gravel bed dynamics on velocity power spectra, *Water Resources Research*, *46*, 1–10, 2010. → page 2

Singh, A., E. Foufoula-Georgiou, F. Porté-Agel, and P. R. Wilcock, Coupled dynamics of the co-evolution of gravel bed topography, flow turbulence and sediment transport in an experimental channel, *Journal of Geophysical Research: Earth Surface*, *117*, 1–20, 2012. → pages 56, 73, 76, 115

Sivan, D., K. Lambeck, R. Toueg, A. Raban, Y. Porath, and B. Shirman, Ancient coastal wells of Caesarea Maritima, Israel, an indicator for relative sea level changes during the last 2000 years, *Earth and Planetary Science Letters*, *222*, 315–330, 2004. → page 1

Slater, L., G. Villarini, S. Archfield, D. Faulkner, R. Lamb, A. Khouakhi, and J. Yin, Global changes in 20-year, 50-year, and 100-year river floods, *Geophysical Research Letters*, *48*, 1–10, 2021. → page 1

Slaymaker, O., T. Spencer, and C. Embleton-Hamann, Recasting geomorphology as a landscape science, *Geomorphology*, *384*, 107,723, 2021. → page 1

Sokolov, I. M., Models of anomalous diffusion in crowded environments, *Soft Matter*, *8*, 9043–9052, 2012. → pages 8, 11, 46, 77

Sornette, D., *Critical Phenomena in the Natural Sciences*, Springer, Berlin, 2006. → page 75

Strahler, A. N., Dynamic basis of geomorphology, *Bulletin of the Geological Society of America*, *63*, 923–938, 1952. → page 121

Strom, K., A. N. Papanicolaou, N. Evangelopoulos, and M. Odeh, Microforms in gravel-bed rivers: formation, disintegration, and effects on bedload transport, *Journal of Hydraulic Engineering*, *130*, 554–567, 2004. → pages 24, 52

Sumer, B. M., L. H. Chua, N. S. Cheng, and J. Fredsøe, Influence of turbulence on bed load sediment transport, *Journal of Hydraulic Engineering*, *129*, 585–596, 2003. → page 2

Sun, Z., and J. Donahue, Statistically derived bedload formula for any fraction of nonuniform sediment, *Journal of Hydraulic Engineering*, *126*, 105–111, 2000. → pages 24, 120

Suweis, S., A. Porporato, A. Rinaldo, and A. Maritan, Prescription-induced jump distributions in multiplicative Poisson processes, *Physical Review E*, *83*, 1–8, 2011. → pages 100, 179

Swift, R. J., A stochastic predator-prey model, *Bulletin of the Irish Mathematical Society*, *48*, 57–63, 2002. → page 61

Szabo, J., D. Lorant, and D. Loczy (Eds.), *Anthropogenic Geomorphology: A Guide to Man-Made Landforms*, Springer, New York, 2010. → page 1

Takayama, S., Bedload movement in torrential mountain streams, *Tokyo Geographical Paper*, *9*, 169–188, 1965. → page 5

Taylor, G. I., Diffusion by continuous movements, *Proceedings of the London Mathematical Society*, *s2-20*, 196–212, 1920. → page 11

Temme, N. M., *Special Functions: An Introduction to the Classical Functions of Mathematical Physics*, John Wiley & Sons Ltd., New York, 1996. → pages 83, 174

Touchette, H., E. Van Der Straeten, and W. Just, Brownian motion with dry friction: Fokker-Planck approach, *Journal of Physics A: Mathematical and Theoretical*, *43*, 1–18, 2010. → page 13

Tregnaghi, M., A. Bottacin-Busolin, A. Marion, and S. Tait, Stochastic determination of entrainment risk in uniformly sized sediment beds at low transport stages: 1. Theory, *Journal of Geophysical Research: Earth Surface*, *117*, 1–15, 2012. → page 20

Tsujimoto, T., Probabilistic model of bed load processes and its application to moving bed problem (In Japanese), Ph.D. thesis, Kyoto University, 1978. → page 23

Tucker, G. E., and D. N. Bradley, Trouble with diffusion: Reassessing hillslope erosion laws with a particle-based model, *Journal of Geophysical Research*, *115*, 1–12, 2010. → page 21

Turowski, J. M., Probability distributions of bed load transport rates: A new derivation and comparison with field data, *Water Resources Research*, *46*, 2010. → pages 25, 27, 30, 34, 35, 48, 49, 92

Valyrakis, M., P. Diplas, C. L. Dancey, K. Greer, and A. O. Celik, Role of instantaneous force magnitude and duration on particle entrainment, *Journal of Geophysical Research: Earth Surface*, *115*, 2010. → pages 2, 4, 33, 51

Van Den Broeck, C., On the relation between white shot noise, Gaussian white noise, and the dichotomic Markov process, *Journal of Statistical Physics*, *31*, 467–483, 1983. → pages 6, 7, 100, 115, 179

Van den Broeck, C., Taylor dispersion revisited, *Physica A: Statistical Mechanics and its Applications*, *168*, 677–696, 1990. → page 9

Van Kampen, N. G., *Stochastic Processes in Physics and Chemistry*, 3rd ed., Elsevier B.V., 2007. → pages 13, 28, 60, 158

van Rijn, L. C., Sediment transport, part I: Bed load transport, *Journal of Hydraulic Engineering*, *110*, 1431–1456, 1984. → pages 9, 11

Venditti, J. G., P. A. Nelson, R. W. Bradley, D. Haught, and A. B. Gitto, Bedforms, structures, patches, and sediment supply in gravel-bed rivers, *Gravel-Bed Rivers: Process and Disasters*, pp. 439–466, 2017. → pages 2, 120

Vicsek, T., and A. Zafeiris, Collective motion, *Physics Reports*, *517*, 71–140, 2012. → page 90

Voepel, H., R. Schumer, and M. A. Hassan, Sediment residence time distributions: Theory and application from bed elevation measurements, *Journal of Geophysical Research: Earth Surface*, *118*, 2557–2567, 2013. → pages 55, 69, 70, 72, 75, 78, 85, 88, 89

Vowinckel, B., T. Kempe, and J. Fröhlich, Fluid-particle interaction in turbulent open channel flow with fully-resolved mobile beds, *Advances in Water Resources*, *72*, 32–44, 2014. → pages 12, 54

Wachs, A., Particle-scale computational approaches to model dry and saturated granular flows of non-Brownian, non-cohesive, and non-spherical rigid bodies, *Acta Mechanica*, *230*, 1919–1980, 2019. → page 12

Walther, G.-r., E. Post, P. Convey, A. Menzel, C. Parmesank, T. J. C. Beebee, J.-m. Fromentin, O. H.-g. I, and F. Bairlein, Ecological response to recent climate change, *Nature*, *416*, 389–395, 2002. → page 1

Warburton, J., Observations of bed load transport and channel bed changes in a proglacial mountain stream, *Arctic & Alpine Research*, *24*, 195–203, 1992. → pages 95, 120

Weeks, E. R., and H. L. Swinney, Anomalous diffusion resulting from strongly asymmetric random walks, *Physical Review E*, *57*, 4915–4920, 1998. → pages 55, 80, 81, 82, 84, 87, 89, 177

Weeks, E. R., J. S. Urbach, and H. L. Swinney, Anomalous diffusion in asymmetric random walks with a quasi-geostrophic flow example, *Physica D: Nonlinear Phenomena*, *97*, 291–310, 1996. → pages 88, 89

Weiss, G. H., The two-state random walk, *Journal of Statistical Physics*, *15*, 157–165, 1976. → page 80

Weiss, G. H., *Aspects and Applications of the Random Walk.*, North Holland, Amsterdam, 1994. → pages 80, 81, 82, 87, 163, 177

Weiss, G. H., Some applications of persistent random walks and the telegrapher's equation, *Physica A: Statistical Mechanics and its Applications*, *311*, 381–410, 2002. → pages 10, 42

Wiberg, P. L., and J. D. Smith, A theoretical model for saltating grains in water, *Journal of Geophysical Research*, *90*, 7341–7354, 1985. → pages 9, 11, 54

Wilcock, P. R., Toward a practical method for estimating sediment-transport rates in gravel-bed rivers, *Earth Surface Processes and Landforms*, *26*, 1395–1408, 2001. → page 3

Wilcock, P. R., and J. C. Crowe, Surface-based transport model for mixed-size sediment, *Journal of Hydraulic Engineering*, *129*, 120–128, 2003. → page 17

Wilcock, P. R., and B. W. McArdell, Partial transport of a sand-gravel sediment, *Water Resources Research*, *33*, 235–245, 1997. → pages 5, 20

Wilcock, P. R., and J. B. Southard, Bed load transport of mixed size sediment: Fractional transport rates, bed forms, and the development of a coarse bed surface layer, *Water Resources Research*, *25*, 1629–1641, 1989. → page 120

Williams, S., and D. Furbish, Particle energy partitioning and transverse diffusion during rarefied travel on an experimental hillslope, *Earth Surface Dynamics Discussions*, pp. 1–33, 2021. → page 96

Willis, K. J., and S. A. Bhagwat, Biodiversity and climate change, *Science*, *326*, 806–808, 2009. → page 1

Witz, M. J., S. Cameron, and V. Nikora, Bed particle dynamics at entrainment, *Journal of Hydraulic Research*, *57*, 464–474, 2019. → page 87

Wolman, M. G., and R. Gerson, Relative scales of time and effectiveness of climate in watershed geomorphology, *Earth Surface Processes*, *3*, 189–208, 1978. → page 121

Wolman, M. G., and J. P. Miller, Magnitude and frequency of forces in geomorphic processes, *The Journal of Geology*, *68*, 54–74, 1960. → page 121

Wong, M., and G. Parker, Reanalysis and correction of bed-load relation of Meyer-Peter and Müller using their own database, *Journal of Hydraulic Engineering*, *132*, 1159–1168, 2006. → page 24

Wong, M., G. Parker, P. DeVries, T. M. Brown, and S. J. Burges, Experiments on dispersion of tracer stones under lower-regime plane-bed equilibrium bed load transport, *Water Resources Research*, *43*, 1–23, 2007. → pages 27, 56, 57, 59, 60, 62, 73

Wu, Z., E. Foufoula-Georgiou, G. Parker, A. Singh, X. Fu, and G. Wang, Analytical solution for anomalous diffusion of bedload tracers gradually undergoing burial, *Journal of Geophysical Research: Earth Surface*, *124*, 21–37, 2019a. → pages 45, 55, 72, 79, 80, 85, 89, 90, 178

Wu, Z., A. Singh, X. Fu, and G. Wang, Transient anomalous diffusion and advective slowdown of bedload tracers by particle burial and exhumation, *Water Resources Research*, *55*, 7964–7982, 2019b. → pages 72, 85, 89

Wu, Z., D. Furbish, and E. Foufoula-Georgiou, Generalization of hop distance-time scaling and particle velocity distributions via a two-regime formalism of bedload particle motions, *Water Resources Research*, *56*, 1–30, 2020. → page 110

Yalin, M. S., An expression for bed-load transportation, *J. Hydraul. Div. Am. Soc. Civ. Eng.*, *89*, 221–250, 1963. → page 11

Yalin, M. S., *Mechanics of Sediment Transport.*, (1972), Pergamon Press, 1972. → pages xv, 17, 18, 19

Yang, C. T., and W. Sayre, Stochastic model for sand dispersion, *Journal of the Hydraulics Division*, *97*, 265–288, 1971. → pages 4, 70, 72, 73, 80

Yang, F. L., and M. L. Hunt, Dynamics of particle-particle collisions in a viscous liquid, 2006. → pages 110, 111

Yano, K., Tracer studies on the movement of sand and gravel, in *Proceedings of the 12th Congress IAHR, Vol 2.*, pp. 121–129, IAHR, Kyoto, Japan, 1969. → pages 55, 78, 80, 87, 88

Yano, K., Y. Tsuchiya, and M. Michiue, Studies on the sand transport in streams with tracers, *Kyoto Univ-Disaster Prevention Research Inst-Bul*, *18*, 1–16, 1969. → page 55

Youse, A., P. Costa, and L. Brandt, Single sediment dynamics in turbulent flow over a porous bed - Insights from interface-resolved simulations, *Journal of Fluid Mechanics*, *893*, 1–28, 2020. → page 12

Zaburdaev, V., M. Schmiedeberg, and H. Stark, Random walks with random velocities, *Physical Review E*, *78*, 1–5, 2008. → page 90

Zaidi, A. A., B. Van Brunt, and G. C. Wake, Solutions to an advanced functional partial differential equation of the pantograph type, *Proc. Roy. Soc. London, Series A.*, *471*, 2015. → page 103

Zhang, Y., M. M. Meerschaert, and A. I. Packman, Linking fluvial bed sediment transport across scales, *Geophysical Research Letters*, *39*, 1–6, 2012. → page 78

Zimmermann, A. E., M. Church, and M. A. Hassan, Video-based gravel transport measurements with a flume mounted light table, *Earth Surface Processes and Landforms*, *33*, 2285–2296, 2008. → page 24

Appendix A

Calculations involved in the dynamical bedload flux model

A.1 Derivation of the master equation for particle position

Here I derive the master equation 2.2 for the probability distribution of particle position from the Langevin equation 2.1. This is closely based off on the approach of *Balakrishnan* (1993).

The master equation satisfies $P(x,t) = \langle\langle \delta(x - x(t))\rangle_\xi\rangle_\eta$, where the averages are over all realizations of the two independent noises. It is most convenient to take these averages after taking Fourier transforms and manipulating time derivatives of the resulting equations.

Integrating the Langevin equation 2.1, substituting the solution in the above definition, and taking the Fourier transform in space gives

$$\tilde{P}(g,t) = \Big\langle \Big\langle \exp\Big[- ig \int_0^t du[V + \sqrt{2D}\xi(u)]\eta(u)\Big]\Big\rangle_\eta \Big\rangle_\xi \tag{A.1}$$

This can be rearranged as

$$\tilde{P}(g,t) = \Big\langle \exp\Big[igV\int_0^t du\eta(u)\Big]\Big\langle \exp\Big[ig\sqrt{2D}\int_0^t du\xi(u)\eta(u)\Big]\Big\rangle_\xi\Big\rangle_\eta. \quad \text{(A.2)}$$

Using the classic identity for an average over white noise of an exponential (*Balakrishnan*, 1993; *Van Kampen*, 2007) gives, after recognizing that the dichotomous noise satisfies $\eta^2 = \eta$ since η is either 0 or 1,

$$\tilde{P}(g,t) = \Big\langle \exp\Big[(igV - g^2D)\int_0^t du\eta(u)\Big]\Big\rangle_\eta. \quad \text{(A.3)}$$

Now I will take time derivatives in order to apply the so-called Furutsu-Novikov formula to evaluate the ensemble average over dichotomous noise (*Shapiro and Loginov*, 1978). Applied to the dichotomous noise in Fig. 1.2, the Furutsu-Novikov formula is, for an arbitrary functional F of the noise,

$$\partial_t\langle\eta(t)F[\eta(t)]\rangle = \langle\eta\partial_t F\rangle + k\big[\langle\eta\rangle\langle F\rangle - \langle\eta F\rangle\big]. \quad \text{(A.4)}$$

Making the shorthands $G = igV - g^2D$ and $F = \exp G\int_0^t \eta(u)du$ and taking a time derivative of Eq. A.3 gives

$$G^{-1}\partial_t\tilde{P}(g,t) = \langle\eta F\rangle. \quad \text{(A.5)}$$

Taking a second time derivative opens up the possibility of using the Furutsu-Novikov formula A.4:

$$G^{-1}\partial_t\tilde{P}(g,t) = \partial_t\langle\eta F\rangle = G\langle\eta F\rangle + k\big[\langle\eta\rangle\tilde{P}(g,t) - G^{-1}\partial_t\tilde{P}(g,t)\big]. \quad \text{(A.6)}$$

Applying Eq. A.5 finally gives

$$\partial_t^2\tilde{P}(g,t) = (igV - g^2D - k)\partial_t\tilde{P} + k_E(igV - g^2D)\tilde{P}, \quad \text{(A.7)}$$

and inverse Fourier transforming provides the master equation 2.2.

A.2 Solution for the position probability distribution

The position probability distribution can be obtained from Eq. 2.2 for the initial conditions $P(x,0) = \delta(x)$ and $\partial_t P(x,0) = \frac{k_E}{k}\big[D\delta''(x) - V\delta'(x)\big]$ using Fourier transforms in space and Laplace transforms in time. Taking these transforms provides

$$\bar{\tilde{P}}(g,s) = \frac{s + k + \varphi D g^2 - igV\varphi}{s(s+k) + (Dg^2 - igV)(s+k_E)}, \tag{A.8}$$

where $\varphi = k_D/k$ is the probability a particle starts at rest.

The numerator terms encode the initial conditions. The denominator terms are where the real structure of the solution is contained. The numerator terms involving g can be expressed as first and second derivatives with respect to x. The problem, then is to calculate the inverse Fourier integral of the denominator. The inverse Fourier transform can be calculated by expanding the denominator of Eq. A.8 in partial fractions and applying the contour integral (e.g. *Arfken*, 1985)

$$\int_{-\infty}^{\infty} \frac{1}{2\pi i} \frac{e^{-igx}}{g - ic} dg = \sigma(c)\theta(-x\sigma(c)) \exp\big(-|cx|\big). \tag{A.9}$$

In this equation $\sigma(c) = \mathrm{sgn}(c)$ is a shorthand for the sign function. The above integral can be obtained with the residue theorem by considering different cases for the signs of x and c and applying square contours around the upper or lower-half regions of the complex plane.

Rearranging the governing equation gives

$$\tilde{\bar{P}}(g,s) = \frac{\varphi D g^2 - igV\varphi + s + k}{D(s+k_E)} \frac{1}{g^2 - i\frac{V}{D}g + \frac{s(s+k)}{D(s+k_E)}}. \tag{A.10}$$

The roots of the denominator are at

$$g_\pm = \frac{iV}{2D}\Big[1 \pm R\Big], \tag{A.11}$$

where

$$R = \sqrt{1 + \frac{4D}{V^2}\frac{s(s+k)}{s+k_E}}. \tag{A.12}$$

The partial fractions expansion is therefore

$$\frac{1}{g^2 - i\frac{V}{D}g + \frac{s(s+k)}{D(s+k_E)}} = \frac{D}{iVR}\Big[\frac{1}{g-g_+} - \frac{1}{g-g_-}\Big], \tag{A.13}$$

giving

$$\tilde{P}(x,s) = \frac{-\varphi D\partial_x^2 + V\varphi\partial_x + s + k}{VR(s+k_E)} \times \left[\int \frac{dg}{2\pi i}\frac{e^{-igx}}{g-g_+} - \int \frac{dg}{2\pi i}\frac{e^{-igx}}{g-g_-}\right], \tag{A.14}$$

or eventually

$$\tilde{P}(x,s) = \frac{-\varphi D\partial_x^2 + V\varphi\partial_x + s + k}{VR(s+k_E)} \times \left[\theta(x)\exp\Big(\frac{Vx}{2D}(1-R)\Big) + \theta(-x)\exp\Big(\frac{Vx}{2D}(1+R)\Big)\right]. \tag{A.15}$$

This simplifies slightly to

$$\tilde{P}(x,s) = \frac{-\varphi D\partial_x^2 + V\varphi\partial_x + s + k}{VR(s+k_E)}\exp\Big[\frac{Vx}{2D} - \frac{V|x|}{2D}R\Big]. \tag{A.16}$$

Taking the inverse Laplace transform symbolically provides the desired probability density function

$$P(x,t) = \mathcal{L}^{-1}\left\{\frac{1}{V}\big[-\varphi D\partial_x^2 + V\varphi\partial_x + k + s\big] \times \exp\Big(\frac{Vx}{2D}\Big)\frac{\exp\Big(-\frac{V|x|R}{2D}\Big)}{(s+k_E)R}\right\}(t). \tag{A.17}$$

Using the shift property of Laplace transforms (e.g. *Arfken*, 1985), this be-

comes

$$P(x,t) = \frac{1}{V}e^{-k_E t}\mathcal{L}^{-1}\Bigg\{\big[-\varphi D\partial_x^2 + V\varphi\partial_x + k_D + s\big] \times \exp\Big(\frac{Vx}{2D}\Big)\frac{\exp\Big(\frac{-V|x|R_*}{2D}\Big)}{sR_\star}\Bigg\}, \quad \text{(A.18)}$$

where

$$R_* = \sqrt{1 + \frac{4D(k_D - k_E)}{V^2} + \frac{4D}{V^2}\Big(s - \frac{k_E k_D}{s}\Big)}. \quad \text{(A.19)}$$

Using the property that $\mathcal{L}^{-1}\big\{s\tilde{f}\big\} = (\delta(t) + \partial_t)f(t)$ (*Arfken*, 1985) gives

$$P(x,t) = \frac{1}{V}e^{-k_E t}\big[-\varphi D\partial_x^2 + V\varphi\partial_x + k_D + \delta(t) + \partial_t\big] \times \exp\Big[\frac{Vx}{2D}\Big]\mathcal{L}^{-1}\Bigg\{\frac{-\exp\Big[\frac{-V|x|R_*}{2D}\Big]}{sR_*}\Bigg\}(t). \quad \text{(A.20)}$$

Finally, using the identity

$$\mathcal{L}^{-1}\Big\{\frac{1}{s}\tilde{g}(s - a/s)\Big\} = \int_0^t \mathcal{I}_0\Big(2\sqrt{au(t-u)}\Big)g(u)du \quad \text{(A.21)}$$

from *Bateman and Erdelyi* (1953), pg. 133 (which can be derived by either u-substitution or series expansion in powers of a) provides

$$P(x,t) = \frac{1}{V}e^{-k_E t}\big[-\varphi D\partial_x^2 + V\varphi\partial_x + k_D + \delta(t) + \partial_t\big]\exp\Big[\frac{Vx}{2D}\Big] \times \int_0^t du\mathcal{I}_0\Big(2\sqrt{k_E k_D u(t-u)}\Big) \times \mathcal{L}^{-1}\Bigg\{\frac{\exp\Big[\frac{-V|x|}{2D}\sqrt{a+bs}\Big]}{\sqrt{a+bs}}\Bigg\}(u), \quad \text{(A.22)}$$

where $a = 1 + 4D(k_E - k_E)/(V^2)$ and $b = 4D/V^2$ are shorthands.

Using the trick of introducing a parameter and integrating over it to remove the square root from the denominator (an integral analogue of "Feyn-

man's trick"), the remaining transform can be evaluated from standard tables (*Prudnikov et al.*, 1992), eventually giving (after integrating over and setting to 1 the fake parameter),

$$P(x,t) = \left[-\varphi D\partial_x^2 + V\varphi\partial_x + k + \delta(t) + \partial_t\right] \int_0^t \mathcal{I}_0\Big(2\sqrt{k_E k_D u(t-u)}\Big) e^{-k_E(t-u)} \times \sqrt{\frac{1}{4\pi D u}} \exp\Big[-k_D u - \frac{(x-Vu)^2}{4Du}\Big] du, \quad \text{(A.23)}$$

as reported in Eq. 2.10.

A.3 Calculation of the scale-dependent rate function $\Lambda(T)$

The central object required to calculate the sediment flux probability distribution in Eq. 2.3 is

$$\Lambda(T) = \rho \int_0^\infty dx_i \int_0^\infty dx P(x + x_i, T). \quad \text{(A.24)}$$

This represents the rate at which particles start at x_i, anywhere to the left of $x = 0$, and manage to cross $x = 0$ by time T.

Again it is easiest to conduct the necessary calculus after Laplace transforming. This gives

$$\tilde{\Lambda}(s) = \rho \int_0^\infty dx_i \int_0^\infty dx \tilde{P}(x + x_i, s). \quad \text{(A.25)}$$

The Laplace transform of the rate function therefore follows after integrating Eq. A.16 twice.

Noting that $x + x_i$ is always positive, The first integration gives

$$\tilde{\Lambda}(s) = \rho \int_0^\infty dx_i \exp\Big[\frac{V(1-R)x_i}{2D}\Big] \times \Big(\varphi \frac{1-R}{2R(s+k_E)} - \frac{\varphi}{R(s+k_E)} - \frac{2D(s+k)}{V^2 R(1-R)(s+k_E)}\Big), \quad \text{(A.26)}$$

and the second integration provides

$$\tilde{\Lambda}(s) = -\frac{\rho\varphi D}{VR(s+k_E)} + \frac{2\rho D\varphi}{VR(1-R)(s+k_E)} + \frac{4\rho D^2(s+k)}{V^3R(1-R)^2(s+k_E)}. \quad \text{(A.27)}$$

Taking the inverse transform, converting the s factor in the numerator of the last term to $\partial_t + \delta(t)$, and using the shift property gives (e.g. *Arfken*, 1985)

$$\Lambda(t) = \rho\mathcal{L}^{-1}\left\{ -\frac{\varphi D}{VR_\star s} + \frac{2D\varphi}{VR_*(1-R_\star)s} + \frac{4D^2\big(\overleftarrow{\partial}_t + k\big)}{V^3R_\star(1-R_\star)^2 s} \right\}. \quad \text{(A.28)}$$

Here the notation $\overleftarrow{\partial}_t$ means the derivative acts from the left on all terms multiplying it (as in $f(t)\overleftarrow{\partial}_t g(t) = \partial_t[f(t)g(t)]$).

After some work, using Eq. A.22 and tabulated Laplace transform pairs (e.g. *Arfken*, 1985; *Prudnikov et al.*, 1992) to perform the inverse Laplace transforms, the net result for the rate constant is

$$\Lambda(t) = \rho\int_0^t \mathcal{I}_0\Big(2\sqrt{k_Ek_Du(t-u)}\Big)e^{-k_E(t-u)-k_Du} \times \left[\sqrt{\frac{D}{\pi u}}\Big([\overleftarrow{\partial}_t + k]u - \frac{k_D}{2k}\Big)e^{-V^2u/4D} + \frac{V}{2}\Big([\overleftarrow{\partial}_t + k]u - \frac{k_D}{k}\Big)\,\mathrm{erfc}\left(-\sqrt{\frac{V^2u}{4D}}\right)\right]du, \quad \text{(A.29)}$$

as reported in Eq. 2.15.

A.4 Asymptotic limits of the flux rate function

Eq. 2.15 is difficult to work with. To explore the behavior at extreme values of the observation time T, one can apply Tauberian theorems (*Weiss*, 1994) to invert the Laplace-transformed rate function of Eq. A.27 at the opposite extreme of s.

For example, at short times, expanding Eq. A.27 as $s \to \infty$ gives

$$\tilde{\Lambda}(s) = \frac{\rho k_E V}{2ks^2} + \frac{\rho k_E}{k}\sqrt{\frac{D}{4s^3}} \tag{A.30}$$

which inverts to

$$\Lambda(t) \sim \frac{\rho k_E V T}{2k} + \frac{\rho k_E}{k}\sqrt{\frac{DT}{\pi}}, \tag{A.31}$$

giving the small T behavior. This has two scaling limits within it. Provided that $T \ll 4D/V^2/\pi < 2D/V^2$, the scaling goes as $\Lambda(T) \sim T^{-1/2}$. But if $T \gg 4D/V^2/\pi$, it goes as $\Lambda(t) \sim T$. For large times, taking $s \to 0$ gives

$$\tilde{\Lambda}(s) = \frac{\rho k_E V}{ks^2}, \tag{A.32}$$

and this inverts to $\Lambda(T) = \rho k_E V T/k$ as the long time solution, providing a mean flux equivalent to the Einstein model (Sec. 1.1.3). These limits are summarized in Eq. 2.16.

Appendix B

Calculations involved in the bed elevation model

B.1 Numerical simulation algorithm

The Gillespie stochastic simulation algorithm (SSA) generates exact realizations of a Markov random process from a sequence of random numbers. It was originally developed for chemical physics by *Gillespie* (1977) and is reviewed in *Gillespie* (1992) and *Gillespie* (2007). The SSA hinges on the defining property of a Markov process. When the transition rates from one state to another are not dependent on the distant past, the process is Markov (*Cox and Miller*, 1965). The following sections demonstrate that the time intervals τ between subsequent transitions are exponentially distributed within the model of Ch. 3. The SSA follows as a consequence of this property.

B.1.1 Times between transitions of any kind

The joint description of bedload transport and bed elevation changes is characterized by a set of states (n, m) where n and m are integers. The description involves four possible transitions (migration in, entrainment, deposition, migration out) with rates given in Eqs. 3.2-3.5.

From the state (n, m), the rate (probability per unit time) for any transition to occur is the sum over all possibilities:

$$A(n,m) = R_{MI}(n+1, m|n, m) + R_E(n+1, m-1|n, m) + R_D(n-1, m+1|n, m) + R_{MO}(n-1, m|n, m). \quad \text{(B.1)}$$

Using this, the probability that no transition occurs from the state (n, m) in a small time interval $\delta\tau$ is $1-A(n,m)\delta\tau$. If $Q(\tau|n, m)$ denotes the probability density that a transition of any kind occurs from the state (n, m) after a time τ, the probability density that a transition happens after a slightly larger time $\tau + \delta\tau$ can be written

$$Q(\tau + \delta\tau|n, m) = \big[1 - A(n, m)\delta\tau\big]Q(\tau|n, m). \quad \text{(B.2)}$$

Taking $\delta\tau \to 0$ produces a master equation $\frac{d}{d\tau}Q(\tau|n, m) = -A(n, m)Q(\tau|n, m)$, from which it follows that the time τ between subsequent transitions is distributed as

$$Q(\tau|n, m) = A(n, m)e^{-A(n,m)\tau}. \quad \text{(B.3)}$$

This equation demonstrates that the time τ to the next transition from a state (n, m) is exponentially distributed with mean value $\bar{\tau} = 1/A(n, m)$. This means if the stochastic process transitioned to the state (n, m) at a time t, the next transition will occur at a time $t + \tau$ with τ a random variable drawn from the exponential distribution in Eq. B.3.

B.1.2 Selection of transitions that occur

So far, Eq. B.3 demonstrates how to step the time from one transition to the next, but it remains unclear how to step the state variables n and m at each transition time. There is a need to characterize the type of transition which occurs at a given transition time.

Intuitively, this will depend on the relative magnitudes of the rates from Eqs. 3.2-3.5. The transition with the highest rate is most likely to occur.

This is formalized by generating the ratios

$$S = \left\{ \frac{R_{MI}(n+1, m|n, m)}{A(n,m)}, \frac{R_E(n+1, m-1|n, m)}{A(n,m)}, \right.$$
$$\left. \frac{R_D(n-1, m+1|n, m)}{A(n,m)}, \frac{R_{MO}(n-1, m|n, m)}{A(n,m)} \right\}. \quad \text{(B.4)}$$

By construction, $\sum S = 1$. Forming cumulative sums of the four ratios partitions the unit interval $[0, 1]$ into four chunks, each associated with a transition – either migration in, entrainment, deposition, or migration out. The transitions with the highest rates have the largest associated chunks. Drawing a random number on $[0, 1]$ can then select the transition which occurs at a given transition time by querying which chunk it falls within.

In summary, to step the process through a single transition, the SSA draws the time interval to the next transition from the distribution (Eq. B.3), draws a uniform random number from $[0, 1]$, then uses this uniform random to select the transition that occurs from the cumulative sum of the ratios in Eq. B.4. Iterating this random number generation and selection process simulates exact realizations of the stochastic process. These are series of n and m through time from which any statistics of interest can be calculated.

B.1.3 Pseudocode for the Gillespie SSA

Simulations are initialized by the initial conditions n_0 and m_0, the model parameters used in Eqs. 3.2-3.5, and the desired simulation duration $t_{\max}$. The SSA uses these inputs to generate timeseries of n and m as follows:

$t = 0$
$n = n_0$ ▷ Set the initial state (n_0, m_0)
$m = m_0$
while $t < t_{\max}$; **do** ▷ Simulation will go until t surpasses $t_{\max}$
  record (n, m, t) ▷ Build timeseries of n and m
  draw τ from Eq. B.3 ▷ Select time to next transition

$t \coloneqq t + \tau$

draw a random number r in $[0, 1]$ ▷ Select type of transition that occurs

compute the ratios r_1, r_2, r_3, r_4 in Eq. B.4

form the cumulative sums $r_i = \sum_{1 \leq j \leq i} r_j$ ▷ Now enact the transition

if $0 \leq r < r_1$ **then** ▷ Migration in

$n \coloneqq n + 1$

else if $r_1 \leq r < r_2$ **then** ▷ Entrainment

$n \coloneqq n + 1$

$m \coloneqq m - 1$

else if $r_2 \leq r < r_3$ **then** ▷ Deposition

$n \coloneqq n - 1$

$m \coloneqq m + 1$

else if $r_3 \leq r \leq 1$ **then** ▷ Migration out

$n \coloneqq n - 1$

end if

end while

B.2 Approximate solutions of the master equation

B.2.1 Mean field solution of particle activity

Assuming the dynamics of the particle activity are totally independent of the bed elevation and summing Eq. 3.7 over all values of m obtains a mean field equation for the particle activity:

$$0 = \nu A(n-1) + [\lambda + \mu(n-1)]A(n-1) + \sigma(n+1)A(n+1) + \gamma(n+1)A(n+1) - (\nu + \lambda + \mu n + \sigma n + \gamma n)A(n). \quad \text{(B.5)}$$

This can be solved by introducing the generating function (*Cox and Miller*, 1965) $G(x) = \sum_n x^n A(n)$, providing

$$0 = (\nu + \lambda)(x-1)G + [\mu x^2 + \sigma + \gamma - (\mu + \sigma + \gamma)x]\frac{\partial G}{\partial x}, \tag{B.6}$$

which is separable and integrates for

$$G(x) = \left(\frac{\gamma + \sigma - \mu}{\gamma + \sigma - \mu x}\right)^{\frac{\nu+\lambda}{\mu}} \tag{B.7}$$

after applying the normalization condition $G(1) = 1$. From the definition of G it follows that $A(n) = \frac{1}{n!}\frac{d^n G}{dx^n}|_{x=0}$, giving the negative binomial distribution of particle activity demonstrated by *Ancey et al.* (2008), stated in Eq. 3.10, and introduced originally in Sec. 1.1.13.

B.2.2 Mean field solution of bed elevations

The negative binomial distribution provides $\langle n|m\rangle = \langle n\rangle$, so Eq. 3.7 produces

$$\begin{aligned} 0 = [\lambda + \mu\langle n\rangle][1 + \kappa(m+1)]M(m+1) + \sigma\langle n\rangle[1 - \kappa(m-1)]M(m-1) \\ - \{[\lambda + \mu\langle n\rangle](1 + \kappa m) + \sigma\langle n\rangle(1 - \kappa m)\}M(m). \end{aligned} \tag{B.8}$$

Identifying $E = \lambda + \mu\langle n\rangle$ and $D = \sigma\langle n\rangle$ and incorporating $E = D$ gives Eq. 3.11:

$$0 = [1 + \kappa(m+1)]M(m+1) + [1 - \kappa(m-1)]M(m-1) - 2M(m). \tag{B.9}$$

This can be solved using the Fokker-Planck expansion (*Gardiner*, 1983) that effectively converts this discrete master equation for m into a diffusion equation for the quasi-continuous variable $z = z_1 m$. This works since z_1 is small. Introducing z and writing $\overline{\kappa} = \kappa/z_1$ gives

$$0 = [1 + \overline{\kappa}(z + z_1)]M(z + z_1) + [1 - \overline{\kappa}(z - z_1)]M(z - z_1) - 2M(z). \tag{B.10}$$

$\overline{\kappa}$ should not depend on z_1 since the magnitude of the feedbacks between bed elevations and entrainment and deposition rates depends on elevation changes, and not on the size of grains or the length of the control volume. Expanding the entire first and second terms to second order z_1 provides the Fokker-Planck equation

$$0 = -2\overline{\kappa} z_1 [zM(z)]' + z_1^2 M''(z). \tag{B.11}$$

Taking into account that this distribution should be normalizable, $\lim_{z\to\pm\infty} M(z) = 0$, the solution is

$$M = M_0 e^{-\kappa(z/z_1)^2} \tag{B.12}$$

as provided in Ch. 3.

B.2.3 Closure equation approach for bed elevations

This section produces an approximate relationship to close $\langle n|m\rangle$ in terms of m valid to first order in κ. Writing

$$\langle n|m\rangle \approx \langle n\rangle - \kappa c m, \tag{B.13}$$

for the mean particle activity conditional to the elevation m into Eq. 3.7, noting $E = D$, and neglecting terms of $O(\kappa^2)$ provides

$$\begin{aligned} 0 \approx \Big[1 + \kappa(m+1)\Big\{1 - \frac{\mu c}{E}\Big\}\Big] M(m+1) + \Big[1 - \kappa(m-1)\Big\{1 + \frac{\sigma c}{E}\Big\}\Big] \\ - \Big[2 - \kappa m \Big\{\frac{(\sigma+\mu)c}{E}\Big\}\Big] M(m) \end{aligned} \tag{B.14}$$

At this point, c is considered an undetermined positive constant that may depend on the entrainment, migration, and deposition rates. Taking the Fokker-Planck expansion and requiring the distribution $M(m)$ to vanish at infinity for normalization yields

$$0 = 2\kappa m \Big(2 + \frac{(\sigma-\mu)c}{E}\Big) M(m) + \Big\{\Big[2 - \kappa m \frac{(\sigma+\mu)c}{E}\Big] M(m)\Big\}'. \tag{B.15}$$

Finally, integrating, expanding to first order in κ, and exponentiating to solve for M produces

$$M(m) = M_0 \exp\Big\{ -\kappa m^2 \Big[1 + \frac{(\sigma - \mu)c}{2E}\Big]\Big\}. \tag{B.16}$$

Since the numerical solutions show $\sigma_m^2 = \frac{1}{4\kappa}$, this suggests the closure relation

$$\langle n|m\rangle = \langle n\rangle \Big(1 - \frac{2\kappa m}{1 - \mu/\sigma}\Big) \tag{B.17}$$

corresponding to $c = 2E/(\sigma - \mu)$. This is the closure relationship provided in Eq. 3.12 and plotted with the numerical simulations in Fig. 3.4. The elevation distribution Eq. 3.13 follows by combining Eqs. B.16 and B.17.

Appendix C

Calculations involved in the sediment burial model

C.1 Calculation of the distribution function

Owing to the convolution structure of Eqs. 4.1 and 4.2, their solution is a formidable problem. Luckily, we have the device of Laplace transforms. These project integro-differential equations into an alternate space in which convolutions are unraveled (e.g. *Arfken*, 1985). The double Laplace transform of a joint probability distribution $p(x,t)$ is defined by

$$\tilde{p}(\eta,s) = \int_0^\infty dx e^{-\eta x} \int_0^\infty dt e^{-st} p(x,t). \tag{C.1}$$

The Laplace-transformed moments of x are linked to derivatives of the double-transformed distribution Eq. C.1 (cf. *Berezhkovskii and Weiss*, 2002). Eq. (C.1) implies

$$\langle \tilde{x}(s)^k \rangle = (-)^k \partial_\eta^k \tilde{p}(\eta,s)\Big|_{\eta=0}. \tag{C.2}$$

This means the variance of position can be derived as as $\sigma_x^2(t) = \langle x^2 \rangle - \langle x \rangle^2 = \mathcal{L}^{-1}\{\langle \tilde{x}^2 \rangle; t\} - \mathcal{L}^{-1}\{\langle \tilde{x} \rangle; t\}^2$, where $\mathcal{L}^{-1}$ denotes the inverse Laplace transform (e.g. *Arfken*, 1985).

Double transforming Eqs. 4.1 using the definition Eq. C.1 gives

$$\tilde{\omega}_0(\eta, s) = \theta_1 \tilde{g}_1(\eta, s) + \tilde{\omega}_2(\eta, s)\tilde{g}_1(\eta, s) - \tilde{\omega}_1(\eta, s), \tag{C.3}$$

$$\tilde{\omega}_1(\eta, s) = \theta_1 \tilde{g}_1(\eta, s+\kappa) + \tilde{\omega}_2(\eta, s)\tilde{g}_1(\eta, s+\kappa), \tag{C.4}$$

$$\tilde{\omega}_2(\eta, s) = \theta_2 \tilde{g}_2(\eta, s) + \tilde{\omega}_1(\eta, s)\tilde{g}_2(\eta, s). \tag{C.5}$$

This algebraic system solves for

$$\tilde{\omega}_0(\eta, s) = \frac{\theta_1 + \theta_2 \tilde{g}_2(\eta, s)}{1 - \tilde{g}_1(\eta, s+\kappa)\tilde{g}_2(\eta, s)} \big\{ \tilde{g}_1(\eta, s) - \tilde{g}_1(\eta, s+\kappa) \big\}, \tag{C.6}$$

$$\tilde{\omega}_1(\eta, s) = \frac{\theta_1 + \theta_2 \tilde{g}_2(\eta, s)}{1 - \tilde{g}_1(\eta, s+\kappa)\tilde{g}_2(\eta, s)} \tilde{g}_1(\eta, s+\kappa), \tag{C.7}$$

$$\tilde{\omega}_2(\eta, s) = \frac{\theta_2 + \theta_1 \tilde{g}_1(\eta, s+\kappa)}{1 - \tilde{g}_1(\eta, s+\kappa)\tilde{g}_2(\eta, s)} \tilde{g}_2(\eta, s). \tag{C.8}$$

Double transforming Eqs. 4.2 gives

$$\tilde{p}_0(\eta, s) = \frac{1}{s}\tilde{\omega}_0(\eta, s), \tag{C.9}$$

$$\tilde{p}_1(\eta, s) = \theta_1 \tilde{G}_1(\eta, s) + \tilde{\omega}_2(\eta, s)\tilde{G}_1(\eta, s), \tag{C.10}$$

$$\tilde{p}_2(\eta, s) = \theta_2 \tilde{G}_2(\eta, s) + \tilde{\omega}_1(\eta, s)\tilde{G}_2(\eta, s). \tag{C.11}$$

The total probability is $p(x,t) = p_0(x,t) + p_1(x,t) + p_2(x,t)$. Using Eqs. C.6-C.11 this becomes, in the double Laplace representation,

$$\begin{aligned}\tilde{p}(\eta, s) = \frac{1}{s}\frac{\theta_1 + \theta_2 \tilde{g}_2(\eta, s)}{1 - \tilde{g}_1(\eta, s+\kappa)\tilde{g}_2(\eta, s)} \big\{ \tilde{g}_1(\eta, s) - \tilde{g}_1(\eta, s+\kappa) \big\} \\ + \frac{\theta_1 \big[\tilde{G}_1(\eta, s) + \tilde{g}_1(\eta, s+\kappa)\tilde{G}_2(\eta, s)\big] + \theta_2 \big[\tilde{G}_2(\eta, s) + \tilde{g}_2(\eta, s)\tilde{G}_1(\eta, s)\big]}{1 - \tilde{g}_1(\eta, s+\kappa)\tilde{g}_2(\eta, s)}.\end{aligned} \tag{C.12}$$

Plugging the propagators outlined in Sec. 4.1.3 into Eq. C.12 gives

$$\tilde{p}(\eta, s) = \frac{1}{s}\frac{(s + \kappa + k')s + \theta_1(s+\kappa)\eta v + \kappa k_2}{(s + \kappa + k_1)\eta v + (s + \kappa + k')s + \kappa k_2}. \tag{C.13}$$

In this equation, $k' = k_1 + k_2$, and the normalization requirement of the initial probabilities $\theta_1 + \theta_2 = 1$ has been incorporated. The double inverse transform of this equation provides the distribution $p(x,t)$. The transform over η is inverted first. Using the results [15.103] (transform of exponential), [15.123] (transform of derivative), and [15.141] (transform of Dirac delta function) from *Arfken* (1985) provides

$$\tilde{p}(x,s) = \theta_1 \frac{s+\kappa}{s(s+\kappa+k_1)}\delta(x) + \frac{1}{v}\Big(\frac{(s+\kappa+k')s+\kappa k_2}{s(s+\kappa+k_1)} - \frac{\theta_1(s+\kappa)[s(s+\kappa+k_1)+\kappa k_2]}{s(s+\kappa+k_1)^2}\Big)\exp\Big[-\frac{(s+\kappa+k')s+\kappa k_2}{s+\kappa+k_1}\frac{x}{v}\Big]. \quad \text{(C.14)}$$

Inverting the remaining transform over s, applying results [15.152] (substitution), [15.164] (translation), and [15.175] (transform of te^{kt}) from *Arfken* (1985), and defining the shorthand notations $\tau = k_1(t - x/v)$, $\xi = k_2 x/v$, and $\Omega = (\kappa + k_1)/k_1$, gives the simpler form

$$p(x,t) = \theta_1\Big[1 - \frac{k_1}{\kappa+k_1}\big(1 - e^{-(\kappa+k_1)t}\big)\Big]\delta(x) + \frac{1}{v}\exp[\Omega\tau - \xi] \times \mathcal{L}^{-1}\Big\{\Big(\theta_2 + \frac{\theta_1 k_1 + \theta_2 k_2}{s} + \frac{\theta_1 k_1 k_2}{s^2} + \frac{\theta_2 \kappa k_2}{s(s-\kappa-k_1)} + \frac{\theta_1 \kappa k_1 k_2}{s^2(s-\kappa-k_1)}\Big) \times \exp\Big[\frac{k_1\xi}{s}\Big]; \tau/k_1\Big\}. \quad \text{(C.15)}$$

Using entries [2.2.2.1], [2.2.2.8], and [1.1.1.13] from *Prudnikov et al.* (1992) in conjunction with the definition of the generalized Marcum Q-function $\mathcal{Q}_\mu(x,t)$ (*Temme*, 1996), and inserting the Heaviside functions to account for the fact that grains can neither travel backwards nor at speeds exceeding v, then finally produces Eq. 4.5 for the joint distribution $p(x,t)$.

C.2 Calculation of the moments

The first two moments of position x and ultimately the variance are computed using Eq. C.2. The first two derivatives of the double Laplace-

transformed distribution Eq. C.13 are

$$\partial_\eta \tilde{p}(\eta, s) = -v\frac{1}{s}\frac{[(s+\kappa+k')s+\kappa k_2][\theta_2(s+\kappa)+k_1]}{[\eta v(s+\kappa+k_1)+(s+\kappa+k')s+\kappa k_2]^2}, \tag{C.16}$$

$$\partial_\eta^2 \tilde{p}(\eta, s) = 2v^2\frac{1}{s}\frac{(s+\kappa+k_1)[(s+\kappa+k')s+\kappa k_2][\theta_2(s+\kappa)+k_1]}{[\eta v(s+\kappa+k_1)+(s+\kappa+k')s+\kappa k_2]^3}. \tag{C.17}$$

Evaluating these at $\eta = 0$ and applying Eq. C.2 provides the Laplace-transformed moments

$$\frac{\langle\tilde{x}(s)\rangle}{v} = \frac{1}{s}\frac{\theta_2(s+\kappa)+k_1}{(s+\kappa+k')s+\kappa k_2} = \frac{1}{s}\frac{\theta_2(s+\kappa)+k_1}{(s+a+b)(s+a-b)}, \tag{C.18}$$

$$\begin{aligned}\frac{\langle\tilde{x}^2(s)\rangle}{2v^2} &= \frac{1}{s}\frac{(s+\kappa+k_1)(\theta_2(s+\kappa)+k_1)}{[(s+\kappa+k')s+\kappa k_2]^2} \\ &= \frac{1}{s}\frac{(s+\kappa+k_1)(\theta_2(s+\kappa)+k_1)}{(s+a+b)^2(s+a-b)^2}.\end{aligned} \tag{C.19}$$

The parameters $a = (\kappa+k')/2$ and $b^2 = a^2-\kappa k_2$ were introduced to factorize the denominators. These equations can be inverted using the properties [15.164] (translation), [15.11.1] (integration), and [15.123] (differentiation) from *Arfken* (1985) after expansion in partial fractions. For the mean, the calculation is

$$\begin{aligned}\frac{2b}{v}\langle x\rangle &= \big[\theta_2 + (k_1+\theta_2\kappa)\int_0^t dt\big]\mathcal{L}^{-1}\Big\{\frac{1}{s+a-b} - \frac{1}{s+a+b}; t\Big\} \\ &= \Big[\theta_2 + \frac{k_1+\theta_2\kappa}{b-a}\Big]e^{(b-a)t} - \Big[\theta_2 - \frac{k_1+\theta_2\kappa}{a+b}\Big]e^{-(a+b)t} \\ &\quad - \Big[\frac{k_1+\theta_2\kappa}{b-a} + \frac{k_1+\theta_2\kappa}{a+b}\Big].\end{aligned} \tag{C.20}$$

This equation rearranges to Eq. 4.6. The second moment (Eq. C.19) is

$$\frac{2b^2}{v^2}\langle x^2\rangle = \Big[\theta_2(\delta(t)+\partial_t) + (\theta_2(2\kappa+k_1)+k_1) + (\kappa+k_1)(\theta_2\kappa+k_1)\int_0^t dt\Big] \times \mathcal{L}^{-1}\Big\{\frac{1}{(s+a-b)^2} + \frac{1}{(s+a+b)^2} - \frac{1}{b(s+a-b)} + \frac{1}{b(s+a+b)}; t\Big\}. \quad \text{(C.21)}$$

This becomes

$$\frac{2b^3}{v^2}\langle x^2\rangle = \Big[\theta_2\partial_t + [\theta_2(2\kappa+k_1)+k_1] + (\kappa+k_1)(\theta_2\kappa+k_1)\int_0^t dt\Big] \times \Big((bt-1)e^{(b-a)t} + (bt+1)e^{-(a+b)t}\Big) \quad \text{(C.22)}$$

which evaluates to Eq. 4.7. Finally, $\sigma_x^2 = \langle x^2\rangle - \langle x\rangle^2$ derives the variance in Eq. 4.8.

C.3 Limiting behavior of the moments

The diffusion exponents γ in the local, intermediate, and global ranges using the two limiting cases described in Sec. 4.1.5. Limit (1) is $\kappa \to 0$. Taking this limit in Eqs. C.18 and C.19 with initial condition $\theta_1 = 1$ obtains

$$\langle \tilde{x}\rangle = vk_1\frac{1}{s^2(s+k')}, \quad \text{(C.23)}$$

$$\langle \tilde{x}^2\rangle = 2v^2k_1\frac{s+k_1}{s^3(s+k')^2}. \quad \text{(C.24)}$$

Laplace inverting and combining these equations provides the variance

$$\sigma_x^2 = 2v^2\frac{k_1}{k'^4}\Big(k_1\big[\frac{1}{2} - k't e^{-k't} - \frac{1}{2}e^{-2k't}\big] + k_2\big[-2 + k't + (2+k't)e^{-k't}\big]\Big). \quad \text{(C.25)}$$

This result encodes two ranges of diffusion and can also be derived from the governing equations of the *Lisle et al.* (1998) and *Lajeunesse et al.* (2017)

models. Expanding for small t provides $\sigma_x^2(t) = v^2 k_1 t^3/3$ – local range super-diffusion. Expanding for large t provides $\sigma_x^2(t) = 2v^2 k_1 k_2 t/k'^3$ – intermediate range normal diffusion.

Limit (1) can be further investigated for arbitrary initial conditions. By applying Tauberian theorems, the $t \to 0$ variance can be determined from the $s \to \infty$ limits of Eqs. C.18 and C.19 (e.g. *Weeks and Swinney*, 1998; *Weiss*, 1994). Expanding these equations in powers of $1/s$ and inverting the resulting transforms gives

$$\langle x \rangle = v\theta_2 t + \frac{1}{2} v(\theta_1 k_1 - \theta_2 k_2) t^2 + O(t^3), \tag{C.26}$$

$$\langle x^2 \rangle = v^2 \theta_2 t^2 + \frac{1}{3} v^2 (\theta_1 k_1 - 2\theta_2 k_2) t^3 + O(t^4). \tag{C.27}$$

This equation highlights the effect of initial conditions on the diffusion characteristics of the local range:

$$\sigma_x^2(t) \sim v^2 \theta_1 \theta_2 t^2 + \frac{1}{3} v^2 (\theta_1 k_1 + \theta_2 k_2) t^3. \tag{C.28}$$

This equation includes only leading order terms for any option of θ_1 and θ_2. Eq. C.28 shows local range exponent $\gamma = 2$ when initial conditions are mixed (both are non-zero) and $\gamma = 3$ when initial conditions are pure (one is zero).

Limit (2) is $1/k_2 \to 0$ and $v \to \infty$ while $v/k_2 = l$. Under this limit, Eqs. C.18 and C.19 provide

$$\langle \tilde{x} \rangle = k_1 l \frac{1}{s(s+\kappa)}, \tag{C.29}$$

$$\langle \tilde{x}^2 \rangle = 2l^2 k_1 \frac{s + \kappa + k_1}{s(s+\kappa)^2}. \tag{C.30}$$

Inverting these equations and introducing the variables $c = lk_1$ (an effective velocity) and $D_d = l^2 k_1$ (a diffusivity) provides positional variance

$$\sigma_x^2(t) = \frac{2D_d(1 - e^{-\kappa t})}{\kappa} + \frac{(1 - e^{-2\kappa t} - 2e^{-\kappa t}\kappa t)c^2}{\kappa^2}. \tag{C.31}$$

This is mathematically identical to the key result of *Wu et al.* (2019a). Expanding for small t provides $\sigma_x^2(t) = 2D_d t$ – intermediate range normal diffusion, while sending $t \to \infty$ provides $\sigma_x^2 = (2D_d\kappa + c^2)/\kappa^2$ – a constant variance in the geomorphic range. The global range is characterized by competition between terms in Eq. C.31 and shows $2 \leq \gamma \leq 3$ depending on the ratio k_1/κ (cf. *Wu et al.*, 2019a). Finally, both Eqs. C.25 and C.31 reduce to the Einstein result $\sigma_x^2(t) = 2D_d t$ in further simplified limits.

Appendix D

Calculations involved in the collisional Langevin model

D.1 Derivation of master equation

To derive the master equation from Eq. 5.4, I temporarily consider the Gaussian white noise (GWN) $\xi(t)$ as a Poisson jump process having rate r and jumps $\sqrt{2\tilde{D}}h$ with h distributed as $f(h)$. I will later take a GWN limit from this noise. Similar derivations are available in some references (e.g. *Kanazawa*, 2017; *Suweis et al.*, 2011), and the precise connection between GWN and Poisson noise is discussed in *Van Den Broeck* (1983).

From this starting point, integrating Eq. 5.4 over a small time interval δt under the Itô interpretation for the collision term provides

$$u(t+\delta t) = \begin{cases} u(t) + \tilde{\Gamma}\delta t & \text{with probability } 1 - r\delta t - \nu\delta t \\ u(t) + \sqrt{2\tilde{D}}h & \text{with probability } r\delta t \\ \varepsilon u(t) & \text{with probability } \nu\delta t \end{cases} . \tag{D.1}$$

Considering the probability $P(u, t+\delta t)$ as a sum over possible paths

from $P(u,t)$ develops

$$\begin{aligned} P(u,t+\delta t) = (1-r\delta t-\nu\delta t)\int_{-\infty}^{\infty} dw\delta(u-w-\tilde{\Gamma}\delta t)P(w,t) \\ + r\delta t\int_{-\infty}^{\infty} dw\int_{-\infty}^{\infty} dhf(h)\delta(u-w-\sqrt{2\tilde{D}}h)P(w,t) \\ + \nu\delta t\int_{-\infty}^{\infty} dw\int_{0}^{1} d\varepsilon\rho(\varepsilon)\delta(u-w\varepsilon)P(w,t). \end{aligned} \tag{D.2}$$

Evaluating all integrals over δ-functions provides

$$\begin{aligned} P(u,t+\delta t) = (1-r\delta t-\nu\delta t)P(u-\tilde{\Gamma}\delta t,t) \\ + r\delta t\int_{-\infty}^{\infty} dhf(h)P(u+\sqrt{2\tilde{D}}h) \\ + \nu\delta t\int_{0}^{1}\frac{\tilde{D}\varepsilon}{\varepsilon}\rho(\varepsilon)P\big(\frac{u}{\varepsilon}\big). \end{aligned} \tag{D.3}$$

Finally, taking $\delta t \to 0$ and limiting the Poisson noise involving $\sqrt{2\tilde{D}}$ to a Gaussian white noise by taking $r \to \infty$ as $h \to 0$ such that $h^2 r = 1$ obtains the master equation 5.5.

D.2 Derivation of steady-state solution

Defining $\tilde{P}(s) = \int_{-\infty}^{\infty} due^{ius}P(u)$ as the Fourier transform (FT) of $P(u)$ and taking the FT of Eq. 5.5 develops the recursion relation

$$\tilde{P}(s) = \frac{\tilde{P}(s\varepsilon)}{q(s)}. \tag{D.4}$$

where

$$q(z) = \tilde{D}z^2 - i\tilde{\Gamma}z + 1. \tag{D.5}$$

Recursing $N+1$ times provides

$$\tilde{P}(s) = \frac{\tilde{P}(s\varepsilon^{N+1})}{q(s\varepsilon^0)q(s\varepsilon^1)\ldots q(s\varepsilon^N)}. \tag{D.6}$$

The polynomials $q(z)$ can always be factored as $q(z) = \tilde{D}(z - i\lambda_-)(z - i\lambda_+)$ where

$$\lambda_\pm = \frac{\tilde{\Gamma}}{2\tilde{D}}\Big[1 \pm \sqrt{1 + 4\tilde{D}/\tilde{\Gamma}^2}\Big]. \tag{D.7}$$

Using these factors to expand $\tilde{P}(s)$ in partial fractions provides

$$\tilde{P}(s) = \tilde{P}(s\varepsilon^{N+1}) \sum_{l=0}^{N} \Big[\frac{R_l^-}{s\varepsilon^l - i\lambda_-} + \frac{R_l^+}{s\varepsilon^l - i\lambda_+}\Big], \tag{D.8}$$

where the coefficients $R_l^\pm$ are the residues (up to constant factors) of the product $[q(s\varepsilon^0) \dots q(s\varepsilon^N)]^{-1}$:

$$R_l^\pm = \frac{s\varepsilon^l - i\lambda_\pm}{q(s\varepsilon^0) \dots q(s\varepsilon^N)}\Big|_{s = i\lambda_\pm \varepsilon^{-l}}. \tag{D.9}$$

The Fourier-transformed Eq. D.6 has a convenient feature as $N \to \infty$: since $0 < \varepsilon < 1$, the prefactor $\tilde{P}(s\varepsilon^{N+1})$ becomes the normalization condition $\tilde{P}(0) = 1$ for the probability distribution $P(u)$. Taking this limit and evaluating the residues provides

$$\begin{aligned}\tilde{P}(s) = &\frac{1}{\tilde{D}(\lambda_+ - \lambda_-)\prod_{m=1}^{\infty} q(i\lambda_-\varepsilon^m)} \sum_{l=0}^{\infty} \frac{i}{(s\varepsilon^l - i\lambda_-)\prod_{m=1}^{l} q(i\lambda_-\varepsilon^{-m})} \\ &+ \frac{1}{\tilde{D}(\lambda_+ - \lambda_-)\prod_{m=1}^{\infty} q(i\lambda_+\varepsilon^m)} \sum_{l=0}^{\infty} \frac{-i}{(s\varepsilon^l - i\lambda_+)\prod_{m=1}^{l} q(i\lambda_+\varepsilon^{-m})}.\end{aligned} \tag{D.10}$$

Finally, the Fourier transforms are inverted term by term with contour integration (another use of the integral given in Eq. A.9), and the definition of $q(z)$ from Eq. D.5 is incorporated to obtain the steady-state solution quoted in Eq. 5.9.

D.3 Calculation of the moments

Taking Eq. 5.5, multiplying by u^k, integrating over all space, and taking account of normalization of $P(u)$ provides a recursion relation for the mo-

ments:

$$0 = \tilde{D}k(k-1)\langle u^{k-2}\rangle + \tilde{\Gamma}k\langle u^{k-1}\rangle + (\varepsilon^k - 1)\langle u^k\rangle. \tag{D.11}$$

$k = 1$ provides the mean (given in Eq. 5.11)

$$\langle u\rangle = \frac{\tilde{\Gamma}}{1-\varepsilon} = \frac{\Gamma}{\nu(1-\varepsilon)}, \tag{D.12}$$

while $k = 2$ provides the second moment

$$\langle u^2\rangle = 2\frac{\tilde{D} + \tilde{\Gamma}\langle u\rangle}{1-\varepsilon^2}, \tag{D.13}$$

leading to the velocity variance

$$\sigma_u^2 = \frac{2\tilde{D} + \tilde{\Gamma}^2}{1-\varepsilon^2} \tag{D.14}$$

given in Eq. 5.13.

D.4 The weak collision limit

Now I will demonstrate that weak collisions imply a Gaussian-like distribution for sediment velocities. The limit is challenging since the steady-state distribution Eq. 5.9 and the moments above all diverge as $\varepsilon \to 1$. Following *Hall and Wake* (1989), this divergence suggests normalizing the distribution $P(u)$ using the scaled variable

$$z = \frac{u - \langle u\rangle}{\sigma_u}, \tag{D.15}$$

giving a scaled distribution

$$Q(z) = \sigma_u P(u). \tag{D.16}$$

The resulting differential equation for $Q(z)$ is well-behaved in the elastic collision limit $\varepsilon \to 1$. Incorporating this transformation into Eq. 5.5 provides

the "normalized" master equation

$$(1-\varepsilon^2)\frac{\tilde{D}}{2\tilde{D}+\tilde{\Gamma}}Q''(z) - \frac{\tilde{\Gamma}\sqrt{1-\varepsilon^2}}{\sqrt{2\tilde{D}+\tilde{\Gamma}^2}}Q'(z) - Q(z) + \frac{1}{\varepsilon}Q\Big(z + \Big[\frac{1-\varepsilon}{\varepsilon}z + \frac{\tilde{\Gamma}\sqrt{1-\varepsilon^2}}{\varepsilon\sqrt{2\tilde{D}+\tilde{\Gamma}^2}}\Big]\Big) = 0. \quad \text{(D.17)}$$

This equation remains exact and is only a change of variables from Eq. 5.5. Now I approximate the equation for $\varepsilon \to 1$ by expanding the final term to second order around $z = 0$ before setting $\varepsilon = 1$, obtaining

$$Q''(z) + zQ'(z) + Q(z) = 0, \quad \text{(D.18)}$$

which is the classic Ornstein-Uhlenbeck Fokker-Planck equation whose solution is the standard normal distribution for $Q(z)$ (e.g. *Gardiner*, 1983). This solution provides Eq. 5.15 when transformed back to the original variables $P(u)$ and u.